FACIES DISTRIBUTION, SEQUENCE STRATIGRAPHY,

CHEMOSTRATIGRAPHY, AND DIAGENESIS OF THE MIDDLE-LATE

TRIASSIC AL AZIZIYAH FORMATION, JIFARAH BASIN, NW LIBYA

A Dissertation

by

MOHAMED SALEM HAMADI MOUSTAFA

Submitted to the Office of Graduate and Professional Studies of
Texas A&M University
in partial fulfillment of the requirements for the degree of

DOCTOR OF PHILOSOPHY

Chair of Committee,	Michael Pope
Committee Members,	Ethan Grossman
	Yuefeng Sun
	Walter Ayers
Head of Department,	Rick Giardino

May 2015

Major Subject: Geology

ABSTRACT

This study presents the depositional facies, sequence stratigraphy, chemostratigraphy and diagenetic evolution of the Middle-Late Triassic Al Aziziyah Formation, Jifarah Basin northwest Libya. Eight measured sections were sampled and analyzed. High-resolution stable carbon isotope data were integrated with an outcrop-based sequence stratigraphic framework, to build the stratigraphic correlation, and to provide better age control of the Al Aziziyah Formation using thin section petrography, cathodoluminescence (CL) microscopy, stable isotope, and trace element analyses.

The Al Aziziyah Formation was deposited on a gently sloping carbonate ramp and consists of gray limestone, dolomite, and dolomitic limestone interbedded with rare shale. The Al Aziziyah Formation is predominantly a 2nd-order sequence (5-20 m.y. duration), with shallow marine sandstone and peritidal carbonate facies restricted to southernmost sections. Seven 3rd-order sequences were identified (S1-S7) within the type section. North of the Ghryan Dome section are three mainly subtidal sequences (S_8-S_{10}) that do not correlate to the south. Shallowing upward trends define 4th-5th order parasequences, but correlating these parasequences between sections is difficult due to unconformities.

The carbon isotope correlation between the Ghryan Dome and Kaf Bates sections indicates five units of $\delta^{13}C$ depletion and enrichment (sequences 3-7). The enrichment of $\delta^{13}C$ values in certain intervals most likely reflects local withdrawal of ^{12}C from the

ocean due to increased productivity, as indicated by the deposition of organic-rich sediment, and/or whole rock sediment composed of calcite admixed with aragonite. The depletion of $\delta^{13}C$ is clearly associated with exposure surfaces and with shallow carbonate facies. Heavier $\delta^{18}O$ values are related to evaporetic enrichment of ^{18}O, whereas depletion of $\delta^{18}O$ is related to diagenesis due to freshwater input.

Al Aziziyah Formation diagenetic events indicate: 1) initial meteoric and shallow burial; 2) three types of dolomite D_1, D_2 and D_3 were most likely formed by microbial, seepage reflux and burial processes, respectively; and 3) diagenetic cements cannot be related to the arid, mega-monsoonal climate of the Triassic and most likely formed subsequently in a humid, meteoric setting.

DEDICATION

This dissertation is dedicated to my father and mother for their encouragement, to my wife and children for their support and patience.

ACKNOWLEDGEMENTS

TABLE OF CONTENTS

CHAPTER

CHAPTER

LIST OF FIGURES

xi

LIST OF TABLES

CHAPTER I

INTRODUCTION

The Triassic rocks of the Jifarah Basin, northwest Libya, contain mixed carbonate and siliciclastic, which make it a potential petroleum play. The Middle-Late Triassic (Ladinian Carnian) Al Aziziyah Formation was deposited on a gently sloping carbonate ramp within the Jifarah Basin of Northwest Libya. The Al Aziziyah Formation consists of gray limestone, dolomite, and dolomitic limestone interbedded with rare shale. Facies of the Al Aziziyah Formation are interpreted from shallowest to deepest as follows: tidal sandstone; peritidal carbonate; barrier; shallow subtidal facies; deep subtidal; and basinal facies (black shale and carbonate mud). Eight measured sections (Ghryan Dome, Ras Mazal East, Ras Mazal West, Kurrush Dome, Kaf Bates, Al Aziziyah Town, Ras Lafal and Bu Arghop), three measured sections were sampled for carbon and oxygen isotope (Ghryan Dome, Kaf Bates and Bu Arghop), and two measured sections (Ghryan Dome and Kaf Bates) were additionally sampled to better understand the diagenesis of this unit. A depositional dip cross section of the Al Aziziyah Formation within the Jifarah Basin was sampled and analyzed for facies, sequence stratigraphy, stable isotope and digenesis to build the stratigraphic framework of Al Aziziyah Formation, to integrate high-resolution carbon isotope data with an outcrop-based sequence stratigraphic framework, and to provide better age control of the Al Aziziyah Formation. This study also discusses the relation between the facies architecture of the Al Aziziyah Formation and the carbon isotope values and the possible influence of depositional environments on the isotopic values. Moreover, this study describes the diagenetic processes and

1

sequence of paragenetic events that affected the Middle–Late Triassic Al Aziziyah carbonate facies to determine if these diagenetic features can be related to the mega-monsoonal climate of the Triassic. Although this Formation was the subject of many previous outcrop and biostratigraphic studies, a regional synthesis of the lithofacies, diagenesis, chemostratigraphy, and sequence stratigraphy has not been reconstructed.

This dissertation is divided into three main parts (chapters two, three and four), each of which presents a separate paper designed for journal publication, each with its own objectives. These major objectives were to: (1) integrate high-resolution carbon isotope data with an outcrop-based sequence stratigraphic framework and facies architectures for the Al Aziziyah Formations; (2) determine the chemostratigraphy of the Al Azizyah Formation and compare it to the global record; and (3) understanding the diagenetic history of the Al Aziziyah Formation.

Chapter two focuses on descriptions of lithofacies with their relationship to depositional environments and sequence stratigraphy. Detailed stratigraphic cross sections were generated to illustrate the new, refined stratigraphic framework. A refined global correlation between the Middle-Late Triassic Al Aziziyah and the global sea level curve is presented.

Chapter three focuses on the stable isotope chemostratigraphic analysis and integration of carbon isotope data with outcrop data to develop a higher resolution age model for the Al Aziziyah Formation. The integration of carbon isotope data with outcrop data suggest that the carbon isotope record of the Al Aziziyah Formation does not represent the entire

original marine signature. Oxygen isotope data were also incorporated into this study, but were not as useful as the carbon isotope data, due to the effects of diagenesis. The effects of depositional environments and lithofacies on the carbon and oxygen isotope data were analyzed and interpreted.

Chapter four focuses on the diagenesis history of the Al Aziziyah Formation emphasizing trace element variations, microprobe analysis, and their relationships with depositional settings. Trace elements representing different facies and depositional settings were plotted to analyze their variations and determine the major diagenetic environments. Microprobe analysis of selected samples indicates different cement generation and diagenetic features and was then linked to cathodoluminescence stages to determine the paragenetic succession of the Al Aziziyah Formation.

CHAPTER II

FACIES ANALYSIS AND SEQUENCE STRATIGRAPHY OF THE MIDDLE–LATE TRIASSIC AL AZIZIYAH FORMATION, NORTHWEST LIBYA

II.1 Overview

The sequence stratigraphic framework of the Middle-Late Triassic (Ladinian-Carnian) Al Aziziyah Formation that was deposited on a gently sloping carbonate ramp within the Jifarah Basin of Northwest Libya consists of gray limestone, dolomite, and dolomitic limestone interbedded with shale. Eight measured sections along a depositional dip cross-section of the Al Aziziyah Formation within the Jifarah Basin were sampled and analyzed for facies and sequence stratigraphy to build the stratigraphic framework of the Al Aziziyah Formation. Facies of the Al Aziziyah Formation were interpreted from shallowest to deepest as: tidal sandstone; peritidal carbonate; ooid shoal barrier; shallow subtidal carbonate; deep subtidal carbonate; and basinal black shale and carbonate mud. The Al Aziziyah Formation is predominantly a 2nd-order sequence (5-20 m.y. duration), comprising of subtidal carbonate ramp, with marine sandstone and peritidal carbonate facies restricted to the southernmost sections. The peritidal facies were arid with mudcracks, evaporite nodules and abundant stromatolites. Ramp crest shoals were predominantly pellet ooid packstone-grainstone, whereas subtidal carbonate is thin-medium hummocky cross-stratified bed, and low- to high-density bioturbation. The transition from the underlying Kurrush Formation to the Al Aziziyah Formation is marked by a change from fine sand and red clay to carbonate. In the most updip location, the transition from the Al Aziziyah Formation to the overlying Abu Shaybah Formation

4

is an iron-rich and phosphatic surface (composite exposure and flooding surface) overlain by a bone bed with fine sandstone. Seven sequences (S_1-S_7) within the Ghryan Dome were identified based on facies stacking patterns, field observations and carbon stable isotopes. North of the Ghryan Dome section are three mainly subtidal sequences (S_8-S_{10}) that may not correlate to the south. Bed thickness variations may define higher-order parasequences, but correlating these parasequences between sections is difficult due to unconformities.

II.1.1 Introduction

The Triassic was a period of global transition associated with the beginning of the break-up of the Pangea supercontinent and the development of the Mesozoic basins in a globally warm and dry climate (Ziegler, 1990; Frakes et al., 1992; Dercourt et al., 1993; Lucas, 1998; Golonka and Ford, 2000; Reinhardt and Ricken, 2000; Boucot and Gray, 2001). The Triassic successions within the basins around the Tethys are characterized by marine and non-marine deposits (Dubois and Umbach, 1974).

Triassic rocks in Libya were deposited in four main domains: (i) predominantly marine rocks of the Nafusah escarpment and offshore Sabrath Basin, (ii) the eastern extension of the Algerian Ghadamis area, (iii) subsurface Triassic in eastern Libya, and (iv) continental rocks of the craton interior (Hallet, 2002). The Triassic sequence of the Nafusah escarpment was subdivided into four sequences separated by unconformities (Rubino et al., 2000). Sequence 1 equates to the Kurrush Formation, sequence 2 to the Al Aziziyah Formation, sequence 3 to the Abu Shaybah Formation, and sequence 4 to

the Abu Ghaylan Formation. Offshore, in the southern Mediterranean, the Triassic strata mostly are too deep to be penetrated by wells (Fig. 2.1), but seismic data show thick Triassic sediments to the north of the Sabrath-Cyrenaica Fault (Swire and Gashgesh, 2000). Triassic rocks are well developed in the Sabrath Basin, and carbonate and evaporite beds are occur in Late Triassic sediments in the western part of the basin (Hallett, 2002; Abohajar et al., 2009).
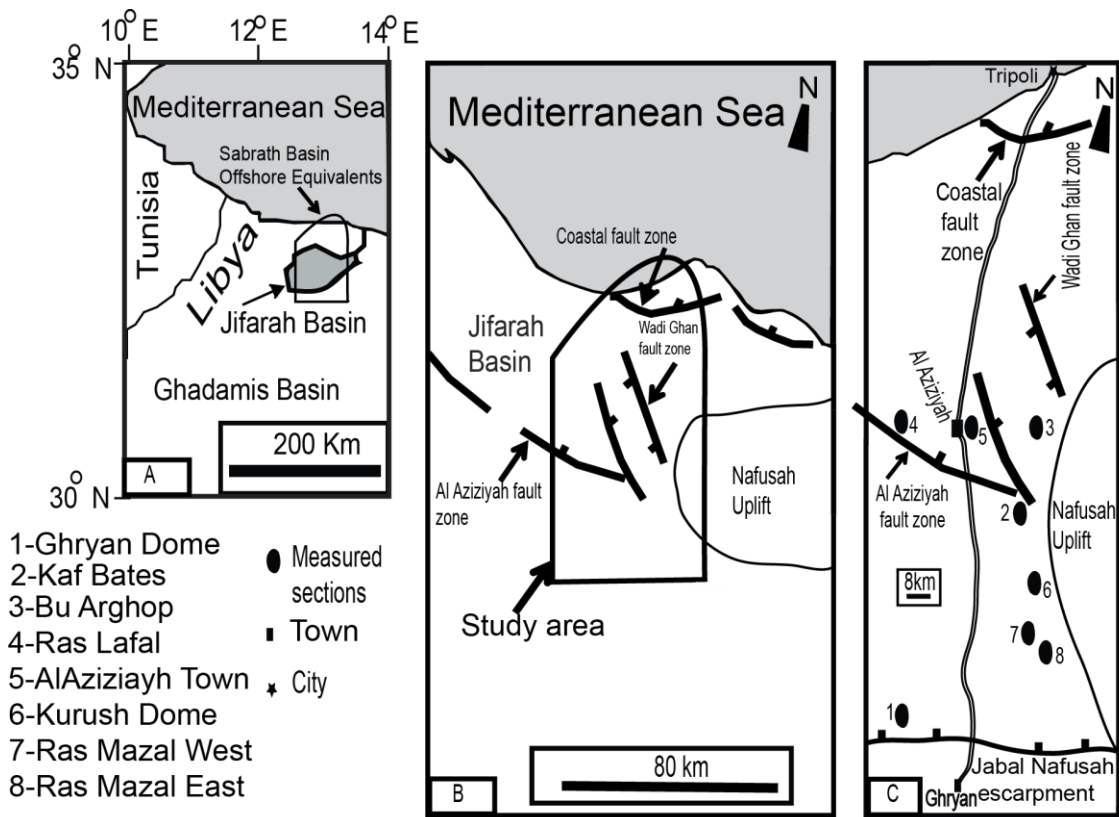
Fig. 2.1. A- Location of the Jifarah Basin. B- Detailed map shows the structural elements of the area. C- Location of measured sections. The Ghryan Dome section (1) is located on the southern margin of the Jifarah Basin. The Al Aziziyah Town section (5) is located north of the Ghryan Dome section, within deep water facies

6

In the Jifarah Basin of northwest Libya (Fig. 2.1A), the Triassic sediments are marine and non-marine deposits (Desio et al., 1960; Desio et al., 1963; Magnier 1963; Asserto and Benelli, 1971; Fatmi, 1977). The Lower Triassic is represented by the Kurrush Formation, which is green and red, sandy shale with sandstone intercalations, and occasional dolomitic limestones (Desio et al., 1960; Desio et al., 1963; Magnier 1963; Asserto and Benelli, 1971; Fatmi, 1977). The Middle-Late Triassic Al Aziziyah Formation is mainly carbonate facies (Desio et al., 1960; Desio et al., 1963; Magnier 1963; Asserto and Benelli, 1971; Fatmi, 1977). The Jifarah Basin covers an area of 1500 km^2 in northwestern Libya, bounded by the Nafusah uplift to the south and the offshore Sabrath Basin to the north (Fig. 2.1B; Hallett, 2002; Abohajar et al., 2009). Cores from wells in the Jifarah Basin indicate deposition of Paleozoic to Jurassic sediments (Hallett, 2002). In addition, the Jifarah escarpment extends 400 km from southeast Tunisia to Northwest Libya, and the Jifarah Arch represents the northern edge of the Ghadamis Basin.

The Jifarah Basin formed at the eastern end of the south Atlas lineament, which defines the southern margin of the Atlas fold belt (Dewey and Burke, 1973). The southern margin of the Atlas fold belt extends from Morocco to Tunisia, where it branches to extend into northwestern Libya (Dewey and Burke, 1973; Anketell and Ghellali, 1991). The Middle-Late Triassic (Ladinian-Carnian) Al Aziziyah Formation consists of massive grey limestone, dolomite and dolomitic limestone interbedded with shale (Fatmi, 1977; Asserto and Benelli, 1971; Magnier 1963; Desio et al., 1963; Desio et al., 1960; Burollet 1963; Muttoni et al., 2001). The Al Aziziyah Formation is a potential oil reservoir

7

interbedded with good source rocks, especially toward the northern part of the Jifarah Basin (Hallett, 2002; Abohajar et al., 2009). Eight measured sections of the Al Aziziyah Formation record a depositional dip cross-section within the Jifarah Basin (Fig. 2.1C). This paper outlines a sequence stratigraphic interpretation of the Al Aziziyah Formation based on bed-by-bed measured sections (Ghryan Dome, Ras Mazal East, Ras Mazal West, Kurrush Dome, Kaf Bates, Al Aziziyah Town, Ras Lafal and Bu Arghop) that provides a modern framework to understand its depositional setting and facies distribution.

II.1.2 Previous studies

The Al Aziziyah Formation was introduced by Parona (1914) after an outcrop study of the limestone in a quarry at an Al Aziziyah Town 42 km south of Tripoli (Al Aziziyah Town section). The type section of the Al Aziziyah Formation (160 m thick) is fully exposed in the Gharyan Dome (El Hinnaway and Chesitev, 1975). The Al Aziziyah Formation outcrops on the Gharyan area and north toward Al Aziziyah Town. However, this unit occurs in the subsurface throughout the Jifarah Basin (Swire and Gashgesh, 2000). In southern and central Tunisia, the lower part of both the Jabal Rehach Dolomite and the Jabal Rheouis Formation in central Tunisia are coeval with the Al-Aziziyah Formation (Bishop, 1975; Swire and Gashgesh, 2000; Hallet. 2002).

The Al Aziziyah Formation was previously interpreted to contain eight Early-Late Triassic biozones (Asserto, and Benelli, 1971; Swire and Gashgesh, 2000). The Al Aziziyah Formation at Ras Lafal was interpreted as two depositional sequences,

8

separated by an unconformity occurring within the lower half of the quarry (Rubino et al., 2000).

The lower boundary of the Al Aziziyah Formation is the first appearance of marine limestone beds overlying non-marine sandstone of the Kurrush Formation as observed at the Ghryan Dome. The upper boundary of the Al Aziziyah Formation is a sharp unconformable surface with overlying rusty colored continental sandstone of the Abu Shaybah Formation (Fatmi et al., 1981). Locally the base of the Abu Shaybah Formation contains phosphate clasts and nodules at the Ghryan Dome section.

II.1.3 Geological setting

During Mesozoic time, northwestern Libya was at the edge of the Tethys Seaway (Fig. 2, Demaison, 1965; Cornell and Tekbali, 1993; Hallet, 2002). Post-Hercynian crustal adjustments resulted in a marginal trough that extended westward into Tunisia and Algeria. Oscillations of the Tethys Seaways resulted in variable environmental conditions. An initial marine transgression occurred in the Ladinian, followed by a more extensive marine flooding during the Carnian. However, during the Carnian circulation was restricted in the western and central parts of the Jifarah Basin, probably due to uplift along the marginal trough (Fig. 2.2, Demaison, 1965; Cornell and Tekbali, 1993; Hallet, 2002). Therefore, evaporitic deposition prevailed in Algeria and Tunisia (Sloss, 1953; Demaison, 1965; Bishop, 1975), whereas terrginous material, sandy limestone, and dolomite of the Al Aziziyah Formation were deposited in a shallow ramp environment (Demaison, 1965; Cornell and Tekbali 1993; Swire and Gashgesh, 2000; Raulin et al.,

2011).The Jifarah Basin is bounded to the north by the east-west oriented subsurface Al Aziziyah fault zone. Toward the east (Fig. 2.1B and C), the Al Aziziyah fault links the Wada Ghan fault zone (Arkell et al., 1957; Swire and Gashgesh, 2000; Raulin et al., 2011).
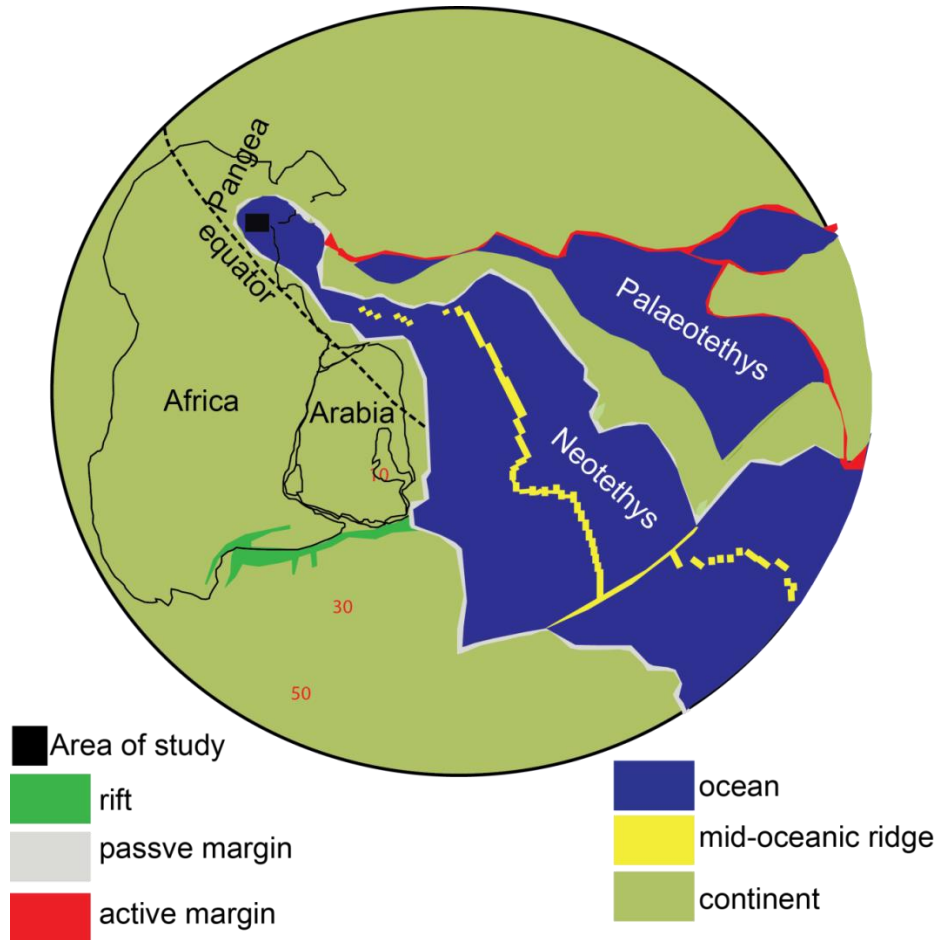
Fig. 2.2. Middle-Late Triassic palaeogeographic reconstruction of the Paleotethys and Neotethys of the northern Gondwana region (modified from Stampfli and Borel, 2002). The trend of these faults parallels older Paleozoic structures. The northwest-southeast structural orientation formed during the Caledonian orogeny, and the east-west structural orientation formed during subsequence Hercynian events (Swire and Gashgesh, 2000). Hercynian structures formed as a result of the collision between Laurussia and Gondwana and produced regional uplift, folding and erosion in northern Africa (Abohajar et al., 2009; Hallet, 2002).

This study integrates high-resolution carbon isotope data with an outcrop-based sequence stratigraphic framework to build the stratigraphic framework of the Al Aziziyah Formation. This study also presents the first stratigraphic framework integrated with high-resolution carbon isotopes for the Al Aziziyah Formation within the Jifarah Basin in northwest Libya. The sequence stratigraphic framework presented here builds on the rock-based stratigraphic framework, using carbon stable isotope chemostratigraphy and available biostratigraphic data. Over the past several decades, carbonate facies models of ramps (Ahr, 1973; Read, 1985), shelves (Read, 1985) and craton settings (Irwin, 1965; Shaw, 1964) were regularly used for describing and interpreting lateral facies relationships in ancient carbonate platforms.
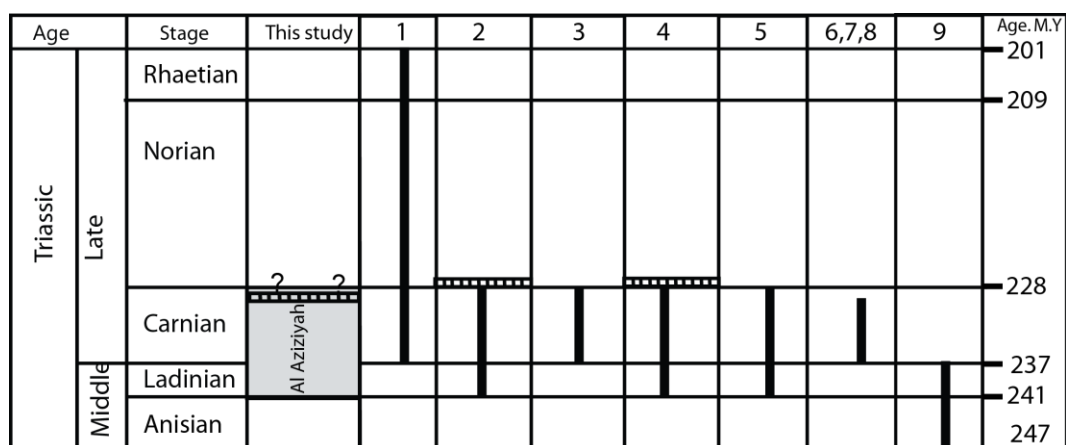
Fig. 2.3. Overview of the previous depositional age interpretation for the Al Aziziyah Formation. Columns 1-9 show different studies that indicate that the age of the Al Aziziyah Formation is disputed. (1- Swire and Gashgeshi, 2000; 2- Fatmi 1977; 3- Asserto and Benelli, 1971; 4- Magnier, 1963; 5- Burollet, 1963; 6- Desic et al., 1963; 7- Hinnawy and Cheshitev, 1975; 8- Muttoni et al., 2001; 9- Christie, 1955.). The correlation between the $\delta^{13}C$ curve from the Al Aziziyah Formation and the global proposed $\delta^{13}C$ curve indicates that the age of the unit may range from Ladinian to Carnian (Moustafa et al., 2014)

11

II.1.4 Methods

Eight full and partial outcrop sections of the Al Aziziyah Formation where measured bed-by-bed (Fig. 2.1C). These sections occur along a depositional dip profile of the Jifarah Basin to provide a more accurate cross-sectional view of the depositional geometries and facies distribution across the basin. These measured sections range in thickness from 24 m to 140 m. Rock color, rock type (limestone or dolomite), facies, sedimentary structures, and stacking pattern of facies were described for each measured section. Carbonate rock types were classified using Dunham's (1962) classification. The contact relationships between the Al Aziziyah Formation and the units above and below were described in detail. 300 thin sections were described to supplement and refine facies interpretations. 287 whole-rock samples for carbon and oxygen isotope analyses were collected at ~ 50-cm intervals from the Ghryan Dome and Kaf Bates section for chemostratigraphy (Moustafa et al., 2014). In addition, fourteen whole rock samples were sampled from the Bu Arghop section for carbon and oxygen isotope analyses to enhance the correlation between the sections from south to north.

II.1.5 Facies analysis and depositional processes

Six major facies are recognized in the Al Aziziyah Formation (Moustafa et al., 2012; 2014). Facies of the Al Aziziyah Formation are interpreted from shallowest to deepest as: tidal sandstone, peritidal carbonate, ooid shoal barrier, shallow subtidal carbonate facies, deep subtidal carbonate and basinal black shale and carbonate mud. A brief description and interpretation of the sediment types in all facies are provided below,

12

arranged from shallowest to deepest. A schematic ramp profile shows the idealized distribution of facies across the ramp (Fig. 2.4). Table 2.1 contains more detailed descriptions and interpretations of the Al Aziziyah Formation facies.

II.1.5.1 Tidal sandstone

This facies contains bidirectionally crossbedded red sandstone beds up to 2 meters thick (Fig. 2.5A) composed primarily of well-rounded and sorted medium sand grains. This facies records high-energy siliciclastic deposition by tidal currents (Hammuda et al., 1985) and occurs only at the Ghryan Dome section (Moustafa et al., 2012).

II.1.5.2 Peritidal carbonate

The peritidal carbonate facies consists mostly of light tan to yellowish cryptalgalaminites (Fig. 2.5B, C), microbial laminites and stromatolites. This facies commonly has well–developed mudcracks, evaporite nodules (Fig. 2.5B), and chert nodules after evaporites. This facies locally is dolomitized. Planar cryptalgalaminites are the most abundant sedimentary structures in this facies, and these small microbial domes are abundant in the Ghryan Dome section (Fig. 2.5C). Pellets occasionally are trapped in the microbial laminites. Peritidal environments were restricted to the southernmost sections of Ghryan Dome, Ras Mazal East, Ras Mazal West, Kurrush Dome and Kaf Bates. The abundance of evaporites and mudcracks, and lack of burrowing, suggests that this facies was deposited in a semi-arid to arid climate. This is the shallowest water carbonate facies in the Al Aziziyah Formation.

Table 2.1 Detailed facies description of the Al Aziziyah Formation

Facies type (Lithofacies)	Description	Sedimentary structures	Biota	Depositional environment
Sandstone	Red to yellow fine-medium sandstone. A few meters thick. Well rounded quartz grains with silica cement.	Bidirectional cross-bedding	none	Tidal environment; the red color indicates iron oxidization.
Mudstone	Tan to yellowish. A few meters to ten meters thick with evaporite nodules, chert, with planar and domal algae.	Mudcracks, microbial laminations, intraclasts	Bioturbated to laminated beds of algae and stromatolites.	peritidal environment
Pellet packstone/ grainstone	Gray to dark color. Up to five meters in thickness. Pellets packstone to grainstone. Grapestone intraclasts and ooids with radial crystal structure. Primary fabric was originally aragonitic ooid and composite ooid. Pellets are rod-like in longitudinal view, round in transverse section and have relatively large and uniform size.	Massive to mechanically laminated beds	Bioturbation beds, gastropod, brachiopods and unidentified fossil fragments	Ramp crest; barrier or shoal
Pellet, skeletal packstone/wackstone/mudstone	Bedding thickness from one to three meters. Dark gray with different cement types, cherty layers and nodules.	Massive to bioturbated beds	Bioturbated beds, of pellets and skeletal fossils like Brachiopods and Gastropods, and other unidentified fossil fragment	Shallow subtidal environment basinward of shoal.
Calcisiltite/ Wackstone	Thickness from a few meters to six meters. Light to dark, with cherty layers and nodules, few pellets.	Massive to mechanical laminations, hummocky cross stratification and stylolites	Fossils are rare in this facies.	Deeper subtidal facies, more abundant in the northern sections.
Carbonate mudstone, black shale	Light to dark gray. The mudstone facies range in thickness from half to one meter. The black shale is very thin organic-rich sediment.	Massive beds	Few unknown fossils.	Basinal environment only occurs in Bu Arghop and Ras Lafa sections.
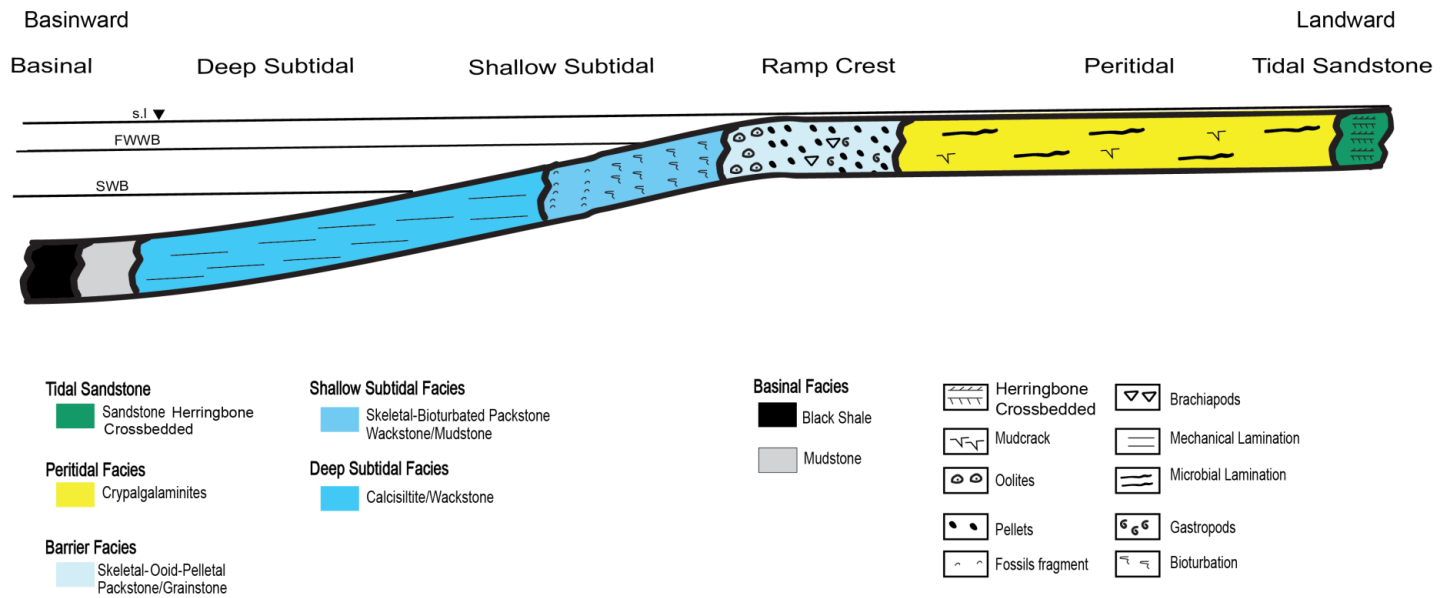
Fig. 2.4. Al Aziziyah Formation depositional profile showing detailed facies distributions. S.1= sea level; FWWB = Fairweather Wave Base; SWB = Storm Wave Base. See table 2.1 for facies descriptions
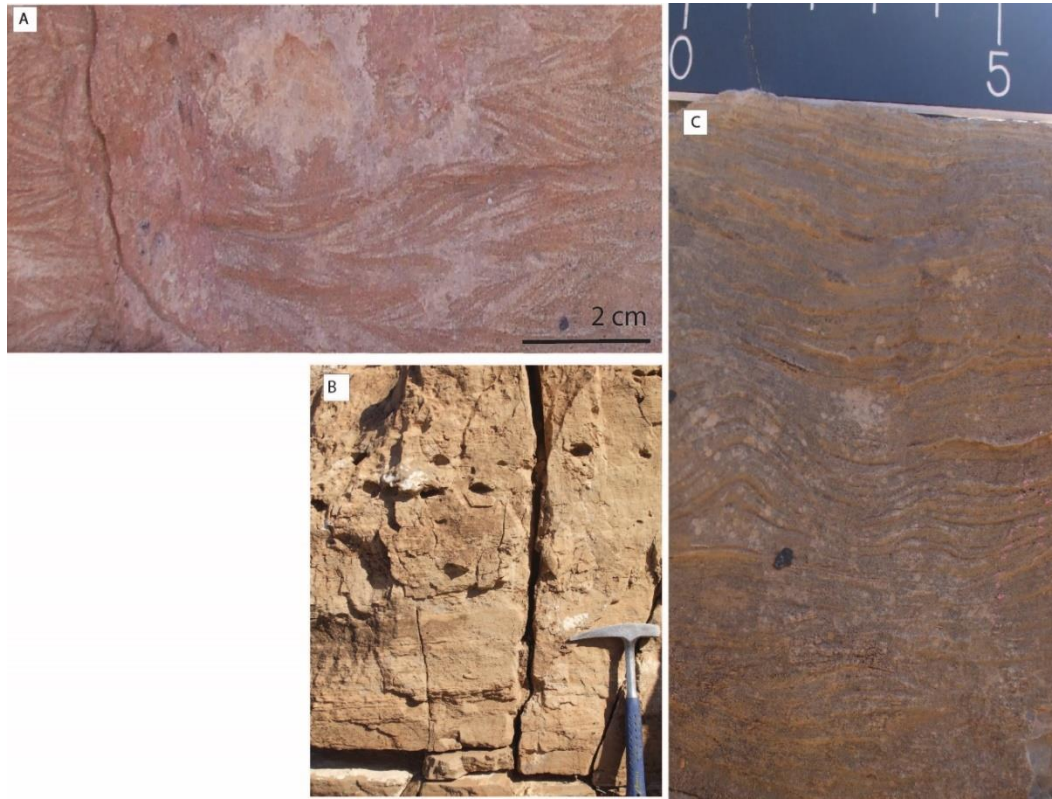
Fig. 2.5. Photography of (A) tidal sand facies showing red bidirectionally crossbedded sandstone. (B) Peritidal facies with evaporite nodules and stromatolites. (C) Peritidal facies with microbial laminations and stromatolites.

II.1.5.3 Ramp crest facies

This ramp crest facies is characterized by ooid-skeletal-pelletal packstone-grainstone locally containing gray to dark gray chert layers (Fig. 2.6A, B). Bed thicknesses in this facies range from less than one meter to almost two meters. The pellets are up to 2 mm, without clear orientation, rod-like in the longitudinal section, circular in the transverse section and are relatively uniform (Fig. 2.6B). The skeletal fragments in this facies are brachiopods, gastropods and small bioclastic fragments. In some sections, these shell fragments are locally mixed with ooids to form grapestone. Some of the oolites have a radial internal structure or are composite ooids, containing more than one ooid grain. The pelletal-ooid packstone/grainstone facies records a high-energy shoal along the ramp crest that separated restricted evaporitic facies to the south from the more open-marine conditions to the north.

II.1.5.4 Shallow subtidal carbonate

The Shallow subtidal carbonate facies consists of thin-medium beds of bioturbated skeletal packstone-wackstone-mudstone in beds up to one meter in thickness (Fig. 7A). Bioturbated, fine-grained, light to dark-gray mudstone and pelletal-skeletal wackstone are the most common lithologies in this unit.
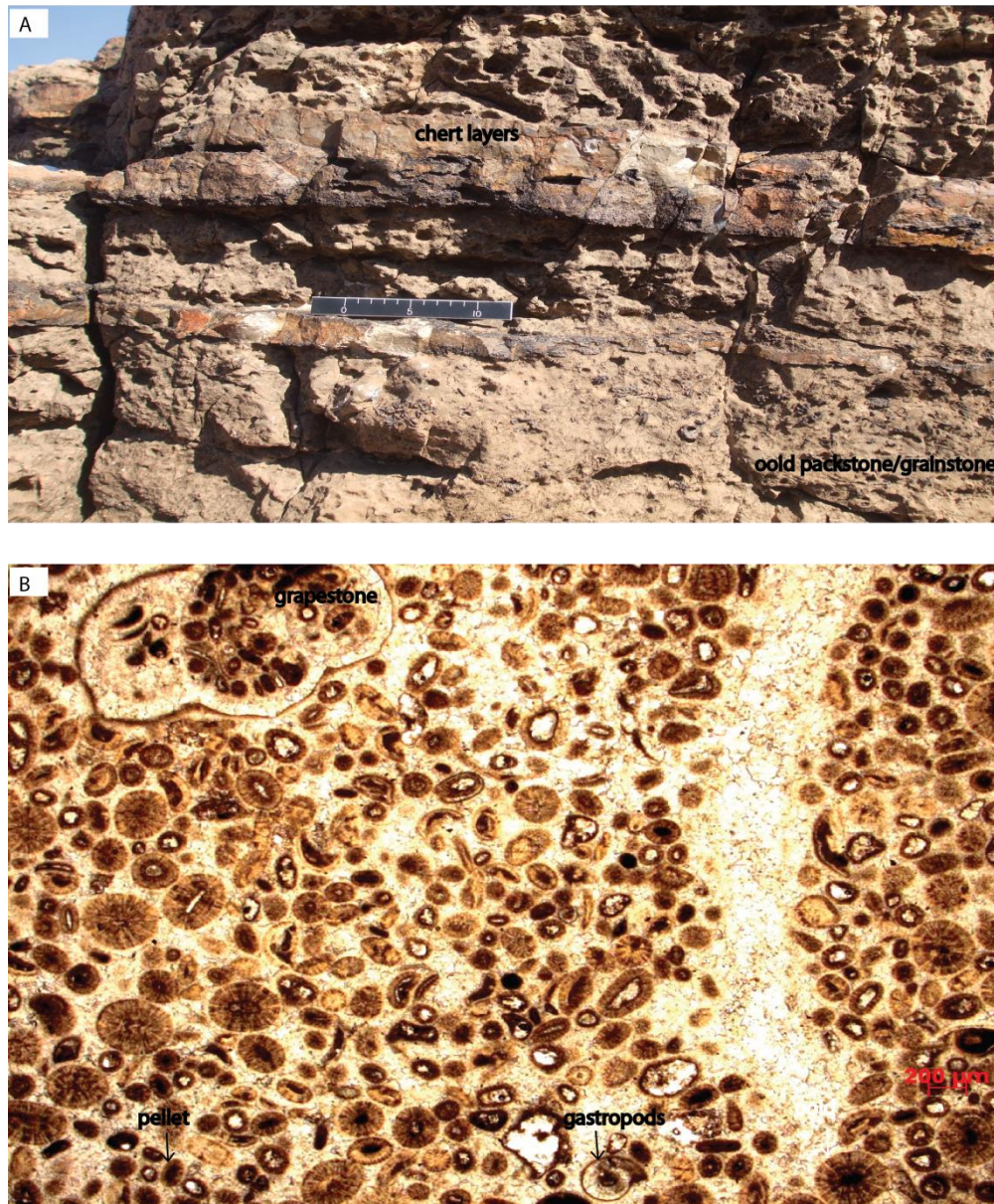
Fig. 2.6. Carbonates barrier facies (A & B). A- Skeletal oolitic-pellet-grainstone with clear ooids, pellets and grapestone. B- Chert layers within the same facies. Note the large thickness of the chert layers.

Bioturbation is grades 1and 4. Grades 1 and 4 refer to low and high levels of bioturbation respectively (Taylor & Goldring 1993), and the few pellets in this facies were likely transported from the ramp crest facies. This facies was deposited in shallow, well-oxygenated waters that promoted abundant bioturbation directly basinward of the ramp crest facies.

II.1.5.5 Deep subtidal facies

The deep subtidal facies is composed of medium-thick beds (up to four meters thick) of calcisiltite, with hummocky cross-stratification, mechanical laminations and local chert layers, interbedded with pellet wackstone or lime mudstone (Fig. 2.7B, C). This facies was deposited within storm wave base and records alternating moderate to high–energy storm events interbedded with lower energy muddy background sedimentation.

II.1.5.6 Basinal facies

The basinal facies consists primarily of thin-bedded lime mudstone layers interbedded with extremely thin black organic-rich shale (Figs. 2.7D). The basinal facies occurs only within the northernmost sections (e.g., Bu Arghop and Ras Lafa; Moustafa et al., 2012, 2014) and may substantially thicken toward the offshore portion of the Jifarah Basin (Abohajar et al., 2009).
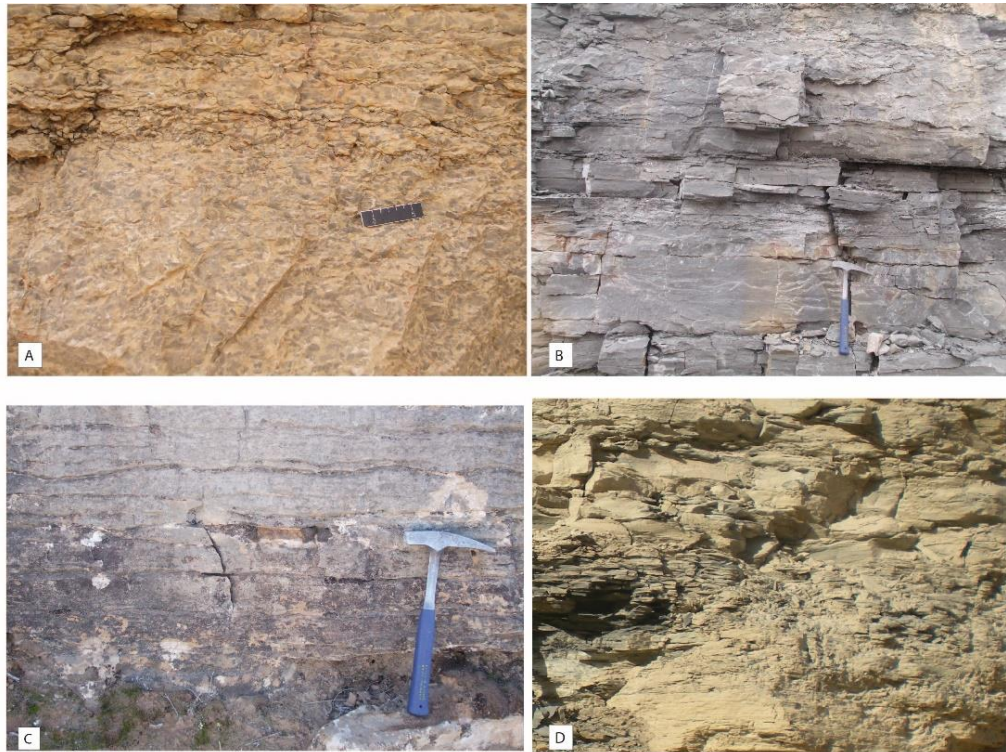
Fig. 2.7. Shallow subtidal facies with high density bioturbation (A); deep subtidal facies with carbonate mud (B); calcisiltite with mechanical laminations (C); and basinal facies with carbonate mud and shale with organic-rich sediment or black shale (D)

II.1.6 Significant surfaces

Subaerial exposure surfaces are absent on the northern part of the Jifarah Basin. The southern part of the basin has major unconformities above and below the Al Aziziyah Formation (Fig. 2.8 A, B, C and D). Major unconformities below the Al Aziziyah Formation occur at the Ghryan Dome, Ras Mazal West, Ras Mazal East, and Kurrush Dome sections. These unconformities are indicated by a decrease in the abundance of sandstone, which represents the transitional contact between the Kurrush and Aziziyah formations. However, the upper unconformity is overlain by the phosphatic bed on the top of the Al Aziziyah Formation and is exposed only at the Ghryan Dome section. Neither the lower or upper unconformities are exposed at the Bu Arghop, Ras Lafa or Al Aziziyah Town sections. In this study, parasequence and sequence boundaries (SB) are a sharp contact with the peritidal facies or barrier facies overlain by subtidal facies. Thus, most sequence boundaries were placed above of shallowing-upward successions, beneath deepening upward units. In this study, the upper contacts are clearly exposed at the Ghryan Dome section and are not exposed at the Kaf Bates section. Flooding surfaces are locally developed on each section of the ramp and are characterized by an abrupt transition from shallow to deep water facies or by condensed intervals of carbonate mud. Flooding surfaces are locally correlative across the study area. Maximum flooding surfaces (MFS) or zones (MFZ) were placed beneath or within the deepest water facies within a sequence.
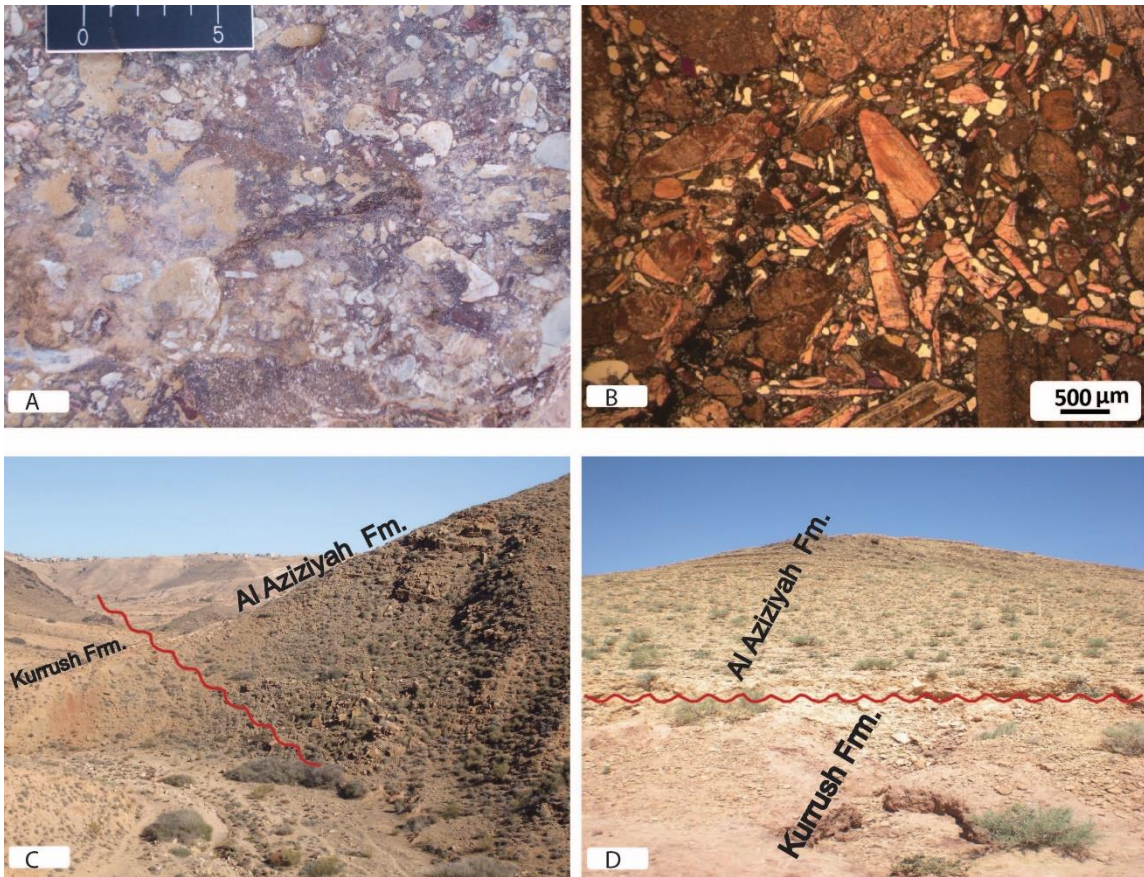
Fig. 2.8. Al Aziziyah Formation's lower boundaries (C and D) and the phosphatic beds, which represent the upper boundary (A and B).

II.1.7 Sequence stratigraphy

Sequences, defined as relatively conformable successions of genetically related strata bounded at their bases and tops by unconformities or their correlative conformities (Vail et al., 1977), were defined using the principles outlined in Sarg (1988), Kerans and Tinker (1997) and Handford and Loucks (1993). The sequence is the fundamental unit of sequence stratigraphy; it is made up of succession of genetically related strata bounded by surfaces of unconformities or their correlative conformities (Mitchum et al., 1977). In general, sequence boundaries (SB) are surfaces marked by a basinward shift of facies and onlap of overlying strata (Van Wagoner et al., 1988). System tracts (e.g. HST and TST) are linkages of contemporaneous depositional systems (Brown and Fisher, 1977) defined on the basis of types of bounding surfaces and their position within a sequence (Van Wagoner et al., 1988). A basic principle of standard sequence stratigraphy holds that sequences and their system tracts are essentially controlled by relative sea level change (Vail et al., 1977; Van Wagoner et al., 1988).

The tectonic model, facies, sequence, and bounding surface between parasequence and sequences are shown in the detailed cross-sections (Figs. 2.9 and 2.10). Parasequences (Fig. 2.11) occur in all sections but they are very difficult to correlate laterally due to unconformities. The global correlation of the sequence stratigraphy of the type section with the global carbon isotope and sea level curves is shown in Figure 2.10. Brief descriptions of the sequences are in Tables 2.2 and 2.3.
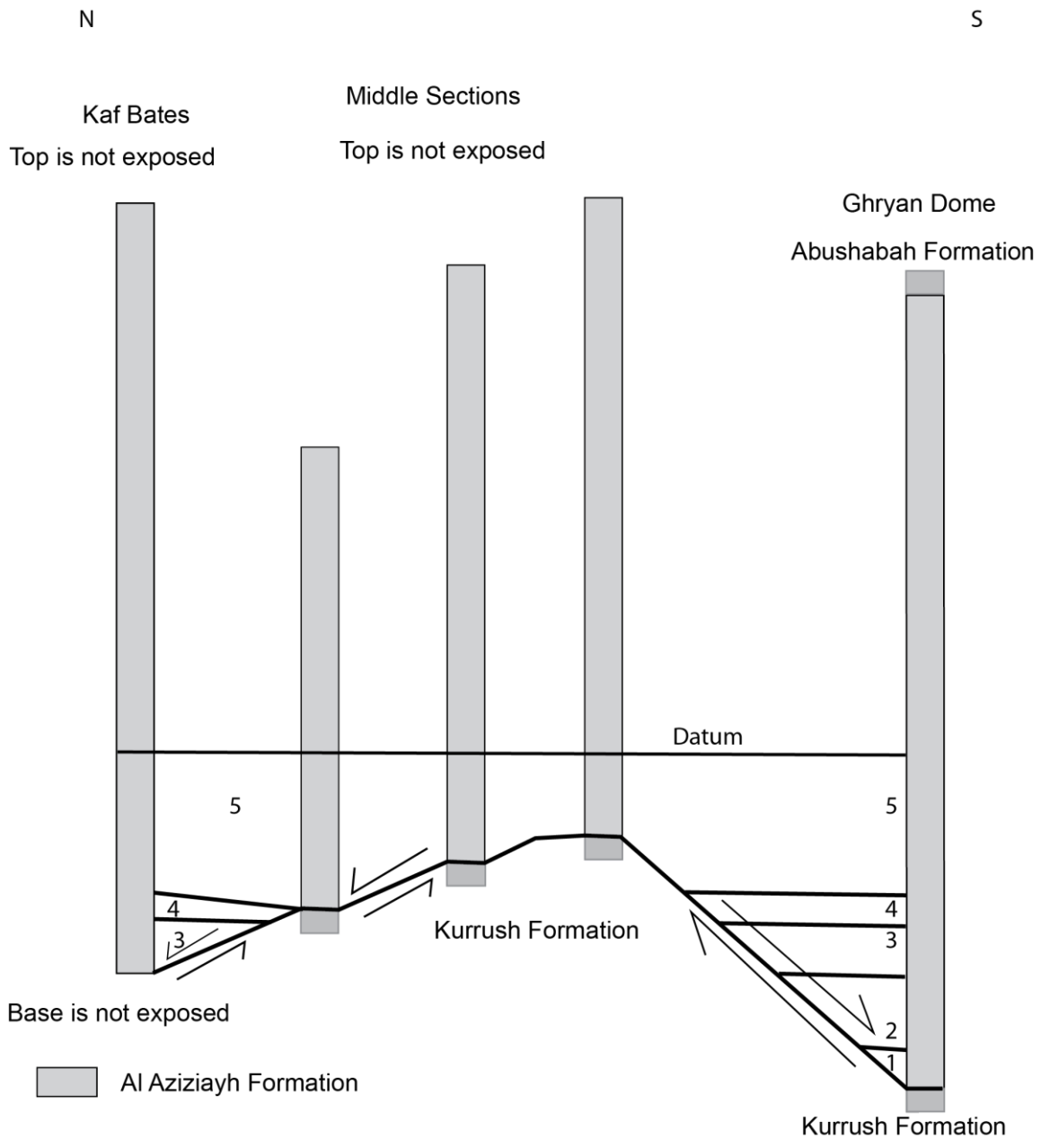
Fig. 2.9. Sketch diagram showing possible tectonic model that affect the Al Aziziyah formation on the study area (not to scale).

Sequences 1 (S1) and 2 (S2) are only exposed at the Ghryan Dome section. Sequence 1 (S1) consists of peritidal and barrier facies with sunstone of lower unit. This mixed sandstone and carbonate represents the lower, transitional contact between the Al Aziziyah and Kurrush formations (Fig. 2.8C and D). Parasequences in this sequence are peritidal capped (Fig. 2.11A). S1 consists predominantly of skeletal pelletal packstone and grainstone beds that shallow-upward to thin microbial mudstone units. The TST of sequence 1 is approximately 5 m thick and consists of an upward-deepening succession of skeletal packstone and grainstone above mixed sandstone and carbonate. The MFS or MFZ of sequence 1 is picked at the base of skeletal packstone, its deepest water facies. The HST is approximately 10 meters of shallowing upward succession of barrier and peritidal facies.

Sequence 2 (S2) is approximately 20 m thick and consists of peritidal, barrier shallow subtidal and deep subtidal facies with multiple thick covered intervals and shallowing upward parasequences (Fig. 2.11A, B and C). The lower boundary of this sequence is sharp contact at the base of peritidal facies. The TST is less than 15 m thick of bioturbated mudstone and wackstone beds. The MFS was placed within the deep subtidal facies. The HST is approximately 5 m and consists of calcisiltite, bioturbated mudstone shallowing upward into peritidal facies.

Sequence 3 (S3) represents the first depositional sequence exposed at the Kaf Bates and consists of approximately 15 m of peritidal, barrier, shallow subtidal and deep subtidal facies with multiple thin covered intervals. This sequence has a basal deepening
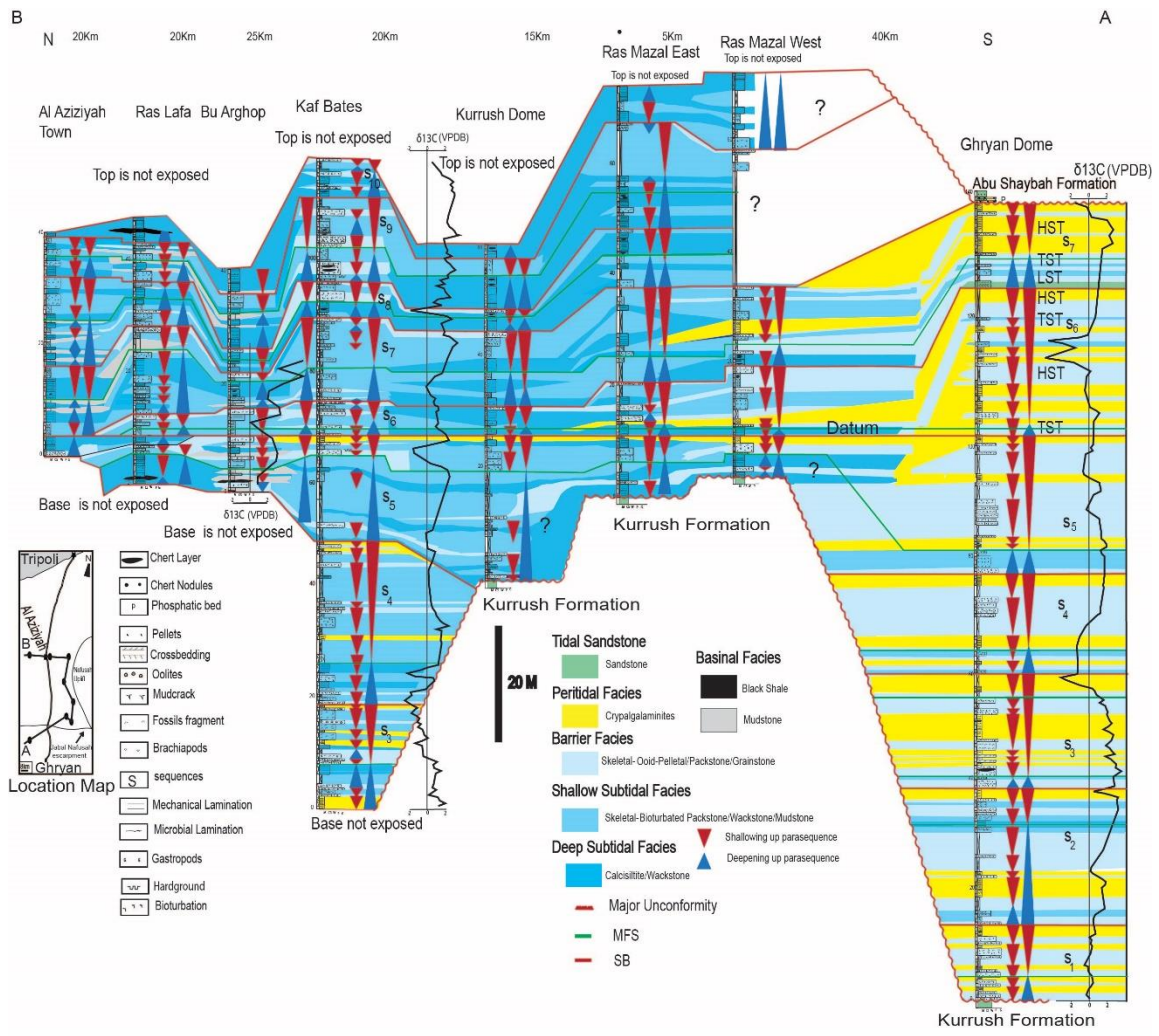
Fig. 2.10. South-north sequence stratigraphy cross section with carbon isotope curves showing the correlation between measured sections based facies stacking pattern and carbon isotope values.

upward parasequence overlain by shallowing upward peritidal parasequences at the Ghryan Dome section and shallowing upward peritidal and ramp crest parasequences at the Kaf Bates section. The TST at the Ghryan Dome section is less than 5 m thick of bioturbated mudstone and wackstone. The MFS was picked at the base of bioturbated mudstone facies at the Ghryan Dome section. However, at the Kaf Bates section, the MFS was picked on the top of the calcisiltite, which here represents the deepest water facies. The HST is approximately 10 to 15 m thick and consists predominantly of shallowing upward units of ooid/pellet barrier and peritidal facies.

Sequence 4 (S4) consists of ~15 m thick of peritidal, barrier, shallow subtidal and deep subtidal facies with multiple thin and thick covered intervals at the Ghryan Dome section and ~20 meters at the Kaf Bates section. Most of the parasequences in this sequence are peritidal capped and ramp crest capped (Fig. 2.11 A and B). The lower boundary of this sequence is sharp contact at the base of peritidal facies. The TST is approximately 5 m thick and consists of an upward deepening unit. The MFS was placed at the top of bioturbated mudstone facies in both sections. The HST is approximately 10 to 15 m thick of shallowing upward successions of barrier and peritidal facies. The Kaf Bates section has higher thickness of HST and thinner facies than the Ghryan Dome section.

Sequence 5 (S5) is the first sequence that correlates across the area from south to north, and its thickness varies from approximately 25 m at the Ghryan Dome and Kurrush Dome sections to ~ 5-20 m at most northern sections. The lower boundary of this sequence is a sharp change from peritidal to barrier facies at the Ghryan and Kaf Bates

27

sections, a transitional contact with the lower unit (Kurrush Formation) at the middle sections. This sequence is the lowest depositional sequence and its base is not exposed at the northern sections. The parasequences in this sequence are peritidal capped; ramp crest capped, shallow and deep subtidal capped (Fig. 2.11A, B, C and D). The TST ranges from 5-15 m thick of pelletal-packstone deepening-upward to bioturbated mudstone beds at the Ghryan Dome and Kaf Bates sections. At the middle sections, the TST deepens upward to bioturbated mudstone and calcisiltite. The MFS was picked at the top of the deepest water facies. The HST is ~5-20 m thick of shallowing upward successions of shallow subtidal, barrier and peritidal facies

Sequence 6 (S6) consists of ~ 5-15 m thick of peritidal, barrier, shallow subtidal and deep subtidal facies with multiple thin and thick covered intervals. S6 is not exposed at the Al Aziziyah Town section.

Table 2.2A Brief sequence description (S_1 to S_5) of the Al Aziziyah Formation.

	S_1	S_2	S_3	S_4	S_5
Occurrence and distribution	Only at the Ghryan Dome section with barrier and peritidal facies	S_2 deposited on S_1 and occurs only at the Ghryan Dome section with more facies than S_1	S_3 deposited on S_2 and occurs at the Ghryan Dome and Kaf Bates sections. It has more peritidal facies at the Ghryan Dome section than at the Kaf Bates section	S_4 deposited on S_3 and occurs at the Ghryan Dome and Kaf Bates sections	S_5 deposited on S_4 at the Ghryan Dome and Kaf Bates sections. S_5 deposited on major unconformity between the Kurrush and Al Aziziyah formations at the middle sections. S_5 is the lowest depositional sequence at the three northern most sections and can be mapped through sections.
Thickness	Approximately 15 m	Approximately 20 m	S_3 about 15 m	Approximately 15 m at Ghryan Dome and 20 m at Kaf Bates	Ranges from 25 m at the Ghryan Dome and Kurrush Dome sections; other sections range from 5-20 m.
Basal sequence boundary	The basal sequence boundary is a transitional contact with the underlying unit (Kurrush Formation).	The basal sequence boundary is the correlative conformity of abrupt change in facies from crypgalaminites (peritidal facies) to skeletal packstone (barrier facies)	The basal sequence boundary is a correlative conformity rapid change in facies from peritidal to barrier at the Ghryan Dome section. At the Kaf Bates section, S_3 is the lower sequence exposed	The basal sequence boundary is the correlative conformity of rapid and sharp change in facies from peritidal facies to skeletal wackstone of shallow subtidal facies	The basal sequence boundary is the correlative conformity of abrupt change in facies from peritidal to barrier at the Ghryan and Kaf Bats sections. At other locations, S_5 is the lower sequence and it has a transition contact with the lower unit (Kurrush Formation) at the middle section and its base is not exposed at the three northern sections

Table 2.2B

Brief sequences description of TST, MFS and HST (S_1 to S_5) of the Al Aziziyah Formation.

	S_1	S_2	S_3	S_4	S_5
TST	The TST is approximately 5 m thick of an upward deepening succession of skeletal packstone and grainstone.	The TST is less than 5 m thick of bioturbated mudstone and wackstone.	The TST is less than 5 m thick of bioturbated mudstone and wackstone.	The TST is approximately 5m thick of an upward deepening of bioturbated mudstone and calcisiltite.	The TST is 5 to 15 m thick of an upward deepening unit. It consists of ramp crest and deep subtidal facies toward the north.
MFS	The MFS was picked at the basal of skeletal packstone, which is the deepest sediment at this sequence.	The MFS was placed within deepest water facies of deep subtidal facies	The MFS was placed at the base of bioturbated mudstone facies at the Ghryan Dome section and on the top of calcisiltite at the Kaf Bates section.	The MFS was placed at the top of bioturbated mudstone facies at Ghryan Dome and at the top of calcisiltite at the Kaf Bates.	The MFS was placed at the top of bioturbated mudstone facies at the Ghryan dome and on the base of ramp crest facies at the Kaf Bates section.
HST	The HST is approximately 10 m of shallowing upward units of ramp crest and peritidal facies.	The HST is approximately 5 m of calcisiltite, bioturbated mudstone, ramp crest and shallowing upward of peritidal facies.	The HST is approximately 10 to 15 m thick of shallowing upward units of barrier and peritidal facies.	Approximately 10 to 15 m thick of shallowing upward ramp crest and peritidal facies. The Kaf Bates section has a thicker HST than the Ghryan Dome section	Approximately 20 m thick succession of shallowing upward ramp crest and peritidal facies.

The lower boundary of this sequence is sharp contact at the base of peritidal facies in all sections except the Bu Arghop, and Ras Lafa sections, where this lower boundary is bioturbated mudstone beds. Parasequences in this sequence are peritidal capped, ramp crest capped and shallow and deep subtidal capped (Fig. 2.11A, B, C and D). The TST is a thin unit of bioturbated mudstone and calcisiltite. The MFS is placed within deeper water facies in each section. The HST is approximately 20 m thick, skeletal packstone that shallowing upward to peritidal mudstone at the Ghryan Dome section. In the northern sections, the HST is 5-10 m of bioturbated mudstone that shallow upward to ooid-skeletal packstone.

Sequence 7 (S7) is ~ 5-20 m thick and it is the last depositional sequence at the Ghryan Dome section. It is bounded at Ghryan Dome section by the major top-Al Azizyah unconformity, and it is capped by barrier and shallow subtidal facies in the other sections. The base of this sequence ranges from shallow marine sandstone facies at the Ghryan Dome section to ooid-pelletal packstone/grainstone ramp crest facies at other sections. This sequence consists of sandstone at the Ghryan Dome with multiple thick covered intervals and microbial mudstone, pelletal packstone, bioturbated mudstone, carbonate mudstone, and black shale. This sequence has multiple thin covered intervals at other sections. The parasequences in this sequence are peritidal capped, ramp crest capped and shallow and deep subtidal capped (Fig. 2.11A, B, C and D). The TST of S7 is about 5-10 meters thick of skeletal bioturbated wackestone with thin covered intervals at the Ghryan Dome and Kaf Bates sections. However, TST of S7 is a thin unit of bioturbated mudstone and black shale north of Ghryan Dome. The MFS on the Ghryan

31

Dome and Kaf Bates sections was picked at a thin skeletal bioturbated wackstone within a thin covered interval; in the other sections, the MFZ was picked within major flooding unit of bioturbated mudstone, black shale, and calcisiltite. The HST is approximately 10 to 15 meters of skeletal packstone that shallowing upwards with microbial mudstone at the Ghryan Dome and Ras Mazal west sections. In the northern sections, the HST is 5-10 m of bioturbated mudstone shallowing upward to ooid-skeletal packstone.

Sequences 8 (S8), 9 (S9) and 10 (S10) were not deposited at the Ghryan Dome section. Sequence 8 is ~5-10 meters across all sections. The base of this sequence ranges from ooid-pelletal packstone/grainstone to bioturbated mudstone facies across sections. The parasequences are ramp crest capped, shallow and deep subtidal capped (Fig. 2.11B, C and D). The TST occurs within a thin unit of bioturbated mudstone, calcisiltite and carbonate mudstone. The MFS is picked within major flooding unit of bioturbated mudstone, calcisiltite and carbonate mud. The HST is 5-10 m of bioturbated mudstone that shallows upward to ooid-skeletal packstone.

Sequence 9 (S_9) is 5 to 10 meters thick and it has ramp crest capped and shallow subtidal capped parasequences. The base of this sequence ranges from ooid-pelletal packstone/grainstone to bioturbated mudstone across all sections. This sequence consists of pelletal packstone, bioturbated mudstone and carbonate mud. Parasequence of this sequence are ramp crest capped, or shallow and deep subtidal carbonate capped (Fig. 2.11B, C and D). The TST is approximately 5 meter of bioturbated mudstone, calcisiltite, and carbonate mudstone. However, the MFz is picked within the deepest

water facies. The HST is 5-10 m of bioturbated mudstone and calcisiltite that shallows upward to ooid-skeletal packstone and bioturbated mudstone.

Sequence 10 (S10) is the youngest depositional sequence and is 2-10 meters thick with shallow to deep subtidal facies. The basal sequence boundary is correlative conformity recording an abrupt facies shift from shallow to deep facies. This sequence consists of pelletal packstone, bioturbated mudstone, carbonate mud and black shale with few shallowing upward ramp crest and deep subtidal parasequences (Fig. 2.11B, and D). The TST is ~ 5-15 meters thick of deepening upward subtidal parasequences. The MFS is difficult to pick in this sequence, however, the TST zone represents the MFS and it is different from section to section (approximately 2-10 meters). The HST of this sequence is unclear.

Table 2.3A

Brief sequence description (S6 to S10) of the Al Aziziyah Formation.

	S_6	S_7	S_8	S_9	S_{10}
Occurrences and distributios	S_6 was deposited on S5. S6 can be mapped through all sections except Al Aziziyah Town section. S_6 thins toward the north.	S_7 was deposited on S_6 and it is the last depositional sequence at the Ghryan Dome section, where it ends with a major unconformity.	S_8 was deposited on S_7 and is mapped throughout all sections. S_8 wasn't deposited at the Ghryan Dome section.	S_9 was deposited on S_8 and is mapped throughout all sections except Ghryan Dome.	S_{10} was deposited on S_9 and is mapped throughout all sections except the Ghryan Dome section. S_{10} thins toward the north.
Thickness	About 15 m at the Ghryan Dome section, thins to 5 m.	S_7 ranges from 5-20 m and it is mapped throughout all sections.	about 5 to 10 m toward the northern sections.	5-10 m and thinner at the Ras Mazal sections.	About 2-10 m, S10 is very thin and incomplete Sequence.
Basal sequence boundary	The basal sequence boundary (cross-section) is the correlative conformity of abrupt change in facies from peritidal to deeper facies at all sections except in northern sections, where their base is bioturbated mudstone.	The basal sequence boundary is the major unconformity indicated by sandstone at the Ghryan Dome section. North of Ghryan Dome, the base of S7 is a correlative conformity of a change in facies from shallow to deep facies.	The basal sequence boundary is correlative conformity of a change in facies from shallow to deep facies characterized with high carbon isotope values at Kaf Bates and Bu Arghop sections.	S9 is correlative conformity of a change in facies from shallow to deep facies characterized with high carbon isotope values at Kaf section, in the base of this sequence.	The basal sequence boundary is correlative conformity recording a facies shift from shallow to deep facies with high carbon isotope values at the Kaf Bates section.

Table 2.3B

Brief sequence description of TST, MFS and HST (S6 to S10) of the Al Aziziyah Formation.

	S_6	S_7	S_8	S_9	S_{10}
TST	The TST is thin with constant thickness in all sections except the Al Aziziyah Town where this sequence does not occur.	The TST in this sequence is approximately 5 to 10 m	The TST in this sequence decreases in thickness (from about 5 to less than 5 m) from southern to northern sections	The TST is approximately 5 m thick of bioturbated mudstone and wackstone and carbonate mud toward the north	The TST is approximately 5 to 15 m thick of deepening upward sediment.
MFS	The MFS is thin and placed within a cover interval, which assumed to be deepest facies in this sequence based on isotope date above and below the cover interval. MFS is picked at deep water facies in other sections.	The MFS was placed within a cover interval between skeletal wackstone and skeletal grainstone. MFS is characterized by high carbon isotope values right above the cover interval.	The MFS was placed within bioturbated mudstone, calcisiltite or carbonate mudstone on the sections.	The MFS was placed within the calcisiltite and bioturbated mudstone on the southern part and on the northern part it was pleased within the carbonate mudstone and calcisiltite cover interval between skeletal wackstone to grainstone.	The MFS difficult to pick in this incomplete sequence. However, the deep facies within the TST zone represent the MFS and it is different from section to section Approximately 2-10 m. S_{10} is very thin and incomplete Sequence.
HST	~5 to 20 m thick of shallowing upward facies, including crypalgalaminites and skeletal packstone facies at the Ghryan Dome section and becomes thin with thin skeletal packstone facies at other sections	10 to 15 m thick of shallow upward facies of ramp crest and peritidal facies. Toward the north, HST consists mainly a skeletal packstone/grainstone of ramp crest.	5 to 10 m thick of shallowing upward successions of skeletal packstone and oolitic packstone/grainstone.	Ranges from 5 to 10 m thick of shallowing upward to ramp crest facies.	S_{10} is incomplete sequence with mostly TST and no clear HST

II.1.8 Parasequences

Parasequences (meter-scale cycles) represent the smallest units of genetically related lithofacies assemblage within sequence, and they commonly are bounded by local flooding surfaces (Arnott, 1995; Embry, 2005). Parasequences in the Al Aziziyah Formation (Fig. 2.11) range in thickness from less than 5 meters in peritidal facies to tens of meters in deep ramp facies. The thickness, geometry, lateral extent and lithology of parasequences vary across depositional settings on the ramp. Representative meter-scale cycles are arranged in order of decreasing water depth (Fig. 2.11). Boundaries of parasequences in the succession were defined using the flooding surface at the tops of upward-shallowing successions. More than 40 parasequences are delineated at the Ghryan Dome section, but no single parasequence is traceable throughout the cross-section of the Al Aziziyah Formation (Fig. 2.10). In general, most parasequences shallow upward. However, a few parasequences deepen upwards.

Peritidal-based parasequence (Fig. 2.11A) are between 5 and 15 meters thick, and they occur in most of the Ghryan Dome section and the lower part of the middle and Kaf Bates sections. These parasequences commonly are composed of skeletal packstone/grainstone shallowing upward into peritidal facies.

Ramp crest-based parasequences (Fig. 2.11B) are 5 to 10 meters thick. They are composed of shallow subtidal facies capped by ramp crest facies. They occur in most sections across the ramp.

Shallow subtidal parasequences (Fig. 2.11C) are composed of calcisiltite shallowing upwards into bioturbated wackstone facies. The thicknesses of these parasequences vary across the ramp and range from 5 to 10 meters. These parasequences dominated most northern sections.

Deep subtidal parasequences (Fig. 2.11D) are composed of calcisiltite shallowing upward into bioturbated mudstone. The thicknesses of these parasequences range from about 5 to less than 10 meters and they occur in most of the Bu Arghop, Ras Lafa and Al Aziziyah sections.
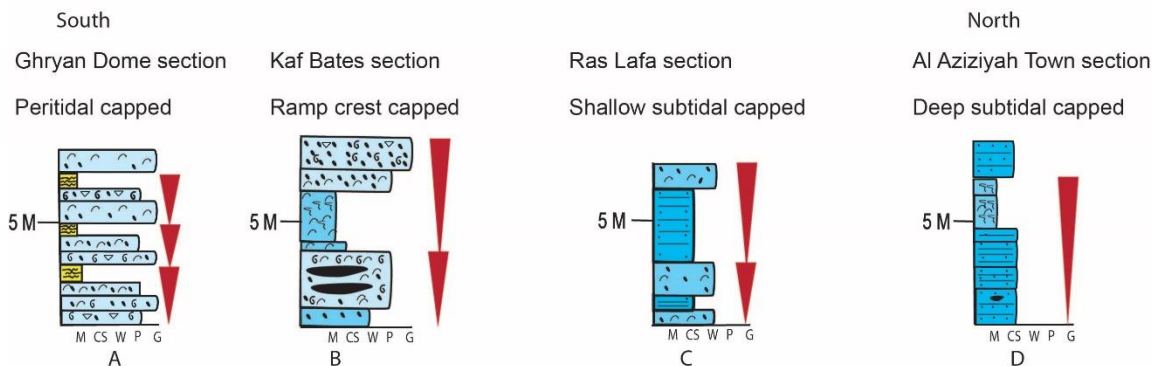
Fig. 2.11. Representative parasequences A-D (individual parasequences indicated by inverted red triangles) illustrate facies stacking geometries according to their position on the ramp. A) Peritidal capped; B) Ramp crest capped; C) Shallow subtidal capped; D) Deep subtidal capped. See 2.10 and table 2.1 for facies descriptions and interpretation.

II.1.9 Discussion

II.1.9.1 Tectonic

The Mesozoic basin-fill of the Jifarah Basin was affected by syn-depositional faulting during the Triassic, and subsidence of the Jifarah Basin continued into the Early and Middle Triassic, indicating the Al Aziziyah Formation, was deposited during a period of active tectonics (Fig. 2.9, Gray, 1971; Anketell and Ghellali, 1991, Muttoni et al., 2001). Ghryan Dome and Kaf Bates sections are much thicker than the middle and northern sections. Thickness variations across the ramp are most likely due to syn-rift events during deposition of the Al Aziziyah Formation, similar to equal events in the western part of the Jifarah Basin, southern Tunisia (Raulin et al., 2011). Furthermore, there are several domal structures around the Ghryan area (e.g., the Ghryan Dome at the southern part of the basin; Gray 1971). In addition, the top of the Al Aziziyah Formation indicates a gentle anticlinal swell (Zivanovic, 1976). Few unpublished studies indicate that, there are also several domal structural at the southeast part of the basin (e.g., Kurrush Dome and Ras Mazal Dome). These domal structures seen around Ghryan today (Gray, 1971), although clearly related to Tertiary volcanism, also show facies and thickness variations patterns indicating that their initiation, together with faulting near Wadi Ghan (Wadi Ghan fault zone, Fig. 1B), was associated with early movement along Al Aziziyah fault zone (Fig. 2.1B; Anketell and Ghellali, 1991). These domal structures likely exposed the Kurrush Formation at the Ghryan area and northeastern part of the Ghryan Dome section (middle sections; Gray 1971). Therefore, deposition of the Al Aziziyah Formation was likely affected by syn-rift, faulting, folding, and domal events causing wide variations in

sedimentary infill across the ramp similar to coeval units in southern Tunisia (Raulin et al., 2011).

II.1.9.2 Al Aziziyah depositional environments

The Al Aziziyah Formation has six facies (Fig. 2.4), from land to the basin the facies are: tidal sandstone, peritidal carbonate, shoal or ramp crest, shallow subtidal and deep subtidal, and basinal. The main Lithofacies are 1) Herringbone cross bedded sandstone, deposited in a tidal setting, 2) cryalgalaminates and carbonate mudstone deposited in peritidal setting, 3) skeletal-ooid-pellet packstone/grainstone that formed a low barrier on the ramp, 4) bioturbated-skeletal wackstone/mudstone deposited in a shallow subtidal setting, 5) hummocky bedded calcisiltite deposited within a deep subtidal setting within storm wave base, and 6) carbonate mud with organic-rich black shale which formed in a basinal setting. The facies in the Al Aziziyah Formation indicate these rocks were deposited on a gently sloping ramp carbonate (e.g., Ahr, 1973; Read, 1980). The Al Aziziyah Formation depositional profile was a very low angle ramp with thin shoal facies and no lagoon facies. Sandstone and carbonate tidal flats passed basinward into a pelletal-oolitic shoal at the ramp crest and then into shallow and deep subtidal facies without a significant break in slope. Most of this ramp is shallow to deep subtidal facies, with the tidal flats restricted to southern exposures. The tidal sandstone facies only formed during pronounced sea level falls. The absence of lagoon facies landward of the ramp crest facies suggests thin ramp crest facies did not produce enough accommodation for thick lagoons to form or formed directly adjustment to shoals. The oolitic nuclei of the ramp crest facies commonly are skeletal fragments or pellets. The radial crystal

structure of the ooids indicates that the ooids likely originally formed as aragonite (Davies et al., 1978; Lehrmann et al., 2012). All of these facies, except the basinal facies, occur in the Ghryan Dome section. Peritidal carbonate facies are abundant at the Ghryan Dome section but are rare north of the Ghryan Dome section. The further north peritidal facies disappear altogether, and the subtidal ramp and basinal facies become more abundant.

II.1.9.3 Carbonate factory and source of carbonate mud

High concentrations of nutrients promote macro-algal and micro-algal growth, reducing water transparency and limiting the growth of carbonate produced such as corals and calcareous algae (Hallock and Schlager, 1986), it has been suggested that carbonate platforms flourish in oligotrophic environments. The absence of sufficient quantities of possible calcium carbonate-producing organisms on the platform surface of the Al Aziziyah Formation, and more non-skeletal fossils such as pellets, ooid and carbonate muds, similar to modern Bahamas (Traverse and Ginsburg, 1966) can indicate oligotrophic environments. However, the Al Aziziyah Formation can be biotically controlled precipitates dominate (tropical type factory, Schlager, 2003), because few photo-autotrophic organisms such as algae, brachiopods are available. The source of the carbonate mud in the Al Aziziyah Formation can be from the atmospheric dust as suggested to the Great Bahama Bank (Swart et al., 2014). Cyanobacteria are responsible for providing nitrogen from the atmosphere dust to the nutrient-poor environment. Providing nitrogen will cause CO_2 to drawdown for beginning the precipitation of

carbonate in the shallow water (Swart et al., 2014). The muds are ingested by worms, generating pellets that harden and eventually form the central portions of ooids.

II.1.9.4 Al Aziziyah composite sequence duration

The Al Aziziyah Formation was deposited during the Ladinian-Carnian with a duration of ~13 m.y. (Gradstein et al., 2012) making it a 2nd-order sequence (Sarg et al., 1999). The (7-10 sequences) Al Aziziyah Formation are each about 1-2 m.y making them 3th–order sequences. In greenhouse times, cycles are likely dominated by high-frequency, low amplitude sea level changes driven by precession (Read, 1995, 1999). Therefore, one would expect to find many more parasequences in the 13 m.y. Al Aziziyah composite sequence due to unconformities. The duration of parasequences in the Al Aziziyah Formation is difficult to evaluate, as they rarely are regionally mapable. The maximum number of parasequences (41) occurs in the Ghryan Dome type section. However, since sequences 8-10 are not exposed here, there are likely at least 50 parasequences in the Al Aziziyah Formation. Given the 13 m.y. duration of the type section, this would suggest that the parasequences are ~260 k.y. This likely the Al Aziziyah Formation contains many missing "beats" due to unconformities (Balog et al., 1997).

II.1.9.5 Climate and paleogeography

The global Triassic climate was a warm greenhouse world (Dickins, 1993), characterized by non-zonal atmosphere patterns, effected by a strong global monsoon system with effects that are most evident in the Tethys realm (Preto et al., 2010). Monsoon is a

climate system in which most of the rainfall is during the summer (Parrish, 1993). The important feature of monsoonal circulation is cross equatorial flow, which results from the thermal and pressure contrasts between the winter and summer hemispheres, and is driven mainly by sensible heat (Parrish, 1993). Monsoonal climate can leave a record in coeval facies. Regional facies comparisons should show that humidity in the equatorial regions of the east (western Tethys) was lower than in the west (e.g., Colorado plateau; Dubiel et al. 1991). Additionally, sedimentary records should reflect a reversal of equatorial flow during maximum intensification of monsoonal circulation in the Late Triassic (Mutti, & Weissert, 1995).

During the Middle and Late Triassic, the climate in the area of study was arid as indicated by the abundance of an evaporite zone stretching from North Africa to northern Scandinavia (Dickins, 1993). The Al Aziziyah Formation contains an abundance of mudcracks, and silicified evaporite nodules in its peritidal facies, also suggesting an arid climate (e.g., Golonka, 2000; Preto et al., 2010) during its deposition. As the Neotethys opened, the sea approached the western shoulder of Gondwana (western Africa) diachronously, land was submerged and the Al Aziziyah Formation was deposited during the Middle-Late Triassic (Fig. 2.2). In addition, the Neotethys shoreline trended northwest to southeast and was inundated by a series of transgressions and regressions during Mesozoic times. A wide spread marine transgression occurred during Landinian, followed by two more extensive sea level rise during the Carnian. However, during the Carnian, the Neotethyan Sea restricted gradually and Carnian ocean circulation was restricted in the western and central parts of the Jifarah Basin, possibly

due to uplift along the marginal trough on the western part of the basin (Fig. 2.2, Demaison, 1965; Cornell and Tekbali, 1993; Hallet, 2002). Therefore, evaporitic deposition predominated in Algeria and Tunisia (Sloss, 1953; Demaison, 1965; Bishop, 1975), whereas terrigenous material, sandy limestone, and dolomites of the (Ladinian-Carnian) Al Aziziyah Formation accumulated in an inner ramp environment (Demaison, 1965; Cornell and Tekbali 1993; Swire and Gashgesh, 2000; Raulin et al., 2011). This climate and environmental setting is reflected in carbon and oxygen isotope data from the Al Aziziyah Formation, which were likely affected by meteoric water charged with light soil CO_2 and excess evaporation as indicated by the abundant evaporites within the peritidal facies (Moustafa et al 2014).

II.1.9.6 Sequence interpretations

Based on field observations, measured sections, thin section petrography, and carbon stable isotope chemostratigraphy, a datum for the regional cross-section (Fig. 10) was placed on the top of peritidal facies on the southernmost five sections at the top of sequence 5. However, at the northern sections, the datum was placed on the bottom of bioturbated lithofacies of shallow subtidal facies associated with gradual increase in carbon isotope values at the Bu Arghop section. The Al Aziziyah Formation sequences were integrated with high-resolution carbon isotopes at the Ghryan Dome and Kaf Bates sections and then correlated within a detailed sequence stratigraphic cross-section from south to north (Fig. 2.10). The sequence stratigraphy correlation between these measured sections focuses on two points: 1) the general facies distribution from south to north; and 2) correlating each sequence to the Ghryan Dome section sequences. The Ghryan Dome

section (type section) has seven sequences, indicated by abundant peritidal facies in the HST of each sequence. However, north of the Ghryan Dome section, sequences and their parasequence stacking patterns are difficult to correlate because the upper and lower contacts of the Al Aziziyah Formation only locally occur and the raise dearth of age diagnostic fossils, marker beds, or abundant subsurface data to correlate strata across the basin. However, suggested structural setting outlined in few studies (Gray 1971; Raulin et al., 2011; Fig. 2.9), facies stacking patterns and positive and negative carbon isotope values from the Ghryan Dome, Kaf Bates and Bu Arghop sections within the south-north cross section of the Al Aziziyah Formation indicate that 1) S3 at the Ghryan Dome and Kaf Bates sections has similar carbon isotope trends. Therefore, the base of S3 also was used as a timeline between the Ghryan Dome and Kaf Bates sections. 2) The middle sections correlate with the upper part of the Ghryan Dome and Kaf Bates sections. Furthermore, the lack of peritidal facies and more positive carbon isotope values in the northern sections indicate that these correlate with the upper part of the Al Aziziyah Formation.

Sequences 1 and 2 are only deposited at the Ghryan Dome section, and sequences 3 and 4 are only exposed at the Ghryan Dome and Kaf Bates sections (Fig. 2.9). S3 is the first sequence at the Kaf Bates sections and is dominated by peritidal and barrier facies at the Ghryan Dome section and by shallow subtidal and barrier facies at the Kaf Bates section. In addition, S3 in both sections is associated with a negative trend in the carbon isotope, and this negative trend was interpreted as a meteoric diagenetic (Moustafa et al., 2014). However, S4 in both sections is associated with a positive trend in carbon isotopes.

44

Sequences 5-7 are correlated from south to north across the ramp with different facies and thickness. The changes in the thickness may be due to differential syn-rift subsidence during the deposition of the Al Azizyah Formation. Sequences 8, 9 and 10 represent shallow to deep subtidal and basinal facies and they are not exposed at the Ghryan Dome section due to major unconformity at the top of sequence 7.

II.1.9.7 Eustatic controls

The relative sea level from the Al Aziziyah type section is linked to the global and local carbon curves and global sea level trends (Fig. 2.12). The global sea level trends in the Triassic are derived from Haq et al. (1987). The local carbon isotope curve also is correlated with the global carbon curve (Fig. 2.12). The carbon isotope values are more negative along many of the sequence boundaries (e.g., see sequence 3 at the Ghryan Dome section; Moustafa et al., 2014). The sea level data reveals a series of short-term fluctuations that are superimposed onto longer-term rising and falling sea level trends. In this study, age control was established using carbon isotope chemostratigraphy (Moustafa et al., 2014, Fig. 2.12). However, the carbon isotope data from this study and the global Triassic ocean suggest that the age of the Al Aziziyah Formation is Middle (Ladinian) to Late (Carnian) Triassic. The long and short terms of relative sea level fluctuations from the Ladinian part of the Al Aziziyah Formation coincides with long and short terms fluctuations of the Ladinian global sea level. Both global and local long terms sea level curves of the Ladinian show gradual rising in sea level. However, during the Carnian global sea level rose during a long-term eustatic rise, where the Al Aziziyah Formation records a gradual long-term relative sea level fall. This negative shift in local

45

relative sea level curve during the Carnian is likely due to restrictions in the Neotethyan Sea and restricted Carnian circulation in the western and central parts of the Jifarah Basin (as discussed earlier).

II.1.9.8 Carbon isotope data and sequence stratigraphy

Carbon stable isotope correlation (Fig. 2.12) indicates that sequences 1 and 2 at the Ghryan Dome section are not exposed at the Kaf Bates section and that sequences 8, 9 and 10 are not exposed at the Ghryan Dome section. Carbon isotope data also indicate that the Al Aziziyah Formation was deposited during the Ladinian–Carnian at its type section. The carbon isotope trends of S3 and S5 at the Ghryan Dome and Kaf Bates sections are used as timeline within the proposed sequence stratigraphic framework. Carbon isotope correlations indicate Ladinian rocks compose only sequences 1 and 2 at the type section (Fig. 2.12). Therefore, the Al Azizyah Formation is Ladinian and Carnian at the Ghryan Dome type section and likely only Carnian north of the Ghryan Dome section.
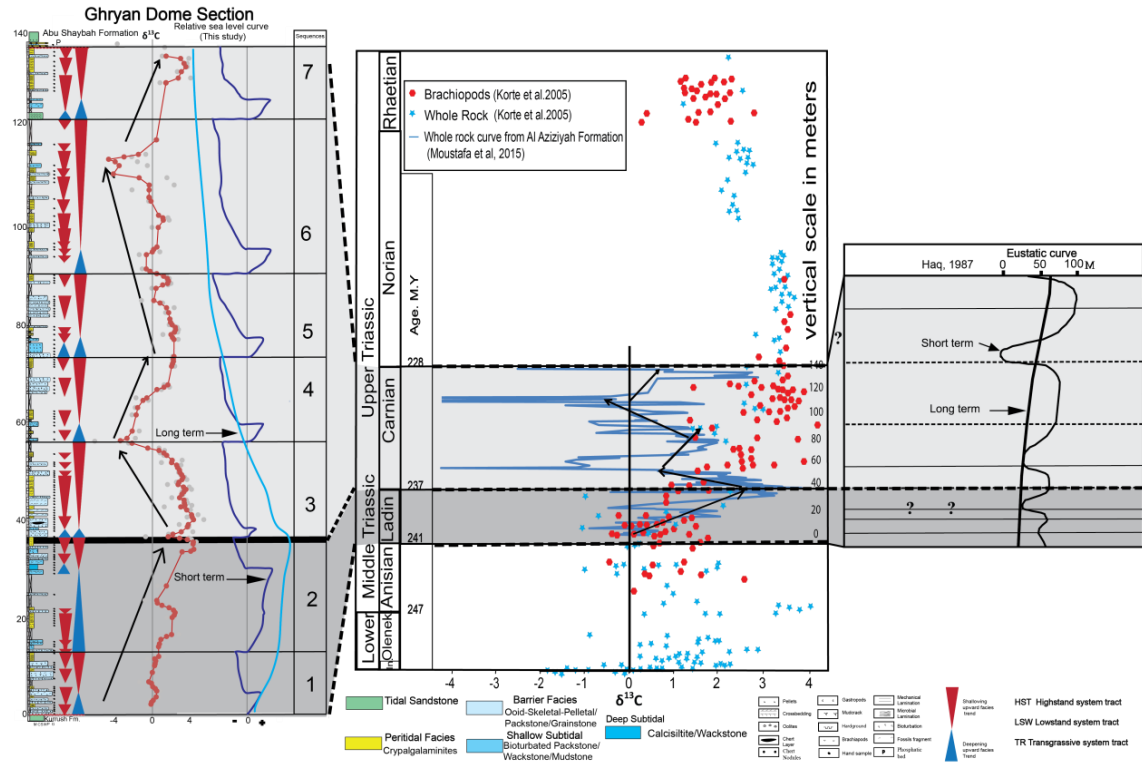
Fig. 2.12. Integrating the Al Aziziyah Formation sequence stratigraphy at the type section with local carbon and oxygen isotope curves. Depletion in both carbon and isotope curves may indicate exposure or sequence boundary (Moustafa et al., 2014). The local carbon isotope curve was integrated with global carbon isotope curve and both local and global sea level curve

47

II.1.10 Conclusions

The Middle-Late Triassic (Ladinian-Carnian) Al Aziziyah Formation was deposited on a shallow carbonate ramp with a pellet ooid shoal that separated cryptalgalaminites deposited in peritidal setting from more an open marine subtidal setting. The main lithofacies are interpreted as 1) tidal-crossbedded sandstone, 2) carbonate mudstone or cryptalgalaminites, deposited in peritidal environments, 3) skeletal-oolitic pelletal packstone/grainstone that formed an extensive shoal at the ramp crest, 4) skeletal bioturbated wackstone/mudstone, formed in shallow subtidal environments, 5-hummocky bedded calcisiltite deposited within a deep subtidal environment within storm wave base, and 6- rare carbonate mud or organic-rich black shale deposited in a basinal setting.

Ghryan Dome and Kaf Bates sections are much thicker than the middle and northern sections of the Al Aziziyah Formation. Thickness variations across the ramp are most likely due to syn-rift events during deposition of the Al Aziziyah Formation, similar to coeval events in the western part of the Jifarah Basin, southern Tunisia. The Al Aziziyah Formation contains an abundance of mudcracks, and silicified evaporite nodules in its peritidal facies, suggesting an arid climate. In addition, ocean circulation during the Carnian was restricted in some parts of the basin as indicated by abundant of deposition of sandstone and evaporites within the upper part of the Al Aziziyah Formation.

Based on field observations, measured sections, thin section petrography, and carbon stable isotope chemostratigraphy, a datum was chosen for the regional cross-section and

was placed on top of the peritidal facies of the southernmost five sections within the top of sequence 5. Seven sequences within the Ghryan Dome were identified (S_1-S_7). North of the Ghryan Dome section are three mainly subtidal sequences (S_8-S_{10}) that may not correlate to the south. Bed thickness variations may define higher-order parasequences, but correlating these parasequences between sections is difficult due to unconformities.

CHAPTER III

CARBON AND OXYGEN ISOTOPE VARIATIONS ON AN ANCIENT CARBONATE PLATFORM: A CASE STUDY FROM THE MIDDLE–LATE TRIASSIC AL AZIZIYAH FORMATION, NORTHWEST LIBYA

III.1 Overview

This study presents the δ^{13}C and δ^{18}O stratigraphies of the Middle-Late Triassic Al Aziziyah Formation. The Al Aziziyah Formation was deposited on a gently sloping carbonate ramp within the Jifarah Basin of northwest Libya and consists of gray limestone, dolomite, and dolomitic limestone interbedded with shale. Facies of the Al Aziziyah are: tidal sandstone, peritidal, barrier, shallow subtidal, deep subtidal and basinal facies. The Ghryan Dome and Kaf Bates sections were sampled and analyzed for carbon and oxygen isotopes (1) to integrate high-resolution carbon isotope stratigraphy with an outcrop-based sequence stratigraphic framework to build the stratigraphic correlation and provide better age control of the Al Aziziyah Formation and (2) to evaluate the influence of depositional environments on the isotopic values. Carbon isotope data identify seven sequences within the Ghryan Dome. Correlations between the sections indicate five sequences in which δ^{13}C value become negative and more positive. Because Carnian ocean circulation was restricted in the some parts of the basin, the Al Aziziyah Formation δ^{13}C curve only partially correlates with the proposed Triassic global δ^{13}C curve. This correlation indicates that the Al Aziziyah Formation was deposited during the Ladinian and part of the Carnian stage. The increase in δ^{13}C values

from -7.8 to +3.9 in certain intervals relative to brachiopod values (-0.5 to +3.0‰) likely reflects local withdrawal of ^{12}C from the ocean due to increased productivity, and/or whole rock sediment composed of calcite admixed with aragonite. The negative $\delta^{13}C$ values are clearly associated with exposure surfaces and with shallow carbonate facies. However, more positive $\delta^{18}O$ values (-9.3 to +0.5‰) relative to Triassic brachiopods (-3.9 to -0.6‰) are related to evaporatic enrichment of ^{18}O, as indicated by the abundance of evaporite within the peritidal facies. In contrast, the negative $\delta^{18}O$ values are related to diagenesis due to freshwater input.

III.1.1 Introduction

Carbon and oxygen isotopic values of shells and whole rocks are commonly used to trace the chemical compositions of the oceans through geological history (Veizer et al., 1999; Brand, 2004; Weissert et al., 2008; Grossman et al., 2008). The variation in $\delta^{18}O$ values result from climate changes associated with glacial versus non-glacial periods, recording depositional water temperatures or the temperature of diagenetic fluids (Emiliani, 1955; Shackleton and Opdyke, 1973; Marshall, 1992; Stoll and Schrag, 2000; Weissert et al., 2008; Grossman et al., 2008; Grossman, 2012a). The carbon isotope composition of carbonate rocks can be used for biostratigraphy and to chronostratigraphy and be used as a relative geochronological tool for the geological record (Veizer et al., 1999; Halverson et al., 2005). Carbon isotope data can also be used as a proxy for sea-level changes where transgressive systems tracts and sea-level rises are associated with positive shifts in the local $\delta^{13}C$ and where highstand systems tracts and sea-level fall are associated with negative shifts in the local $\delta^{13}C$ (Fanton and

Holmden, 2007). In addition, several isotopic studies of shallow carbonate platforms suggest that positive and negative shifts in carbon and oxygen isotopes may not be related to the global carbon and oxygen isotope compositions of the oceans but may rather reflect local environmental diagenetic processes (Allan and Matthews, 1982; Patterson and Walter, 1994; Immenhauser et al., 2003). Various diagenetic processes can alter carbonate and produce apparently related δ^{13}C changes. Shallow-water carbonate platforms tend to become exposed to meteoric water during sea-level falls and are more susceptible to alteration during these periods (Allan and Matthews, 1982; Immenhauser et al., 2003).

In addition, due to the absence of pelagic sediments older than 200 Myr, pre-Jurassic records must be based on macrofossils, like brachiopods and belemnites, or bulk sediments, which are often deposited in restricted environments such as epeiric seas, ramps and carbonate platforms. While these records can be correlated in some cases with trends in the oceanic δ^{13}C records (Vahrenkamp, 1996), skeletal and bulk δ^{13}C records from such environments can present significant interpretive problems in that true open ocean conditions may not have been present at these locations (Panchuk and Holmden, 2006; Woodard et al., 2013) and there may have been vital (Woodruff et al., 1980; Wefer and Berger, 1991) or mineralogical (Swart, 2008) effects which produced carbonate with different δ^{13}C values, or the sediments and fossils may have been diagenetically altered (Immenhauser et al., 2003; Swart and Eberli, 2005; Swart, 2008; Swart et al., 2009).

Studies of the stable carbon and oxygen isotopic compositions of biotic and whole rock carbonate (commonly mud) provide a record of the evolution of Triassic sea water (e.g., Morante, 1996; Krull and Retallack, 2000; Mundil et al. 2004; Payne et al. 2004; Krull et al. 2004; Korte et al. 2005; Payne and Kump, 2007). The first composite albeit imperfect, stable isotope curve for Triassic sea water was derived from brachiopod shells and from whole rock carbonates (Korte et al., 2005).

This study integrates high-resolution carbon isotope data with an outcrop-based sequence stratigraphic framework to build the stratigraphic correlation and provide better age control of the Al Aziziyah Formation. The Middle-Late Triassic (Ladinian-Carnian) Al Aziziyah Formation was deposited on a gently sloping carbonate ramp within the Jifarah Basin in northwest Libya (Fig. 3.1) and consists of gray limestone, dolostone and dolomitic limestone interbedded with shale to the north (Desio et al., 1963; Asserto and Benelli, 1971; Fatmi, 1977; Fatmi et al., 1980; Moustafa et al., 2012; Moustafa et al., 2014). This study also discusses the relation between facies architecture of the Al Aziziyah Formation and carbon isotope values and the possible influence of depositional environments on the isotopic values. Last, this study compares the Al Aziziyah isotopic values with global Triassic isotopic values to evaluate whether the isotopic signature from the Al Aziziyah Formation is similar to the global Triassic isotopic curve and will thus be useful for regional correlation.
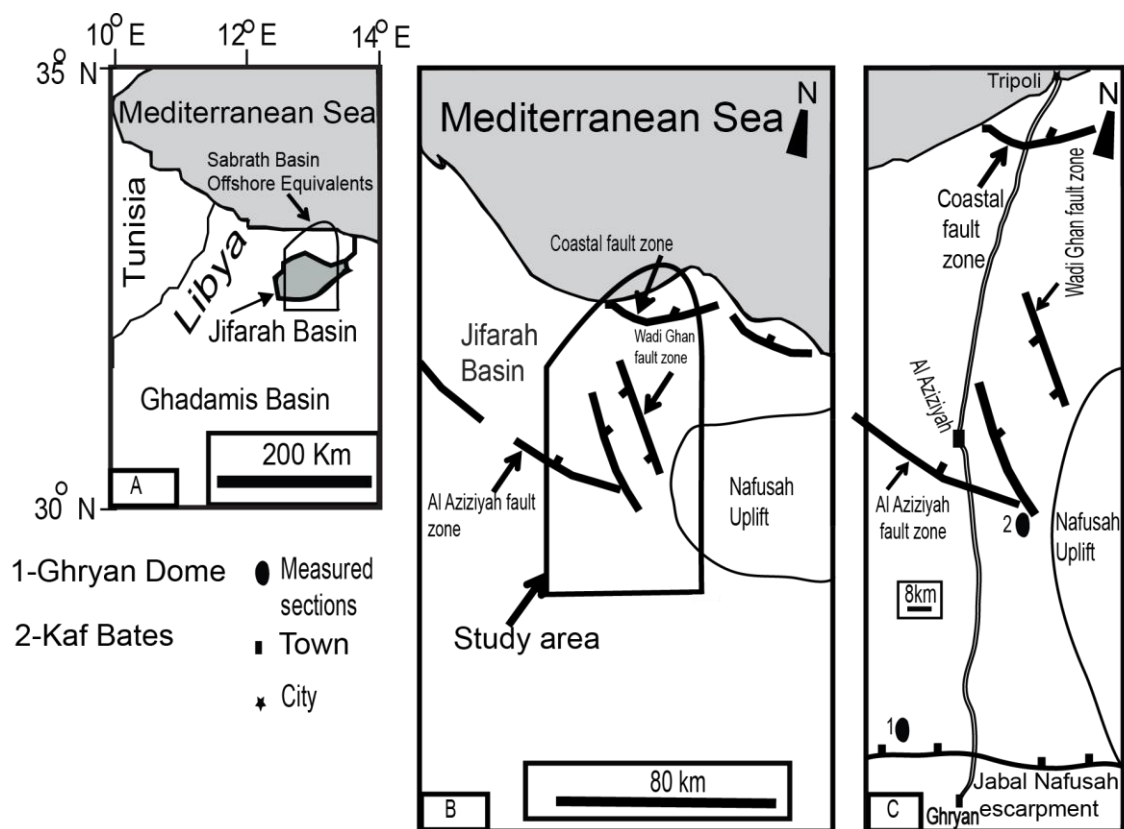
Fig. 3.1. A- Index map shows the location of the Jifarah Basin, Libya. B- Simplified structure map of the area. C- Location of measured sections. The distance between the two sections (Ghryan Dome and Kaf Bates) is approximately 80 km. The Ghryan Dome section (1) is located on the southern margin of the Jifarah Basin. The Kaf Bates section (2) is located north of the Ghryan Dome section, within the deep water facies.

54

III.1.2 Previous studies

Many stable isotope studies have focused on the Permian/Triassic (P/T) boundary and on the Early Triassic biotic rebound following this extinction event (e.g., Holser et al., 1989; Renne and Basu, 1991; Knoll et al., 1996; Isozaki, 1997; Krull et al., 2000; Becker et al., 2004; Korte and Kozur, 2010; Saltzman and Sedlacek, 2013). However, the remainder of the Triassic has been much less studied, which raises challenges for reconstructing pre-Jurassic carbon and oxygen isotope secular variations. Two materials are commonly used for reconstructing pre-Jurassic secular variations in marine carbon isotope ratios: (1) Carefully selected carbonate components, such as marine cements and non-luminescent brachiopod shells, which are most likely to preserve primary signatures; and (2) whole-rock lime mudstone or dolomite, assuming through mass-balance criteria that inorganic carbon isotopes are only slightly affected by diagenetic alterations in carbonate-rich and organic carbon-poor sediments (Grossman, 1994; Scholle, 1995; Saltzman and Thomas, 2012). The global carbon isotopic record of the Triassic is primarily derived from the Tethyan and Muschelkalk Sea and shows a negative trend beginning in the Permian and continuing into the Lower Triassic (Morante, 1996; Krull and Retallack, 2000; Mundil et al., 2004; Krull et al., 2004; Payne et al. 2004; Korte et al., 2005; Payne and Kump, 2007). The negative carbon isotope excursion (CIE) at the (P/T) boundary is recorded in $\delta^{13}C$ from both organic material (Galfetti et al., 2007) and from carbonate rocks (Korte et al., 2005). The negative carbon isotope excursion (CIE) occurs within marine strata in the Tethyan and Neotethyan realms in South China (Korte et al., 2005). This CIE was linked to the biotic events

across the Permian–Triassic boundary and to the overturning of a deep anoxic ocean, which released isotopically light CO_2 and potentially caused anoxia (Knoll et al., 1996; Korte et al., 2005). Alternatively, the CIE may have been caused by the short-term release of isotopically light carbon by the thermal metamorphism of coals during the initial eruption of the Siberian Traps basalt (Payne and Kump, 2007). Others suggest that no single mechanism operating in isolation can account for this isotopic record but that multiple processes operating synergistically caused these changes (Berner, 2002; Tanner, 2010). The Lower Triassic records increasing $\delta^{13}C$ values. A marked recovery of $\delta^{13}C$ values occurs at the Meishan section (South China) from -2‰ at the P/T boundary to +2‰ and is attributed to increased ocean productivity (Chen et al., 2007). During the Middle Triassic, $\delta^{13}C$ values range from -1 to 2‰. However, $\delta^{13}C$ rises to approximately 3.5‰ during the Late Triassic (Payne et al. 2004; Korte et al., 2005). Most of the Middle and Late Triassic values have relatively few variations, with gently rising $\delta^{13}C$ values. The $\delta^{13}C$ carbonate data from brachiopod and from whole rock samples show a positive carbon isotope trend at the base of the Anisian (Korte et al., 2005). The Anisian and Ladinian stages have some negative $\delta^{13}C$ values (Payne et al., 2004; Korte et al., 2005). The Triassic $\delta^{13}C$ values rise into the uppermost Ladinian (Atudorei, 1999; Payne et al., 2004; Korte et al., 2005) and continue to rise through the Carnian (Stanley and Swart, 1995; Payne et al. 2004; Korte et al., 2005). In addition, the $\delta^{13}C$ values of well-preserved coral from the Late Triassic range from +2.5 to +3.5‰ (Stanley and Swart, 1995). The Middle-Late Triassic carbon-isotope trend from organic material, particularly

from leaves and amber (Dal Corso et al., 2011) and from brachiopod calcite (Korte et al., 2005), shows similar patterns.

The oxygen isotopic curve for the Triassic and for its corresponding seawater temperature was summarized by Grossman (2012a). The $\delta^{18}O$ values from brachiopod shells screened for diagenetic influence (Korte et al., 2005; Grossman, 2012a, b) and from whole-rock carbonate (Korte et al., 2005) indicate a broad trend of rising and decreasing $\delta^{18}O$ values. The oxygen isotope from brachiopod shows a range of -3.9 to -0.6‰ within the Triassic, with an increase of 2‰ in the Early Carnian (Grossman, 2012a). This increase in $\delta^{18}O$ values is attributed to global cooling and evaporation (Korte et al., 2005). In addition, these data also indicate that the $\delta^{18}O$ of the Triassic ocean was affected by the northward movement of Europe during the Triassic, which caused a shift in the samples from tropical to temperate climate zones (Grossman, 2012a). The $\delta^{18}O$ of the Triassic ocean was interpreted to be lower than that of the modern ocean, with the $\delta^{18}O$ for well-preserved Late Triassic coral ranging from -4 to -2‰ (Stanley and Swart, 1995), and that for well-preserved Middle-Late Triassic brachiopods ranging from -3.9 to -0.6‰ (Korte et al., 2005). The -0.6‰ value represents the highest values from the Tethyan realm. The paucity of thick-shelled brachiopods in the Triassic deposits is the main reason for using $\delta^{18}O$ data from whole-rock samples to fill the gaps where brachiopod are not available (Korte et al., 2005). However, the whole-rock $\delta^{18}O$ record cannot always be utilized because of diagenetic effects (e.g., Marshall, 1992; Grossman, 1994). The whole rock $\delta^{18}O$ data that represent the Late Carnian and Norian from the Silicka Brezova section in South China are relatively

enriched (up to -0.3‰) compared with the articulate brachiopod data from the Early Carnian because of the variability in ambient seawater temperature due to bathymetric differences or seasonal upwelling (Korte et al., 2005).

III.1.3 Geological setting

Northwestern Libya was at the edge of the Tethys during Mesozoic time (Cornell and Tekbali, 1993; Hallet, 2002). Post-Hercynian crustal adjustments resulted in a marginal trough extended westward into Tunisia and Algeria. During the Carnian circulation was restricted (Demaison, 1965; Cornell and Tekbali, 1993) in the western and central parts of the Jifarah Basin, maybe due to a major uplift alone the marginal trough (Demaison, 1965; Cornell and Tekbali, 1993).

The Jifarah Basin covers an area of 1500 km^2 in northwestern Libya (Fig. 3.1). This area is bounded by the Nafasah uplift to the south and by the offshore Sabrath Basin to the north (Hallett, 2002; Abohajar et al., 2009). Core data from wells in the Jifarah Basin indicate the deposition of Paleozoic to Jurassic sediments (Hallett, 2002). The Jifarah escarpment extends 400 km from southern Tunisia to southwest Libya and marks the southwest limit of outcrops in the Jifarah Basin (Fig. 3.1). The Jifarah Basin formed at the eastern end of the South Atlas lineament, which defines the southern margin of the Atlas fold belt that extends from Morocco to Tunisia (Dewey and Burke, 1973), where it branches to extend into northwest Libya as the Jifarah axis (Anketell and Ghellali, 1991).

The Jifarah Basin is situated at the junction of two major structures: the north-northwest trending Tripoli-Tibesti Arch, which formed in the Caledonian, and the east-west trending Jifarah Arch, which formed because of Hercynian deformation (Anketell and Ghellali, 1991; Abohajar et al., 2009; Swire and Gashgesh, 2000). The structural pattern of the Jifarah Basin was created by these Paleozoic structural trends (Anketell and Ghellali, 1991; Abohajar et al., 2009; Hallet, 2002). The subsidence of the Jifarah Basin continued into the Early and Late Triassic (Muttoni et al., 2001).

The Jifarah Basin is bounded to the south by the east-west oriented subsurface Al Aziziyah fault zone. Toward the east, the Al Aziziyah fault links the Wada Ghan fault zone (Arkell et al., 1957; Swire and Gashgesh, 2000; Raulin et al., 2011) and was active during the Triassic (Swire and Gashgesh, 2000; Raulin et al., 2011). The trend of these faults parallels Paleozoic structures.

The age of the Al Aziziyah Formation has been disputed (Fatmi, 1977; Asserto and Benelli, 1971; Magnier 1963; Desio et al., 1963; Desio et al., 1960; Burollet 1963; Muttoni et al., 2001). The Al Aziziyah Formation was deposited during the Carnian based on "Mojsisovicsites" ammonites in the upper part of the Ghryan Dome section (Fatmi, 1977). This ammonite genus ranges from Carnian to Anisian and occurs in the Alps, Spain, Sardina, Himalaya and in parts of the USA (Fatmi, 1977). However, a Late Triassic (Carnian to Rhaetian) range for the Al Aziziyah Formation was proposed based on the abundance of microflora, including miospore taxa *Infernopollenites spp., Crassicappites spp., Parillinites spp., and Pseudenzonalasporites summus* (Swire and

59

Gashgesh, 2000). The Al Aziziyah Formation ranges in age from Ladinian to Carnian based on ammonites in the upper part of the formation (El Hinnawy and Cheshitev, 1975; Magnier, 1963).

III.1.4 Methods

Eight full and partial sections of the Al Aziziyah Formation were measured between January and April of 2011. Two of the outcrops (Kaf Bates and Ghryan Dome) were sampled for carbon and oxygen isotope chemostratigraphy. Whole-rock samples for carbon and oxygen isotope analyses were collected at ~ 50 cm intervals from both sections. In total, 287 carbonate samples were drilled from freshly cut rock, avoiding sparry cement, skeletal components and vein fill. Samples were analyzed at the Texas A&M Stable Isotope Geoscience Facility, College Station, Texas. One hundred and seventy-six sample powders were analyzed using a Gas Bench II gas handling system and a Delta plus XP isotope ratio mass spectrometer. The precision was 0.04‰ for $\delta^{13}C$ and 0.10‰ for $\delta^{18}O$ based on replicate analyses of NBS-19. One hundred and eleven samples in this data set were analyzed using a Kiel IV carbonate device coupled to a Thermo Scientific MAT 253 isotope ratio mass spectrometer. The precision for these analyses was 0.02‰ for $\delta^{13}C$ and 0.06‰ for $\delta^{18}O$ using the NBS-19 standard. All data are reported versus VPDB using the NBS-19 standard ($\delta^{13}C = 1.95$‰, $\delta^{18}O = -2.20$‰).

III.1.5 Stratigraphic framework

III.1.5.1 Al Aziziyah facies distributions

Six major facies are recognized in the Al Aziziyah Formation (Figs. 3.2, 3.3 and 3.4, Moustafa et al., 2012, 2014). The shallowest to deepest facies are: tidal sandstone, peritidal carbonate, ramp crest barrier, shallow subtidal, deep subtidal and basinal carbonate. Four facies from the Ghryan Dome and Kaf Bates sections (peritidal carbonate, ramp crest barrier, shallow subtidal and deep subtidal carbonate) were isotopically analyzed. A brief description and interpretations of the sediment types in all facies are provided below, arranged from shallowest to deepest. Table 3.1 contains more detailed descriptions and interpretations of the Al Aziziyah Formation facies.

III.1.5.1.1 Tidal sandstone facies

This facies contains bidirectionally crossbedded red sandstone beds which are 2 meters thick (Fig. 3.5A) and primarily composed of well-rounded, well-sorted medium sand grains, recording high-energy siliciclastic deposition by tidal currents (Hammuda et al., 1985). This facies is the shallowest in the area and only occurs at the Ghryan Dome section (Moustafa et al., 2012).

Table 3.1

Facies description of the Al Aziziyah Formation.

Facies type (Lithofacies)	Description	Sedimentary structures	Isotopic composition (δ^{13}C & δ^{18}O versus VPDB)	Fossils	Depositional environment
Sandstone	Red to yellow fine-medium sandstone. A few meters thick. Well rounded quartz grains with silica cement.	Bidirectional cross-bedding	none	none	Tidal environment indicates marine setting. The red color indicates iron oxidization.
Carbonate mudstone	Tan to yellowish. A few meters to ten meters thick with evaporite nodules, chert, with planar and domal algae.	Mudcracks, microbial laminations, intraclasts	δ^{13}C ranges from **-4.4 to +3.9 ‰** δ^{18}O ranges from **-7.8 to +0.5 ‰**	Bioturbated to laminated beds of algae and stromatolites.	peritidal environment
Pellet packstone/ grainstone	Gray to dark color. Up to five meters in thickness. Pellets packstone to grainstone. Grapestone intraclasts and ooids with radial crystal structure. Primary fabric was originally calcitic ooid and composite ooid. Pellets are rod-like in longitudinal view, round in transverse section and have relatively large and uniform size.	Massive to mechanically laminated beds	δ^{13}C ranges from **-7.8 to +3.4 ‰** δ^{18}O ranges from **-7.5 to -0.1 ‰**	Bioturbation beds, gastropod, brachiopods and unidentified fossil fragments	Ramp crest barrier or shoal
Pellet, skeletal packstone/wackstone/mudstone	Thickness from one to three meters. Dark gray with different cement types, cherty layers and nodules.	Massive to bioturbated beds	δ^{13}C ranges from **-3.1 to +3.4 ‰** δ^{18}O ranges from **-9.3 to -0.1 ‰**	Bioturbated beds, of pellets and skeletal fossils like Brachiopods and Gastropods, and other unidentified fossil fragment	Shallow subtidal
Calcisiltite/ Wackstone	Thickness from a few meters to six meters. Light to dark, with cherty layers and nodules, few pellets.	Massive to mechanical laminations and stylolites	δ^{13}C ranges from **-2.9 to +3.2 ‰** δ^{18}O ranges from **-7.3 to -1.6 ‰**	Fossils are rare in this facies.	Deeper subtidal facies, more abundant in the northern sections.
Carbonate mudstone, black shale	Light to dark gray. The mudstone facies range in thickness from half to one meter. The black shale is very thin with organic rich sediment.	Massive beds	none	Few unknown fossils.	Basinal environment
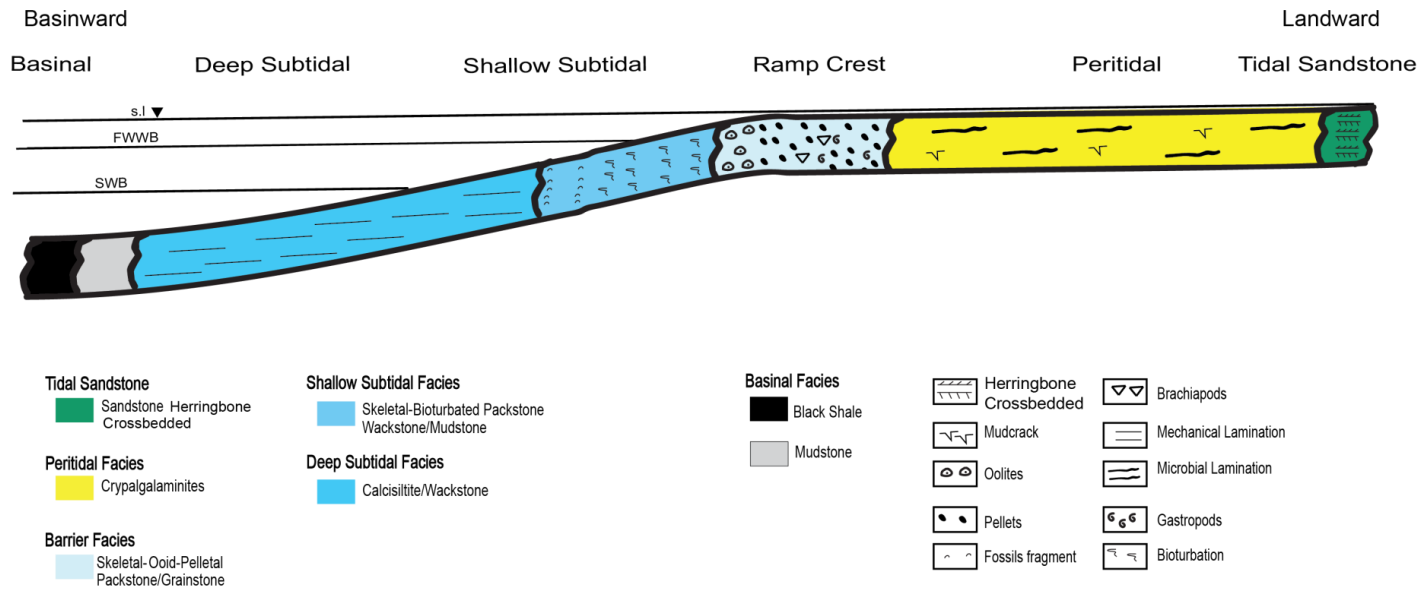
Fig. 3.2. Al Aziziyah Formation depositional profile showing facies distributions. S.l = sea level; FWWB = Fairweather Wave Base; SWB = Storm Wave Base. See Table 1 for a detailed description.

63
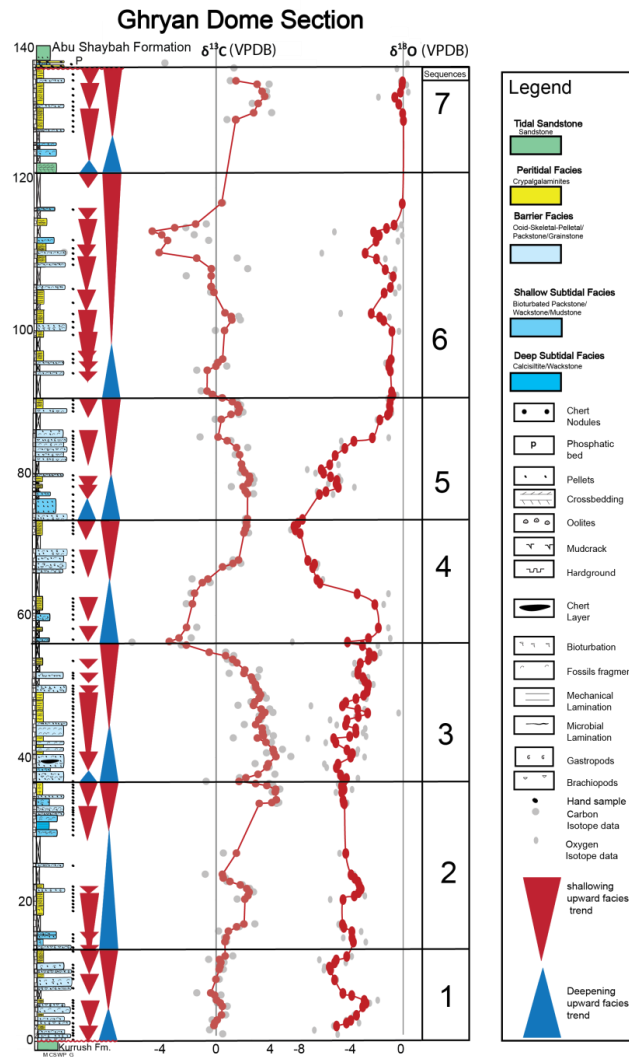
Fig. 3.3. Ghryan Dome measured section plotted with a three-point running average of $\delta^{13}C$ and $\delta^{18}O$ (solid red line). Grey symbols represent the actual carbon and oxygen isotopic data. The Ghryan Dome measured section shows a seven-sequence stratigraphy, with different facies and different carbon and oxygen isotopic trends. The peritidal and barrier facies dominated this section. Note the positive and negative covariance between the carbon and oxygen isotopic values within different intervals of the measured section.
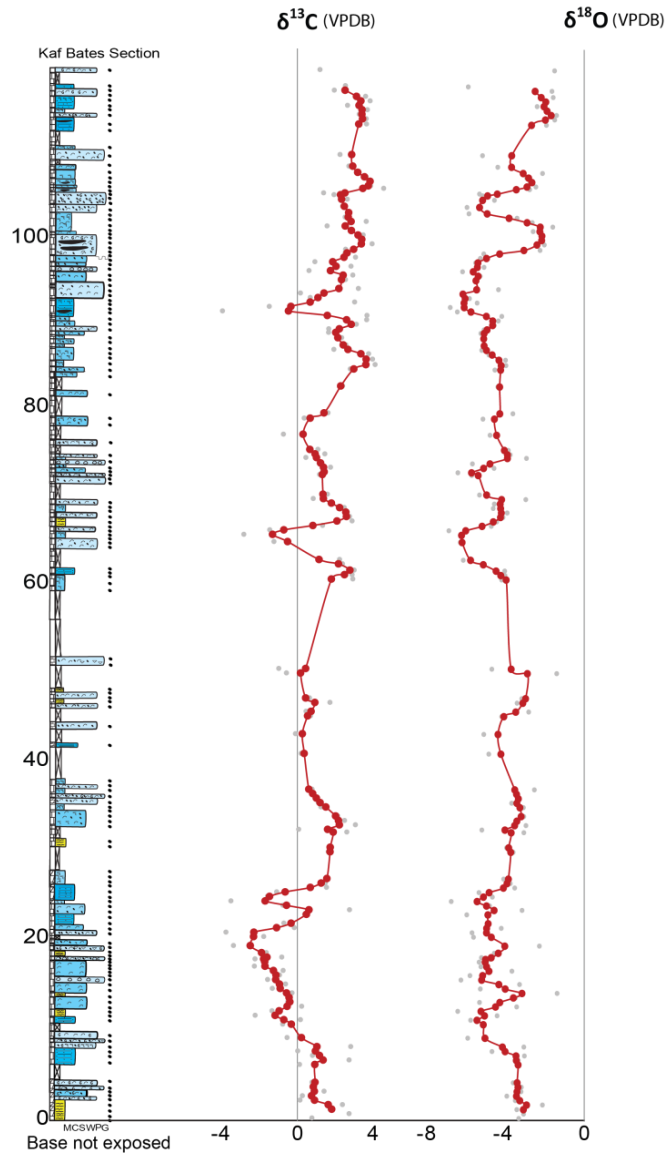
Fig. 3.4. Kaf Bates measured section plotted with a three-point running average of δ¹³C and δ¹⁸O (solid red line). Grey symbols represent the actual carbon and oxygen isotopic data: Note the positive and negative covariance between the carbon and oxygen isotopic values within different intervals of the measured section.

III.1.5.1.2 Peritidal carbonate facies

The light tan to yellowish cryptalgalaminites (Fig. 3.5B, C), microbial laminations and stromatolites of the facies commonly contain well–developed mudcracks, evaporite nodules (Fig. 3.5B), and chert nodules. This facies is locally dolomitized. Planar cryptalgalaminites are the most abundant sedimentary structures in this unit and primarily occur in the Ghryan Dome section. Small microbial domes are also more abundant in the Ghryan Dome section (Fig. 3.5C). Occasionally, pellets are trapped in the microbial laminations. This mud-facies was deposited in shallow-water peritidal environments restricted to the southernmost sections of the Ghryan Dome, Ras Mazal East, Ras Mazal West, Kurrush Dome and Kaf Bates. The abundance of evaporites and mudcracks, and lack of burrowing, suggests that this facies was deposited in a semi-arid to arid climate. This facies represents the shallowest water carbonate facies.
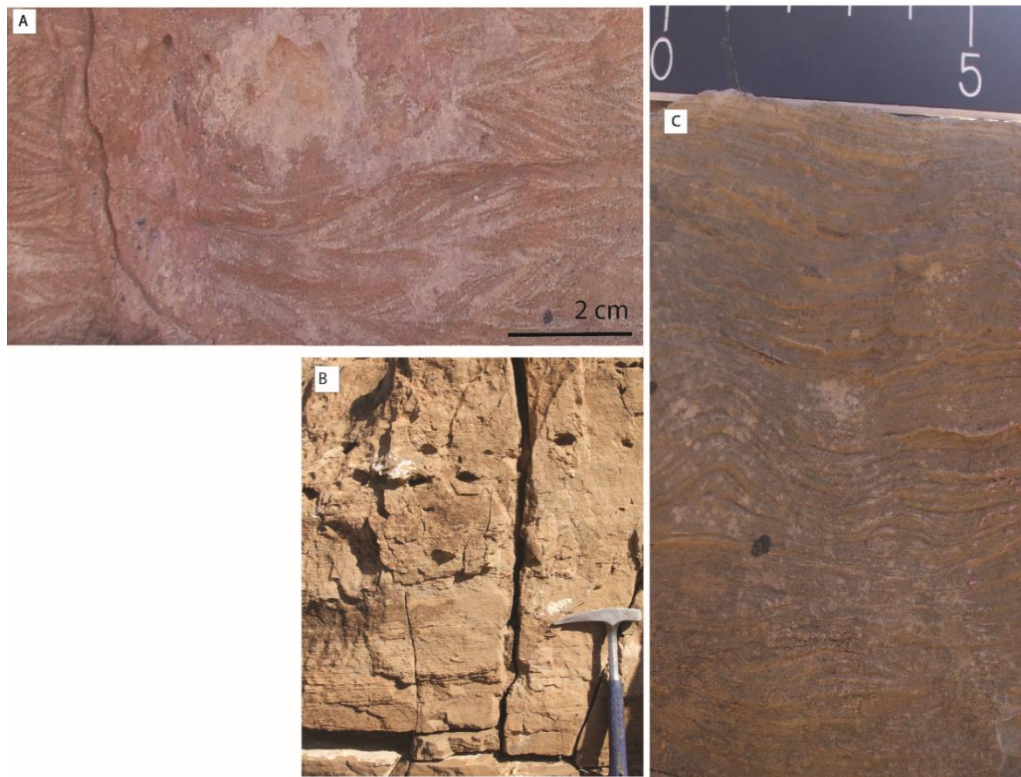
Fig. 3.5. Photographs of (A) Tidal sandstone facies showing red bidirectionally crossbedding sandstone. (B) Peritidal facies with evaporite nodules and stromatolites. (C) Peritidal facies with microbial laminations and stromatolites. Note small microbial domes.

III.1.5.1.3 Ramp crest barrier carbonate facies

This facies is characterized by ooid-skeletal-pelletal packstone-grainstone contains ooids, pellets and bioclast fragments, as well as locally contains gray to dark gray chert layers (Fig. 3.6A, B). The pellets are up to 2 mm, without clear orientation, rod-like in the longitudinal section, circular in the transverse section and are relatively uniform (Fig. 6B). This facies ranges in thickness from less than one meter to almost two meters. The skeletal fragments in this facies are brachiopods, gastropods and small unidentified bioclastic fragments. In some sections, these shell fragments are locally mixed with ooids to form grapestone. Some of the oolites have an internal structure (radial) or are composite ooids, containing more than one ooid grain. The oolitic nuclei are commonly skeletal fragments and non-skeletal grains and are most commonly pellets. The radial crystal structures of the ooids indicate that the ooids likely originally formed as aragonite (Davies et al., 1978; Lehrmann et al., 2012). The pelletal-ooid packstone/grainstone facies indicates high-energy depositional conditions along the ramp crest that separated restricted evaporitic facies to the south from the open-marine conditions to the north.
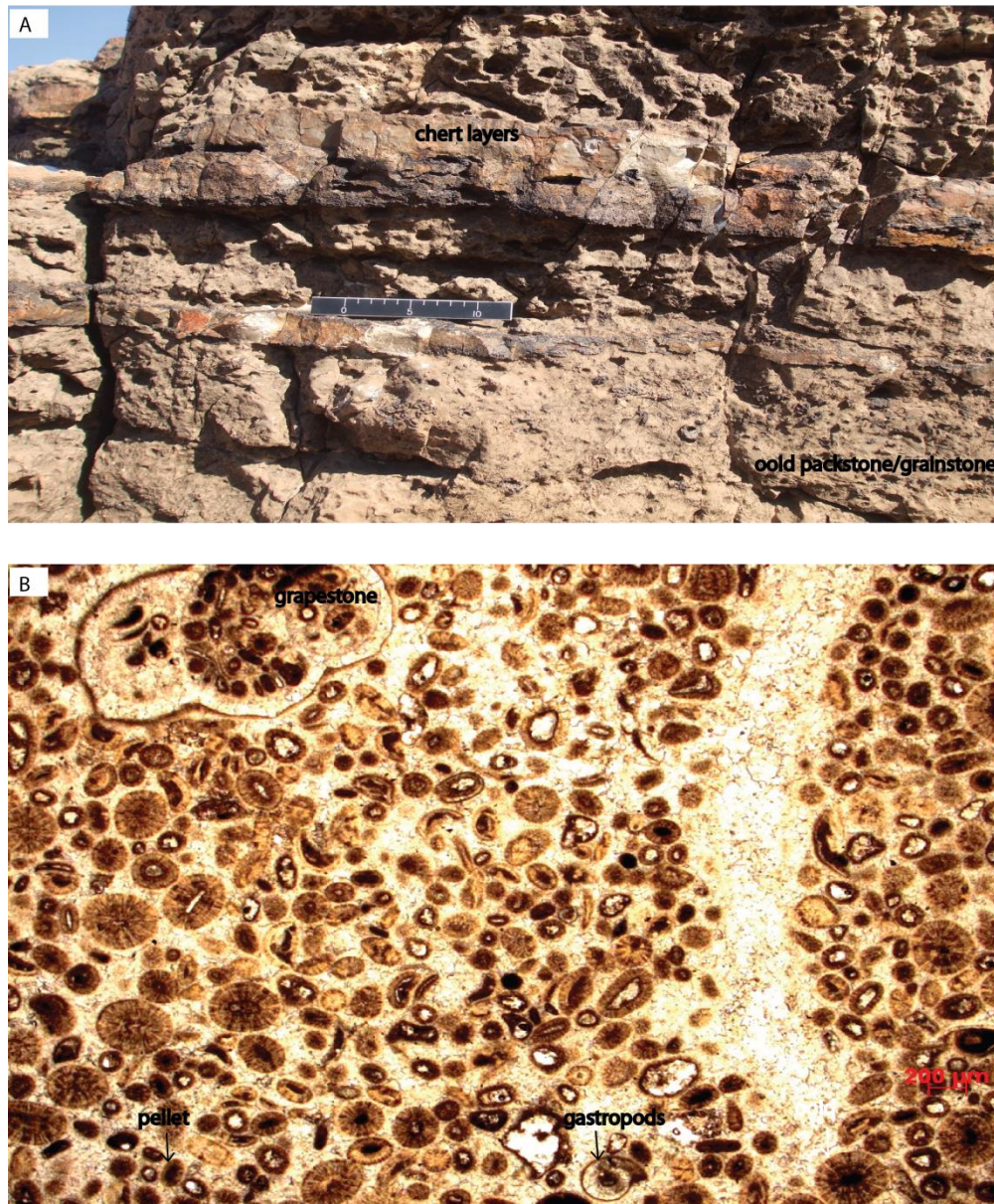
Fig. 3.6. Carbonate from the barrier facies of the Ghryan Dome (A & B). A- Chert layers within skeletal oolitic-pellet-grainstone. Note the large thickness of the chert layers. B-The skeletal oolitic-pellet-grainstone with ooids, pellets and grapestone.

III.1.5.1.4 Shallow subtidal facies

This facies consists of thin-medium beds of bioturbated skeletal packstone-wackstone-mudstone in beds ranging up to one meter in thickness (Fig. 3.7A). Bioturbated, fine-grained, light to dark-gray mudstone and pelletal-skeletal wackstone are the most common lithologies in this unit. Bioturbation varies from low to high density, and the few pellets and fossil fragments in this facies were likely transported from the ramp crest facies. This facies was deposited in shallow, well-oxygenated waters that promoted abundant bioturbation directly basinward of the ramp crest facies.

III.1.5.1.5 Deep subtidal facies:

The deep subtidal facies is composed of medium-thick beds (up to four meters thick) of calcisiltite, with hummocky cross-stratification, mechanical laminations and local chert layers, interbedded with pelletal wackstone or with lime mudstone (Fig. 3.7B, C). This facies was deposited within a storm wave base and recorded alternating moderate to high–energy storm events interbedded with lower energy muddy background sedimentation.

III.1.5.1.6 Basinal facies (black shale and mudstone)

This facies primarily consists of thin-bedded mudstone layers interbedded with extremely thin black shale or organic-rich shale (Figs. 3.7D). The Basinal Facies occurs within the northernmost sections (e.g., Bu Arghop and Ras Lafa; Moustafa et al., 2012,

2014) and may substantially thicken toward the offshore portion of the Jifarah Basin (Abohajar et al., 2009).
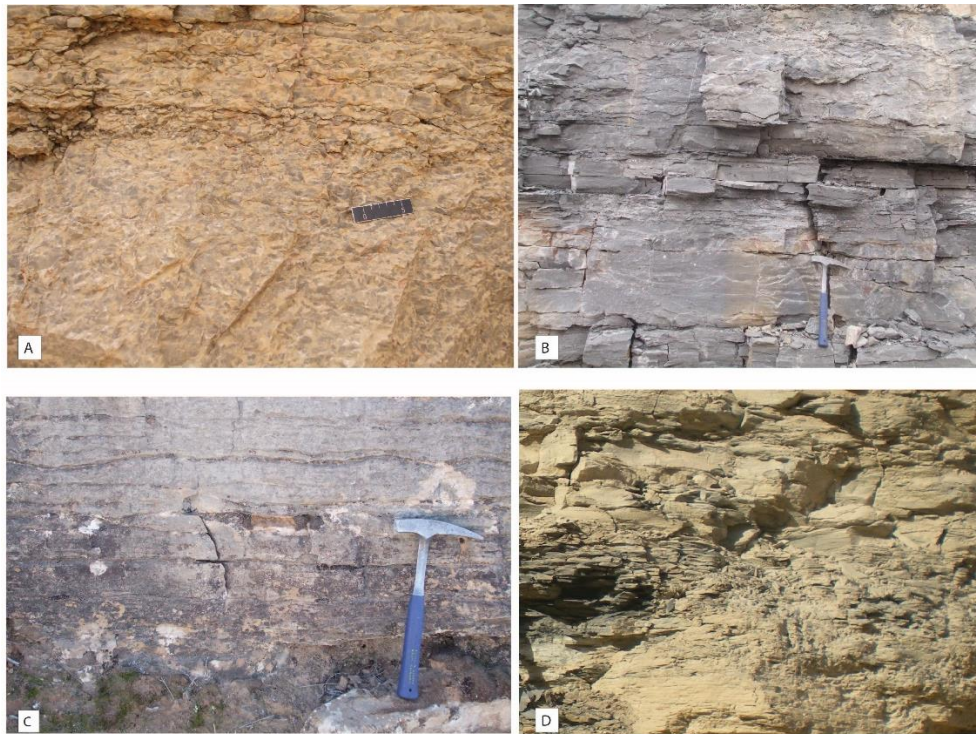
Fig. 3.7. Shallow subtidal facies with high density bioturbation (A); deep subtidal facies with carbonate mud (B); calcisiltite with mechanical laminations (C); and basinal facies with carbonate mudstone and shale with organic-rich sediment or black shale (D).

III.1.6 Sequence stratigraphy

Employing sequence-stratigraphic interpretation procedures (Vail et al., 1977; Mitchum et al., 1977; Brown and Fisher, 1977), seven sequences within the Ghryan Dome have been identified based on facies stacking patterns, field observations and stable carbon isotopes. The Ghryan Dome section, which represents the reference section of the Al Aziziyah Formation because of its thickness (140 meters thick) and exposure of upper and lower contact (a gradational basal contact and a sharp upper surface), represents the southernmost section of the Jifarah Basin. At the Ghryan Dome section, each sequence ends with peritidal facies, with one sequence ending with tidal sand and another sequence ending with phosphatic bed. Each sequence also has a transgressive system tract (TST) and a highstand system tract (HST) (Moustafa et al., 2014).

The Al Aziziyah Formation is predominantly a 2nd-order (5-20 m.y. duration) subtidal carbonate ramp with peritidal facies restricted to the southernmost sections (Moustafa et al., 2012). The transition from the underlying Kurrush Formation to the Al Aziziyah Formation is marked by a change from fine sand and red clay to carbonate. In the most updip location, the transition from the Al Aziziyah Formation to the overlying Abu Shaybah Formation is an iron and phosphatic surface (composite exposure and flooding surface) overlain by a bone bed and by fine sand (Moustafa et al., 2012).

72

III.1.7 Carbon and oxygen isotopes

III.1.7.1 Carbon isotope record

A detailed outcrop-based sequence stratigraphy cross-section integrated with the carbon isotope curves shows a southern section in the southern margin of the Jifarah Basin that recorded a peritidal facies dominated section (Ghryan Dome) and northern section (Kaf Bates) that recorded a transition from peritidal facies to deep subtidal facies (Fig. 3.8). The δ^{13}C of the two sections of the Al Aziziyah Formation range from -7.8 to +3.9‰, with the majority of values higher than +1‰ (Fig. 3.8). Samples with low δ^{13}C values are concentrated near peritidal and barrier facies. The δ^{13}C values of the both sections of the Al Aziziyah Formation are on average similar (Fig. 3.9A and B).

The δ^{13}C curve of the Ghryan Dome section, the reference section for the formation (as stated earlier) shows multiple episodes of depletion and enrichment. This δ^{13}C curve partially correlates with the proposed Triassic global δ^{13}C curve (Fig. 3.10). Carbon isotope values (Fig. 3.3) fluctuate within the range of -0.5‰ to 1‰ at sequence 1 and increase to the highest values at the top of sequences 2 and lower part of sequence 3. Strong depletion of the carbon isotope curve occurs at the top of sequence 3 and at the upper part of sequence 6. Sequence 7 has relatively high carbon isotope values. The carbon isotope values at the Ghryan Dome section are depleted below or at the sequence boundaries in most of the Ghryan Dome section sequences (e.g., sequences 1, 2, 3 and 5; Fig. 3.3). Carbon isotope values at the Kaf Bates section also show depletion and enrichment throughout the section. The carbon isotope curve of the Kaf Bates section (Fig. 3.4, 3.8) has sharp depletion at its lower part and gradual enrichment in the middle

73

part, with little depletion. The carbon isotope curve of the upper part of the section increases gradually, with little depletion.

The $\delta^{13}C$ curves of the Ghryan Dome and Kaf Bates sections of the Al Aziziyah Formation were correlated within detailed sequence stratigraphic cross sections from south to north (Fig. 3.8). The base of sequence 3 at the Ghryan Dome and the base of sequence 3 at the Kaf Bates have the shallowest facies, with the most similar carbon isotope values and patterns in both sections. These changes in $\delta^{13}C$ values (at the base of sequence 3 in both sections), which occur during the same period, can define a stratigraphic line (Swart and Eberli, 2005). Therefore, the base of these sequences is used as the datum for this chemostratigraphic correlation between the Ghryan Dome and Kaf bates sections. Based on carbon isotope variations (Fig. 3.8), the correlation between the Ghryan Dome and Kaf Bates sections indicates five sequences (sequences 3-7) of $\delta^{13}C$ depletion and enrichment (Fig. 3.8).

III.1.7.2 Oxygen isotope record

The oxygen isotope compositions of the two sections cluster in a wide range, with higher maximum values for the Ghryan Dome section (-9.3 to +0.5‰) than for the Kaf Bates section (-8.2 to -1.5‰; Fig. 3.9A and B). The Ghryan Dome section has the heaviest $\delta^{18}O$ values associated with peritidal and barrier facies (Figs 3.3, 3.9A). The oxygen isotope curve of the Ghryan Dome section fluctuates between -2‰ and -5‰ at sequences 1 to 3 and shifts toward low values at sequence 4, then toward heavy values at sequences 5 to 7 (Fig. 3.3). These $\delta^{18}O$ shifts are generally associated with peritidal and

barrier facies. The oxygen isotope curve of the Ghryan Dome section is slightly enriched at exposure surfaces (e.g., at the end of sequences 1 to 7; Fig. 3.3). The oxygen isotope curve of the Kaf Bates section (Fig. 3.4) shifts toward heavy values at the top and fluctuates between -3‰ and -6‰ for most of the section.

III.1.7.3 Carbon and oxygen isotope covariance

The carbon and oxygen isotopic curves of the Ghryan Dome section (Fig. 3.3) show both positive covariance (Sequences 2 and 3) and negative covariance (Sequences 3.4, 3.5 and 3.7). Most of the carbon and oxygen isotope minima are associated with peritidal and barrier facies (Sequence 1-7, Fig. 3.3). However, at the end of sequence 7, beneath the major unconformity between the Al Azizyah Formation and the overlying Abu Shaba Formation, the carbon isotope curve decreases while the oxygen isotope curve slightly increases (Fig. 3.3). This contact is a major unconformity surface overlain by a phosphatic bed in the base of the Abu Shaba Formation (Fig. 3.3). However, the depletion of carbon and oxygen isotope values also occurs at the beginning of sequence 1 (Fig. 3).

The carbon and oxygen isotopic curves of the Kaf Bates section also show positive and negative covariances (Fig. 3.4). Carbon and oxygen isotope curves are depleted at the beginning of the section. However, at the end of the section, the carbon isotope curve is depleted while the oxygen isotope curve is enriched (Fig. 3.4).
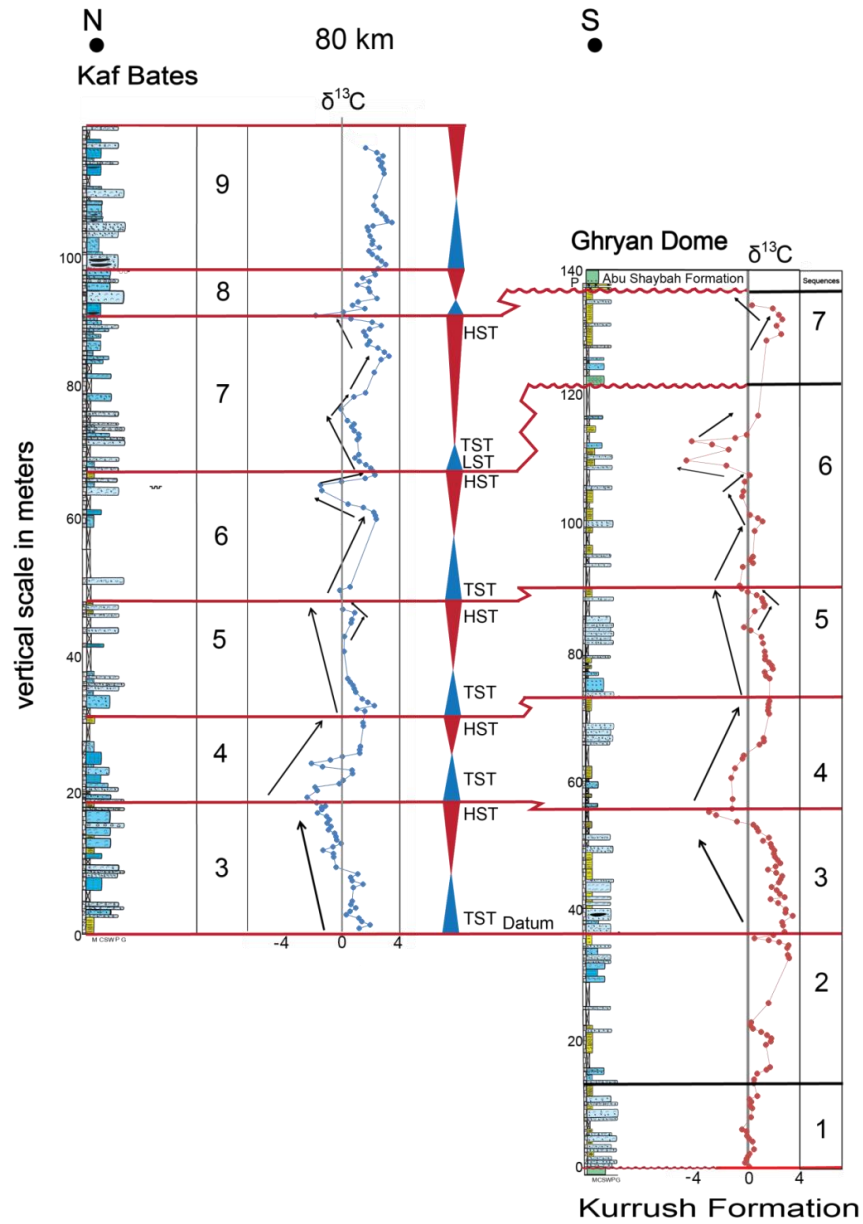
Fig. 3.8. The correlation between the Ghryan Dome and the Kaf Bates sections based on δ¹³C. Note the similar carbon isotope patterns in sequence 3 at the Ghryan Dome and Kaf Bates sections. The base of this sequence is used as a datum.
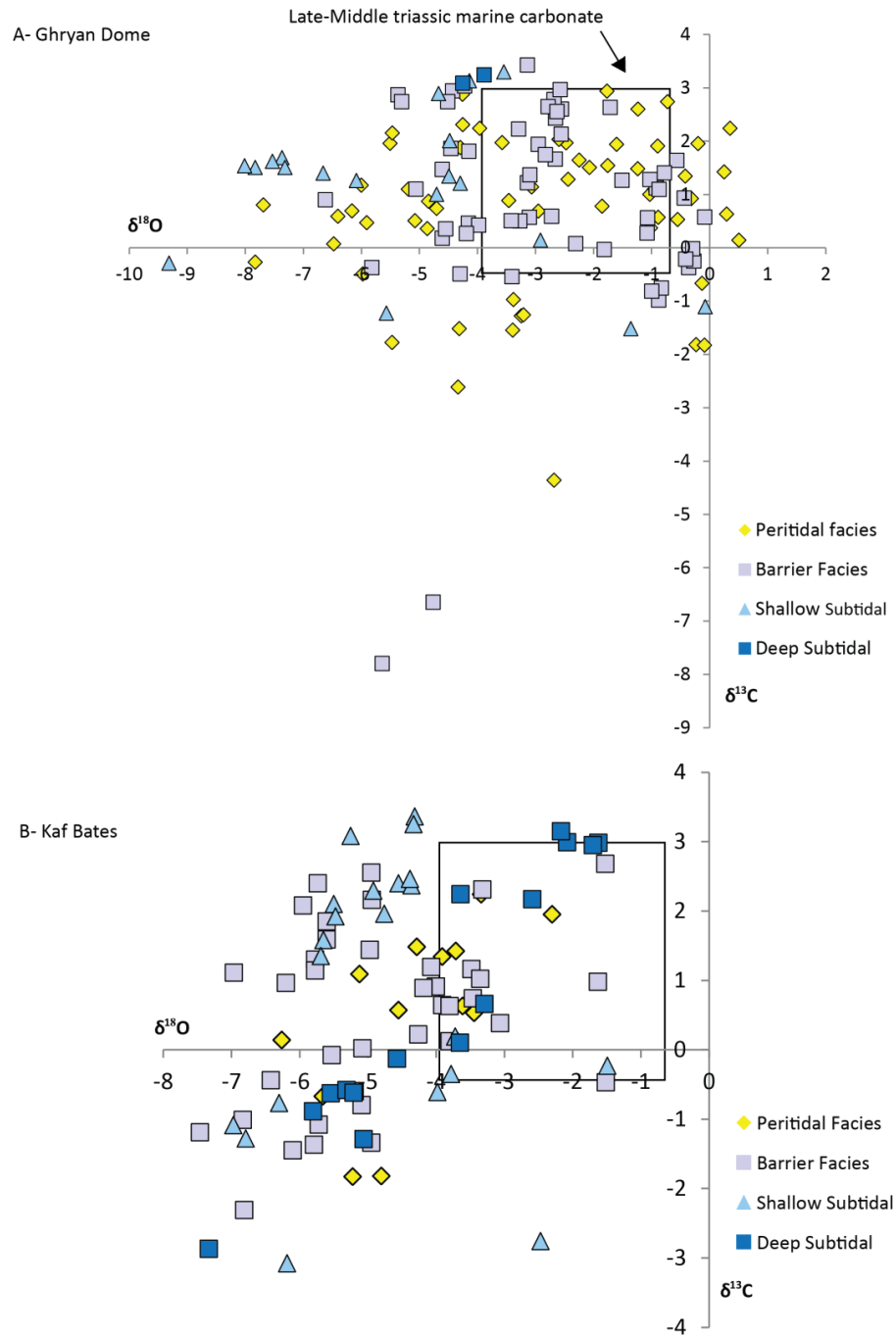
Fig. 3.9. Scatter diagram of $\delta^{13}C$ versus $\delta^{18}O$ keyed for each facies from the Ghryan Dome section (A) and the Kaf Bates section (B).

III.1.8 Discussion

III.1.8.1 Ramp geometry

As discussed earlier, the Al Aziziyah Formation depositional profile has six facies (Fig. 3.2). From land to the basin, they are tidal sandstone, peritidal carbonate, ramp crest barrier, shallow subtidal, deep subtidal, and basinal. The facies indicate that these rocks were deposited on a gently sloping carbonate ramp (e.g., Ahr, 1973; Read, 1985) with tidal flats that passed basinward into a thin pelletal-oolitic ramp crest and then into shallow and deep subtidal facies without a significant break in the slope. Most of this ramp is shallow to deep subtidal facies, with the tidal sandstone and peritidal facies restricted to southern exposures. The absence of a lagoon facies landward of the ramp crest facies suggests that the thin ramp crest facies did not produce enough accommodation space for subtidal lagoons to form.

III.1.8.2 Climate

Globally, the Triassic climate was warm (Dickins, 1993). During the Middle and Late Triassic the climate in the study area was arid as indicated by the abundance of an evaporite zone stretching from North Africa to northern Scandinavia (Dickins, 1993). The Al Aziziyah Formation has an abundance of mudcracks and silicified evaporite nodules in its peritidal facies, suggesting an arid climate during its deposition (e.g., Golonka, 2000; Preto et al., 2010). In addition, a wide marine transgression occurred during the Ladinian followed by more extensive sea invasion during the Carnian. However, during the Carnian circulation was restricted (Demaison, 1965; Cornell and Tekbali, 1993) in the western and central parts of the Jifarah Basin due to a major uplift

78

along the marginal trough in Tunisia and Algeria (Demaison, 1965; Cornell and Tekbali, 1993). Therefore, thick evaporitic deposition occurred in Algeria and Tunisia (Sloss, 1953; Demaison, 1965; Bishop, 1975), whereas terrigenous material, sandy limestone, evaporites and dolomites of the Al Aziziyah Formation (Ladinian-Carnian) accumulated in the shallow ramp environment, especially in the peritidal facies (Demaison, 1965; Cornell and Tekbali 1993; Swire and Gashgesh, 2000; Raulin et al., 2011). This climatic setting is reflected in carbon and oxygen isotope data from the Al Aziziyah Formation, which were likely affected by meteoric water charged with light soil CO_2 and excess evaporation (due to restriction in ocean circulation) as indicated by the abundant evaporites within the peritidal facies mostly in the upper part of the Al Aziziyah Formation.

III.1.8.3 Stable isotope patterns and interpretations

Because the oxygen and carbon isotopic composition of seawater can vary through geologic time (e.g., Veizer et al., 1999; Grossman, 2012a), it is necessary to understand the initial composition of the Triassic marine carbonate to make global correlations. Accordingly, the isotopic values of well-preserved brachiopod shells from Triassic seawater range from -0.5 to +3.0‰ $\delta^{13}C$ and -3.9 to -0.6‰ $\delta^{18}O$ (Korte et al., 2005). In addition, the isotopic values of well-preserved corals from the Late Triassic range from +2.5 to +3.5‰ $\delta^{13}C$ and -4 to -2‰ $\delta^{18}O$ (Stanley and Swart, 1995). In the following discussion, the isotope ratios of the Al Aziziyah Formation obtained in this study are compared with the primary range of Triassic values suggested by Korte et al. (2005).

The Ghryan Dome and Kaf Bates sections have similar $\delta^{13}C$ values (Fig. 3.9A and B), and some of their values are heavier than the isotopic signature of well-preserved brachiopod shells from Triassic seawater, but the majority are lower, especially in the upper half . The Kaf Bates section recorded more open marine depositional conditions than the Ghryan Dome section as indicated by its lower occurrence of peritidal facies and greater occurrence of deep subtidal facies. The ^{13}C depletion of the Al Aziziyah Formation relative contemporary brachiopod shells could be related to the effects of the ^{13}C-depleted meteoric water and environmental restriction as evidenced by the abundant evaporites within the peritidal facies. The $\delta^{13}C$ of dissolved inorganic carbon (DIC) in meteoric water can rapidly decline as water percolates through a sediment soil zone containing CO_2 produced by the oxidization of organic matter (Allan and Matthews, 1982; Lohmann, 1988; Immenhauser, 2003). This CO_2 subsequently dissolves $CaCO_3$ to produce bicarbonate. The uptake of this bicarbonate in biogenic or inorganic precipitates results in carbonate materials with depleted $\delta^{13}C$ values. Similar depletion in $\delta^{13}C$ values can also result from influx of fresh continental water influenced by similar processes (Simms and Ruffell, 1990). Therefore, freshwater limestone has negative $\delta^{13}C$ values which depend on the relative contribution of oxidation of organic carbon. Indeed, the Al Aziziyah Formation was deposited in a shallow ramp within a warm and semi-arid climate and was affected by freshwater diagenesis. Therefore, local changes in freshwater diagenesis may affect the $\delta^{13}C$ value (Immenhauser et al., 2003). In addition, an abundance of evaporites is associated with depletion in $\delta^{13}C$ values due to environmental restriction and to "aging" (Patterson and Walter 1994; Holmden et al.,

80

1998; Swart et al., 2009). This aging enables the accumulation of CO_2 from oxidized organic matter enriched in ^{12}C, resulting in carbonate materials with lower $\delta^{13}C$ values (as discussed above). Moreover, lower $\delta^{13}C$ can occur in normal-salinity waters when isotopically light organic carbon is oxidized in intermediate and deep waters, and these waters are upwelled into the basin (Patterson and Walter 1994; Immenhauser et al., 2003).

The interval of ^{13}C enrichment of whole rock relative to brachiopod shells may be attributable to local primary productivity, which preferentially removes ^{12}C from seawater DIC and increases its $\delta^{13}C$ (Broecker, 1982; Kump and Arthur, 1999; Panchuk et al., 2006; Grotzinger et al., 2011; Hajikazemi et al., 2012). This primary production is indicated by the abundance of organic-rich sediment. Alternatively, the enrichment of whole rock carbonate relative to brachiopod shells may be due to the admixing of aragonite with calcite, since aragonitic sediments are typically enriched in ^{13}C relative to calcitic sediments (Swart, 2008; Swart et al., 2009). The Al Aziziyah Formation facies described in this study is interbedded with shale and organic-rich sediment, particularly toward the northern portion of the Jifarah Basin, as shale thickness increases into the subsurface (Abohajar et al., 2009; Moustafa et al., 2014). Therefore, a combination of factors, such as freshwater diagenesis associated with light soil CO_2 and environmental restriction as indicated by the abundance of evaporite in peritidal environments and in portions of the barrier facies are most likely responsible for the ^{13}C depletion of Al Aziziyah carbonates relative to well-preserved brachiopod shells representing contemporary seawater. In contrast, the ^{13}C enrichment of Al Aziziyah carbonates versus

81

contemporary brachiopod shells may be due to local withdrawal of ^{12}C from the seawater DIC and/or admixing of calcite and aragonite sediment.

In summary, the Ghryan Dome section has relatively high δ^{18}O values (Fig. 3.9A) interpreted as ^{18}O enrichment of water, consistent with a dominant lithology of peritidal and barrier facies deposited in evaporitic conditions. On the other hand, the wide range of low δ^{18}O values likely indicates freshwater diagenetic effects (Fig. 3.9A).

III.1.8.3.1 Isotopes and depositional facies

Investigating the relation between the isotopic composition and facies is critical when evaluating chemostratigraphic correlations because a strong correlation between isotope values and depositional facies may indicate that the original ocean signature is not preserved (Kaufman and Knoll, 1995). To determine the relation between depositional facies and isotope values in the Al Aziziyah Formation, carbon and oxygen isotope data (Fig. 3.9A and B) were plotted and keyed to facies.

III.1.8.3.1.1 Peritidal facies

The peritidal facies in both sections has a wide range of positive and negative δ^{13}C and δ^{18}O values, from -4.4 to +3.9‰ and -7.8 to +0.5‰, respectively. As discussed previously, the Ghryan Dome section has many peritidal samples with heavy oxygen values associated with the evaporites in this facies. The Ghryan Dome section also shows peritidal facies with a wide range of positive and negative δ^{18}O values, interpreted as due to less evaporation and a greater freshwater diagenesis during deposition of some intervals. The δ^{13}C values in the peritidal facies at the Ghryan Dome section are mostly

positive (Fig. 3.9A). Although freshwater diagenesis also can result in low $\delta^{13}C$, freshwater diagenesis would likely result in low, rather than high, $\delta^{18}O$. The lowest $\delta^{13}C$ values are in sequences 3 and 6 (Fig. 3.3 and 3.8). Peritidal facies at the Kaf Bates section (Fig. 3.9B) are less abundant than in the Ghryan Dome section (Fig. 3.9A) and do not show the heavy $\delta^{13}C$ and $\delta^{18}O$ values seen in similar facies in the Ghryan Dome section. As previously discussed, the light $\delta^{13}C$ and $\delta^{18}O$ values in both sections are likely due to freshwater diagenesis.

III.1.8.3.1.2 Ramp crest barrier facies

Ramp crest barrier facies is ooid-skeletal-pelletal packstone-grainstone with isotope values ranging from -7.8 to +3.4‰ for $\delta^{13}C$ and -7.5 to -0.1‰ for $\delta^{18}O$. In the Ghryan Dome section, carbonates from this facies have high oxygen isotope values (close to 0‰) and depleted carbon isotope values relative to Triassic brachiopod shells, suggesting that this facies formed during evaporite deposition. On the other hand, some carbonates from the ramp crest barrier facies of the Ghryan Dome section have low $\delta^{18}O$ and $\delta^{13}C$ values relative to contemporary brachiopods, indicating alteration during freshwater diagenesis. The heavy $\delta^{13}C$ may be due to increased productivity, as evidenced by deposition of organic-rich sediment at northern sections of the Al Aziziyah Formation and/or admixing of aragonite-rich sediment. Carbonates of the ramp crest barrier facies at the Kaf Bates section have very low δ18O values and a wide range of ^{13}C-enriched and ^{13}C-depleted $\delta^{13}C$ values (Fig. 3.9B). The heavy $\delta^{18}O$ and light $\delta^{13}C$ values are due to evaporite formation, which is associated with this facies.

83

III.1.8.3.1.3 Shallow subtidal facies

This facies consists of thin-medium beds of bioturbated skeletal packstone-wackstone-mudstone with ^{13}C-enriched and ^{13}C-depleted δ^{13}C values but with only depleted δ^{18}O isotopic values in both sections (Fig. 3.9 A and B). At the Kaf Bates section, this facies only has high δ^{13}C values and a wide range of δ^{18}O values (Fig. 3.9A). In both sections, the δ^{13}C and δ^{18}O values of this facies range from -3.1 to +3.7‰ for δ^{13}C and from -9.3 to -0.1‰ for δ^{18}O (Table 3.1). The light oxygen and carbon values are due to freshwater diagenesis.

III.1.8.3.1.4 Deep subtidal facies

This facies, with medium-thick beds of calcisiltite with hummocky cross-stratification, mechanical laminations and local chert layers interbedded with pelletal wackstone or lime mudstone, has high δ^{13}C and low δ^{18}O isotopic values at the Ghryan Dome section (Fig. 3.9A). For the Kaf Bates section the facies shows a strong correlation between δ^{13}C and δ^{18}O values (R^2=0.92). This strong correlation implies a single-phase alteration pattern (e.g., Hudson, 1977; Fig. 3.9B). In both sections, the δ^{13}C and δ^{18}O values of this facies range from -2.9 to +3.2‰ for δ^{13}C and from -7.4 to -1.6‰ for δ^{18}O. The high δ^{13}C values in deep subtidal facies may be related to the deposition of organic-rich sediment within northern sections of the Al Aziziyah Formation or to the preservation of the original marine signal. The light δ^{18}O and δ^{13}C values in this facies are likely produced by freshwater diagenesis.

III.1.8.3.2 Summary

The differences and similarities in isotopic data between both sections of the Al Aziziyah Formation may be related to differences and similarities in lithology between the sections. The Ghryan Dome section is dominated by dolomitized peritidal facies with evaporites. However, the Kaf Bates section has much less peritidal facies and evaporites. The carbon isotope values at the Ghryan Dome section were likely decrease due to freshwater diagenesis and environmental restriction as indicated by the evaporites within the peritidal facies. The ^{18}O-enriched carbonates at the Ghryan Dome section were produced during the formation of evaporites within the peritidal facies. The flushing of freshwater with soil CO_2 and lithology differences most likely controlled the isotope distribution within the measured sections. The isotopic correlation with facies for the Ghryan Dome (Fig. 3.9A) and Kaf Bates sections (Fig. 3.9B) suggests that the isotopic values were influenced by facies and thus depositional environment, particularly in the Ghryan Dome section, where peritidal and barrier facies show high δ^{18}O values and a wider range of negative δ^{18}O values.

III.1.8.4. Carbon isotope correlation and relative sea-level changes

III.1.8.4.1. Carbon isotope correlation

The carbon isotope curves of the Ghryan Dome and Kaf Bates sections were correlated within detailed sequence stratigraphic cross sections from south to north (Fig. 3.8) in the Al Aziziyah formation. The base of sequence 3 at the Ghryan Dome and the base of sequence 3 at the Kaf Bates have the shallowest facies, with the most similar δ^{13}C values

and patterns in both sections. These changes in $\delta^{13}C$ values (at the base of sequence 3 in both sections), which occur during the same period, can be correlated and the base of these sequences is used as the datum for this chemostratigraphic correlation between the Ghryan Dome and Kaf bates sections. Based on carbon isotope variations (Fig. 3.8), the correlation between the Ghryan Dome and Kaf Bates sections indicates five coincident sequences (Sequences 3-7) of $\delta^{13}C$ depletion and enrichment (Fig. 3.8).

Sequence 3 from the Ghryan Dome and Kaf Bates sections shows a gradual up-section decline of $\delta^{13}C$. This $\delta^{13}C$ decrease is associated with transgressive system tracts (TSTs) and highstand system tracts (HSTs). Peritidal facies dominate sequence 3 at the Ghryan Dome section, whereas peritidal facies are less abundant in sequence 3 at the Kaf Bates section. Therefore, sequence 3 at the Ghryan Dome and Kaf Bates sections is interpreted as an approximate timeline based on carbon isotope variation. Sequence 4 at the Ghryan Dome and Kaf Bates shows a gradual increase in $\delta^{13}C$ values. This increase is not consistent with highstand system tracts (HSTs) and with transgressive system tracts (TSTs) in the sections. Sequence 5 at the Ghryan Dome and Kaf Bates sections shows gradual $\delta^{13}C$ decline. This decline is consistent with transgression and highstand system tracts. Sequences 6 and 7 at the Ghryan Dome and Kaf Bates sections indicate the gradual decrease and increase of $\delta^{13}C$ values in both sections (Fig. 3.8).

The carbon isotope correlation (Fig. 3.8) suggests that sequences 1 and 2 at the Ghryan Dome section are not exposed at the Kaf Bates section and that sequences 8 and 9 at the Kaf Bates section are not exposed at the Ghryan Dome section. Several studies indicate

that the Al Aziziyah Formation at the Ghryan Dome section is the most completely exposed section, with an exposed lower and upper contact (Desio et al., 1960; Desio et al., 1963; Magnier 1963; Asserto and Benelli, 1971; Fatmi, 1977; Hammuda et al. 1985, Sebat, 2008). However, toward the north, the upper contact is not exposed, and it becomes difficult to see the lower contact (Desio et al., 1960; Desio et al., 1963; Magnier 1963; Asserto and Benelli, 1971; Fatmi, 1977; Hammuda et al. 1985, Sebat, 2008). In this study, the lower and upper contacts are clearly exposed at the Ghryan Dome section and are not exposed at the Kaf Bates section. The upper contact at the Ghryan Dome section is a major unconformity overlain by phosphatic beds. The development of this unconformity may explain why sequences 8 and 9 at the Kaf Bates section are not recorded at the Ghryan Dome section.

III.1.8.4.2 Relative sea level changes with $\delta^{13}C$

Lateral variations in $\delta^{13}C$ can be recorded in stratigraphic profiles during the rise and fall of local sea-level (e.g., mixing of open ocean and restricted platform water masses, Immenhauser et al., 2002; Immenhauser et al., 2003; Fanton and Holmden, 2007). During times of a high relative sea level, carbonate platforms are flooded and the carbonate factory is turned on (Swart and Eberli, 2005). Transgressive systems tracts (TSTs) and relative sea-level rises are associated with positive shifts of the $\delta^{13}C$ curve, and highstand systems tracts (HSTs) and relative sea-level falls are associated with negative shifts of the $\delta^{13}C$ curve (Immenhauser et al., 2003; Swart and Eberli, 2005 Fanton and Holmden, 2007). In addition, storing much organic matter in marginal areas

results in the local enrichment of ^{13}C. However, during the subsequent sea level fall, the stored organic matter is eroded and oxidized, resulting in ^{12}C increase in deep basins (Broecker, 1982; Hajikazemi et al., 2012). Therefore, δ^{13}C values and associated changes can indicate eustatic sea-level changes.

 Shallow carbonate platforms may reflect local alterations rather than global ocean signatures (Holmden et al., 1998; Immenhauser et al., 2003; Swart and Eberli, 2005). The Ghryan Dome facies show some evidence of exposure surfaces (e.g., top of sequence 5, top of sequence 7, Fig. 3.3); these boundaries record low δ^{13}C values. This decline is commonly due to meteoric water associated with light CO_2. However, oxygen isotope values were low in both sections. Oxygen isotope data also recorded enriched values at the Ghryan Dome section (e.g., top of sequence 5 to sequence 7, Fig. 3.3) associated with peritidal facies. The carbon isotope data for the shallow carbonate in the Al Aziziyah Formation were affected by meteoric water charged with light soil CO_2 at a few exposure surfaces (e.g., Fig. 3.3; top of sequences 3, 5 and 7). The carbon isotope curves of the Al Aziziyah Formation do not show positive shifts in all or even most interpreted transgressive systems tracts (Fig. 3.8, see sequences 4 and 6 in both sections). Similarly, these curves also do not show an increasingly negative trend in all interpreted highstand systems tracts (Fig. 3.8 see sequence 4 in both sections) within the Al Aziziyah cross section (Fig. 3.8). In this study, the overall relation observed between the sequence stratigraphy and δ^{13}C at both sections suggests that sea-level fluctuations are not the dominant mechanism governing changes in δ^{13}C on this ramp. The Al Aziziyah Formation carbon isotope record was affected by freshwater diagenesis and by lithologic

(environmental) variations (e.g., an abundance of evaporite in some facies), suggesting that changes in its stable carbon isotope curve may dominantly reflect local diagenetic processes rather than global change (e.g., Holmden et al., 1998; Immenhauser et al., 2003; Patterson and Walter, 1994; Hajikazemi et al., 2012).

III.1.8.4.3 Comparison with the Tethyan δ^{13}C Triassic reference curve

and global correlations

Carbon isotope values obtained from whole rock carbonate samples are often used as a proxy for the δ^{13}C of seawater because δ^{13}C, in contrast to δ^{18}O, is more resistant to diagenetic alteration, i.e., high fluid/rock ratios are required to significantly change the δ^{13}C value of carbonate sediments during diagenesis (Grotzinger et al., 2011). The reconstruction of the Triassic δ^{13}C stable isotope curve, which is based on articulate brachiopods (Korte et al., 2005), is currently the most reliable data set (Preto et al., 2009). Therefore, the whole rock carbon isotope curve from the Middle–Late Triassic Al Aziziyah Formation were compared with this proposed global δ^{13}C curve to achieve different goals (e.g., to evaluate the age of the Al Aziziyah Formation). The

Middle–Late (Ladinian-Carnian) Triassic part of the global carbon-isotope curve is relatively stable, with a gradual increase in δ^{13}C from approximately 0 to 2‰ in the Ladinian to approximately 3-4‰ in the Carnian. This increase is followed by a plateau in the δ^{13}C data at approximately +3.5‰ in the Carnian-Norian, followed by a gradual decrease to values of +1-2 during the Norian-Rhaetian (e.g., Korte et al., 2005; Preto et al., 2009). The δ^{13}C curve of the Al Aziziyah Formation shows multiple rise and decline

throughout the Ghryan Dome section (Fig. 3.10). The δ^{13}C curve of the Al Aziziyah Formation can be divided into five parts (Fig. 3.10). The first part of the curve has gradual increase through sequence 2; the second part has rapid decline through sequence 3 followed by a gradual increase (third part) from sequence 4 to the lower part of sequence 5; the fourth part of the curve has gradual depletion from the lower part of sequence 5 to the lower part of sequence 6, and the fifth part has increased from the lower part of sequence 6 to the upper part of sequence 7. Most of the depleted intervals of the δ^{13}C curve are associated with peritidal and barrier facies (Fig. 3.3). However, the lower part of the δ^{13}C curve of the Al Aziziyah Formation has a clear gradual increase, whereas the upper part of the curve is more variegated, with multiple carbon excursions. These multiple carbon excursions are likely due to restriction of the Carnian ocean circulation (as discussed earlier) as indicated by clastic material, evaporite, sandy limestone, and dolomites particularly in the upper part of the Al Aziziyah Formation (Fig. 3.3). Indeed, many decreases in δ^{13}C from the upper part of the curve are associated with abundant peritidal and barrier facies with evaporite or with exposure surfaces (e.g., peritidal and tidal sandstone facies at sequence 6, Fig. 3.3).
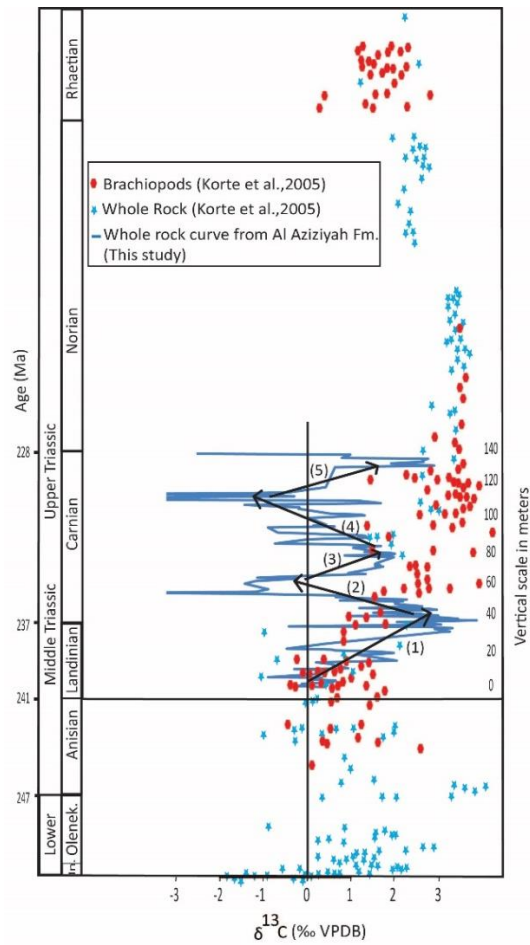
Fig. 3.10. The whole rock carbon isotope curve from the Middle–Late Triassic Al Aziziyah Formation compared with the proposed global δ13C (Korte et al., 2005). The results indicate five parts: (1) gradual increase through sequence 2; (2) rapid decrease through sequence 3; (3) gradual i from sequence 4 to the lower part of sequence 5; (4) gradual depletion from the lower part of sequence 5 to the lower part of sequence 6; and (5) enrichment from the lower part of sequence 6 to the upper part of sequence 7.

Therefore, the Al Aziziyah Formation δ^{13}C chemostratigraphic curve can be partially correlated with the proposed Triassic global δ^{13}C curve (Fig. 3.10, Korte et al., 2005). The lower part of the Al Aziziyah Formation δ^{13}C curve correlates well with the Ladinian to the lower Carnian part of the proposed global δ^{13}C curve. However, the upper part of the Al Aziziyah Formation δ^{13}C curve does not correlate well with the

91

remaining Carnian of the proposed global δ^{13}C curve most likely due to restriction in the Carnian ocean circulation and the subsequent diagenetic modification of the stable isotope values. This correlation indicates that the Al Aziziyah Formation was deposited during the Ladinian and during part of the Carnian stage (Fig. 3.11).
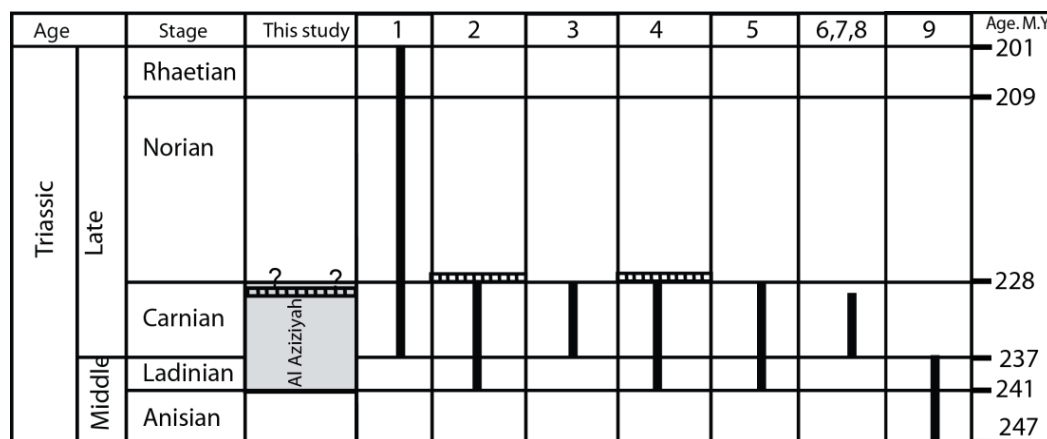
Fig. 3.11. Overview of the previous depositional age interpretations for the Al Aziziyah Formation. Columns 1-9 show different studies that indicate that the age of the Al Aziziyah Formation is disputed. The dashed line represents major unconformity between the Al Aziziyah and Abu Shaybah Formations. The correlation between the δ^{13}C curves from the Al Aziziyah Formation and the global proposed δ^{13}C curve indicates that the age of the unit may range from Ladinian to Carnian. The time scale is from Gradstein et al. (2012).

III.1.9 Conclusions

Samples of the Middle-Late Triassic Al Aziziyah Formation Ghryan Dome and Kaf Bates sections in northwest Libya were analyzed to determine their stable isotope chemostratigraphy. The isotope data were integrated into the detailed sequence stratigraphy of this unit. Seven sequences within the Ghryan Dome have been identified based on facies stacking patterns, field observations and stable carbon isotopes. The correlation between the Ghryan Dome and Kaf Bates sections indicates five sequences (sequences 3-7) of δ13C depletion and enrichment. The Ghryan Dome section has a wider δ13C range (-7.8 to +3.9‰) than the Kaf Bates section (-3.2 to +3.7‰). The Ghryan Dome section also shows a wider range in δ18O (-9.3 to +0.5‰ versus -8.2 to -1.5 ‰).

Isotope values of the Al Aziziyah carbonate rocks are partially controlled by their facies. For example, carbonates from the peritidal facies in the Ghryan Dome section have the highest oxygen isotopic values suggesting evaporative enrichment of ^{18}O in waters. This interpretation is supported by the abundances of evaporites within the peritidal facies. In another example of facies influence, δ^{18}O and δ^{13}C values in carbonates from the deep subtidal facies in the Kaf Bates section show a strong positive correlation suggesting a simple, single phase of meteoric diagenesis altering the original marine signal. In addition, high productivity during the deposition of the Al Aziziyah Formation and/or the abundance of aragonite mixing with calcite are the most likely causes of the local δ^{13}C enrichment relative to the general δ^{13}C curve for brachiopod shells.

Ocean circulation during the Carnian was restricted in some parts of the basin as indicated by abundant sandstone and evaporites within the upper part of the Al Aziziyah Formation. Therefore, the δ^{13}C curve of the Al Aziziyah Formation shows similar patterns with the late Middle Triassic (Ladinian) portion of the global δ^{13}C curve based on brachiopod and whole rock data. These data indicate that this unit was likely deposited during the Ladinian and part of Carnian stages.

CHAPTER IV

DIAGENESIS OF THE MIDDLE-LATE TRIASSIC AL AZIZIYAH

FORMATION, JIFARAH BASIN, NORTHWEST LIBYA

IV.1 Overview

The Middle-Late Triassic (Ladinian-Carnian) Al Aziziyah Formation was deposited on a gently sloping carbonate ramp in the Jifarah Basin of northwest Libya and consists of gray limestone, dolomite, and dolomitic limestone interbedded with minor shale. Facies of the Al Aziziyah Formation ramp are interpreted from shallowest to deepest as: tidal sandstone; peritidal carbonate; pellet-ooid shoal; shallow subtidal carbonate; deep subtidal carbonate; and basinal black carbonate mud and shale. Two measured sections (Ghryan Dome and Kaf Bates) of the Al Aziziyah Formation within the Jifarah Basin were extensively sampled to describe the diagenetic processes and sequence of paragenetic events that affected the Middle–Late Triassic Al Aziziyah carbonate facies and to determine if these diagenetic features are related to the mega-monsoonal climate of the Triassic. The diagenetic events of the Al Aziziyah Formation were determined by thin section petrography, cathodoluminescence (CL) microscopy, stable isotope, and trace element analyses. The diagenetic events in the Al Aziziyah Formation are 1- Early (syndepositional), which include micritization, type one (D_1) dolomite and isopachous fibrous cements); 2- Intermediate (dissolution, blocky calcite cement, neomorphism, physical compaction and type two(D_2) dolomite; and 3- Late including (pore filling blocky calcite cement, silica, stylolitization, type three (D_3) dolomite and fracturing.

Carbon isotope values of the late calcite cement and pore-filling dolomite cement (D_3) range from -1.5 to -0.9‰ and -1.3 to +1.8 respectively, and oxygen isotope values of the calcite and pore-filling dolomite cements range from -6.2 to -4.3‰ and -7.6 to -4.1 respectively, indicating lighter dolomite cement than calcite cement.. Three types (D_1-D_3) of dolomite occur within the Al Azizyah Formation. D_1 is very fine- to fine-crystalline (≤50 µm crystal diameter) and preserves depositional fabric well. D_2 is coarse crystalline dolomite (100 to 300 µm crystal diameter) that destroyed the depositional fabric and some crystals have a clear outer rim surrounding a precursor cloudy coarse dolomite core. D_3 is a coarse to very coarse dolomite that formed last in a shallow burial environment. Diagenesis lowered the carbon and oxygen isotope values of whole rock and cement from the Al Aziziyah carbonate and introduced a strong correlation between $\delta^{13}C$ and $\delta^{18}O$ values within the deep subtidal carbonate facies of the Kaf Bates section. Peritidal facies have more positive $\delta^{18}O$ values at the Ghryan Dome section due to evaporation. This diagenetic analyses indicates the Al Aziziyah Formation: 1) experienced early marine syndepositional, meteoric and shallow burial cements; 2) dolomite type one, dolomite type two and dolomite type three were likely formed by microbial in early stage, seepage reflux in intermediate stage and burial in late stage respectively; and 3) an arid climate is indicated from the abundance of evaporite nodules, and dissolution and meteoric cements were likely produced by the low rainfall patterns consistent with a monsoonal climate.

IV.1.1 Introduction

The Triassic was a period of global transition associated with the beginning of the break-up of the Pangea supercontinent and the development of Mesozoic basins, in a globally warm, dry climate (Frakes et al., 1992; Dercourt et al., 1993; Lucas, 1998; Golonka and Ford, 2000; Reinhardt and Ricken, 2000; Boucot and Gray, 2001). The Triassic climate was characterized by non-zonal atmosphere patterns, dictated by a strong global monsoon system whose effects are most evident in the Tethys realm (Preto et al., 2010). A monsoon climate is one in which most of the rainfall is during the summer (Parrish, 1993). The important feature of monsoonal circulation is cross equatorial flow, which results from the thermal and pressure contrasts between the winter and summer hemispheres, and is driven mainly by sensible heat (Parrish, 1993). Monsoonal climate can leave a record in coeval facies such as sandstone and evaporite. Regional facies comparisons should show that humidity in the equatorial regions of the east (western Tethys) was lower than in the west (e.g., Colorado Plateau; Dubiel et al., 1991). This indicates more monsoonal climate effect in the equatorial regions of the western Tethys than in the equatorial regions of the east Tethys.

Several studies explained how sediments formed under extremely variable climate condition related to a monsoonal climate (Frisia-Bruni et al., 1989; Frisia, 1991). For example, Triassic shallow marine carbonate strata in the Alps deposited in the eastern equatorial region of Pangea reflect changing depositional environments ranging from carbonate platform to siliciclastic deltaic systems. In addition, a diagenetic study from

97

the Dolomia Principale, Italy, shows multiple phases of dolomite and highly evaporative conditions (Frisia, 1994).

The Jifarah Basin of northwest Libya (Fig. 4.1A and B) was penetrated by numerous wells which record Paleozoic to Jurassic sediments (Hallett, 2002; Abohajar et al., 2009) and has over 1.5 km of Triassic marine and non-marine deposits (Parona 1914; Desio et al., 1960; Desio et al., 1963; Magnier, 1963; Asserto and Benelli, 1971; Fatmi 1977: Hallett 2002). The Middle-Late Triassic carbonate facies are the Al Aziziyah Formation (Desio et al. 1960; Desio et al. 1963; Magnier 1963; Asserto and Benelli 1971; Fatmi, 1977). Al Aziziyah Formation consists of massive grey limestone, dolostone and dolomitic limestone with rare interbedded shale to the north. Thin anhydrite and oolitic horizons also were described (Hammuda et al., 2000). The Al Aziziyah Formation contains an abundant algal and pelecypod fauna (Assereto and Benelli, 1971; Muttoni et al., 2001; Hallett, 2002). The lower boundary of the Al Aziziyah Formation (Fig. 4.2) is the first appearance of marine limestone beds overlying non-marine sandstone of the Kurrush Formation as observed at the Ghryan Dome. The upper boundary of the Al Aziziyah Formation is a sharp unconformable surface with overlying rusty colored continental sandstone of the Abu Shaybah Formation (Fatmi, 1977; Asserto and Benelli 1971; Magnier, 1963; Desio et al., 1963; Desio et al., 1960; Burollet, 1963; Muttoni et al., 2001). Locally the base of the Abu Shaybah Formation contains phosphate clasts and nodules at the Ghryan Dome section. Two stratigraphic sections from the Al Aziziyah Formation in northwest Jifarah Basin (Figs. 4.1C) were measured bed-by-bed. This study describes the diagenetic processes and sequence of diagenetic events that affected

the Middle–Late Triassic Al Aziziyah carbonate facies to understand its diagenesis events and to determine if these diagenetic features can be related to the mega-monsoonal climate of the Triassic.
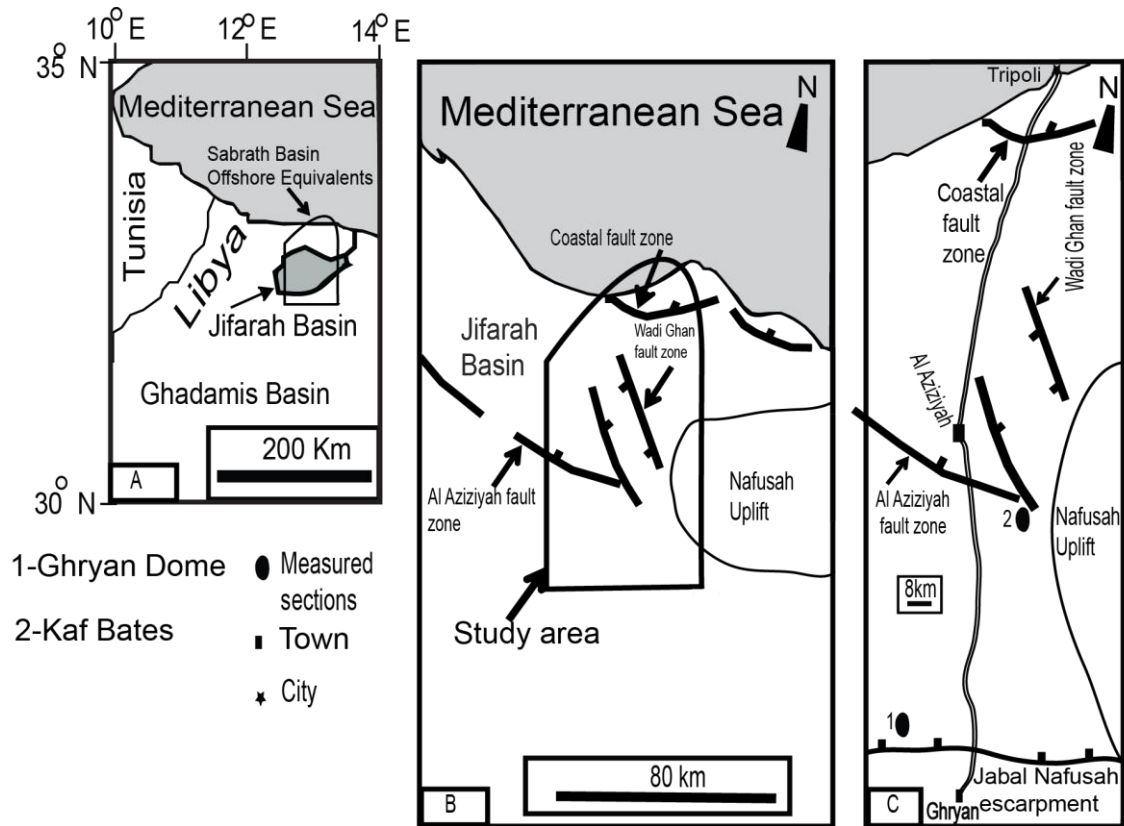
Fig. 4.1. A- Index map of the Jifarah Basin northwest Libya. B- Detailed map of the structural setting of the area. C- Location of measured stratigraphic sections. Ghryan Dome (1), Kaf Bates (2). The Ghryan Dome section was deposited on the southern margin of the Jifarah Basin, whereas Kaf Bates section was deposited down ramp in a more subtidal location in the basin.

Age		Stage	Formations	Units
Triassic	Late	Norian	Abu Shaybah	
		Carnian	Al Aziziyah	
	Middle	Ladinian		
		Anisian	Kurrush	

Fig. 4.2. Stratigraphic column of the middle-Late Triassic units in the study area (Modified after Swire and Gashgesh 2000 and Moustafa et al., 2014).

IV.1.2 Geological setting

The Jifarah Basin encompasses an area of 1500 km^2 in northwestern Libya (Fig. 4.1B), bounded by the Nafusah uplift to the south and the offshore Sabrath Basin to the north (Hallett, 2002; Abohajar et al., 2009). The Jifarah escarpment extends 400 km from southern Tunisia to southwest Libya, and marks the southwestern limit of outcrops in the Jifarah Basin (Fig. 4.1). The Jifarah Basin formed at the eastern end of the south Atlas lineament, which defines the southern margin of the Atlas fold belt that extends from Morocco to Tunisia (Dewey and Burke, 1973) where it branches to extend into northwest Libya as the Jifarah Arch (Anketell and Ghellali, 1991).

The Jifarah Basin is situated at the junction of two major structures: the north-northwest trending Tripoli-Tibesti Arch, which formed in the Caledonian, and the east-west trending Jifarah Arch, which formed as a result of Hercynian deformation (Anketell and Ghellali, 1991; Abohajar et al., 2009; Swire and Gashgesh, 2000). The structural pattern of the Jifarah Basin was created by these Paleozoic structural trends (Anketell and Ghellali 1991; Abohajar et al. 2009; Hallet 2002) but, subsequent subsidence of the Jifarah Basin continued into the Early and Late Triassic (Muttoni et al. 2001).

The Jifarah Basin is bounded to the south by the east-west oriented subsurface Al Aziziyah fault zone. Toward the east, the Al Aziziyah fault links to the Wada Ghan fault zone (Arkell et al., 1957; Swire and Gashgesh, 2000; Raulin et al., 2011). The Al Aziziyah fault was active during the Triassic (Swire and Gashgesh, 2000; Raulin et al., 2011), and parallels the Paleozoic structures.

The age of the Al Aziziyah Formation is disputed (Fatmi 1977; Asserto and Benelli, 1971, Magnier 1963; Desio et al., 1963, Desio et al., 1960, Burollet, 1963, Muttoni et al., 2001). The occurrence of "Mojsisovicsites" ammonites in the upper part of the Ghryan Dome section (Fatmi, 1977) suggests the Al Aziziyah Formation was deposited during the Carnian. This ammonite genus ranges from Carnian to Anisian and also occurs in the Alps, Spain, Sardina, Himalaya and parts of the USA (Fatmi, 1977). However, the abundance of microflora including miospore taxa infernopollenites spp., Crassicappites spp., Parillinites spp., pseudenzonalasporites summus suggests a Late Triassic (Carnian to Rhaetian) range for the Al Aziziyah Formation (Swire and Gashgesh, 2000). Ammonites in the upper part of the Al Aziziyah Formation (El Hinnawy and Cheshitev, 1975; Mapnier, 1963) and its whole-rock carbon isotope data indicate this unit was deposited during the Ladinian to Carnian (Figs. 4.2 and 4.3, Moustafa et al., 2014).
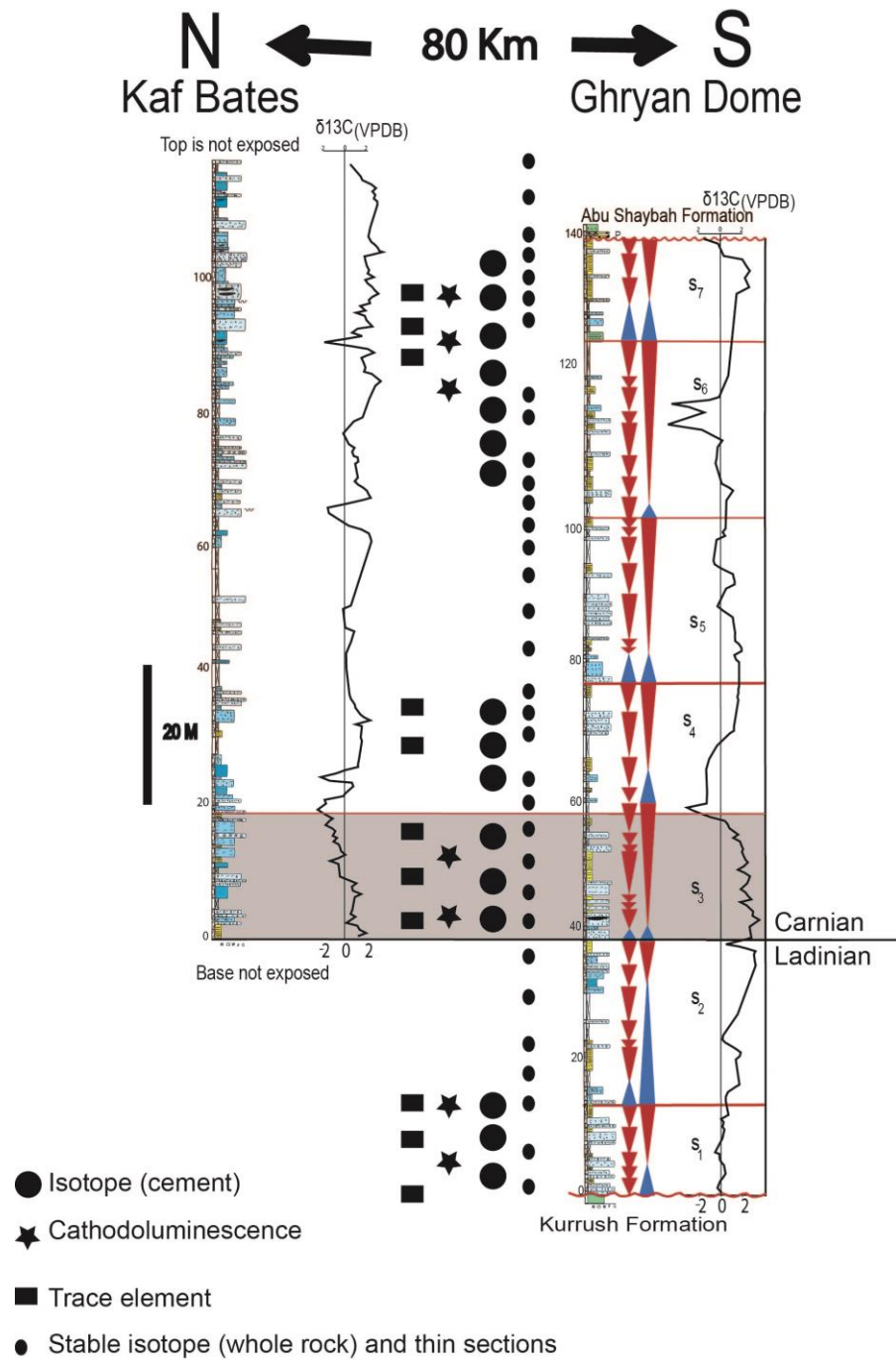
Fig. 4.3. Two measured sections of the Al Azizyah Formation with sample locations. The gray areas indicate the chemostratigraphically based correlation between the Ghryan Dome and Kaf Bates sections.

IV.1.3 Depositional environments

The Middle-Late Triassic Al Aziziyah Formation in the study area is composed of both carbonate and siliciclastic rocks. Based on field relationships and petrographic studies, five carbonate facies associations (Fig. 4.4; Table 4.1), and one siliciclastic lithofacies were identified (Fatmi, 1977; Asserto and Benelli, 1971; Magnier, 1963; Desio et al., 1963; Desio et al., 1960; Burollet, 1963, Muttoni et al., 2001; Moustafa et al., 2012; 2014). The facies (Fig. 4.5) from shallowest to deepest are: tidal sandstone, peritidal carbonate, pellet-ooid ramp crest barrier, shallow subtidal carbonate, deep subtidal carbonate and basinal carbonate mudstone and shale. A brief description and interpretations of the sediment types in all facies is given below, arranged from shallowest to deepest (Moustafa et al., 2014). More detailed descriptions and interpretations of the Al Aziziyah Formation facies are in Table 4.1 and Moustafa et al., (2012; 2014).

Table 4.1 Description of the Al Aziziyah Formation facies.

Facies type (Lithofacies)	Description	Sedimentary structures	Fossils	Depositional environment
Sandstone	Red to yellow fine-medium sandstone. A few meter thick beds. Well rounded quartz grains with silica cement.	Bidirectional cross-bedding	none	Tidal environment indicates marine setting. The red color indicates iron oxidization.
Carbonate mudstone	Tan to yellowish. Units few meters to ten meters thick with evaporite nodules, chert, planar and domal stromatolites.	Mudcracks, microbial laminations, intraclasts	Bioturbated to laminated beds of algae and stromatolites.	Peritidal environment
Pellet packstone/ grainstone	Gray to dark color. Beds up to five meters in thickness. Pellets packstone to grainstone. Grapestone intraclasts and ooids with radial crystal structure. Primary fabric was originally calcitic ooid and composite ooid. Pellets are rod-like in longitudinal view, round in transverse section and have relatively large and uniform size.	Massive to mechanically laminated beds	Bioturbation beds, gastropod, brachiopods and unidentified fossil fragments	Ramp crest barrier or shoal
Pellet, skeletal packstone/ wackestone/ mudstone	Bed thickness from one to three meters. Dark gray with different cement types (rimming calcite, blocky or equant spar dolomite (equant spar), pore-filling dolomite and silica).cherty layers and nodules.	Massive to bioturbated beds	Bioturbated beds, of pellets and skeletal fossils brachiopods and gastropods, and other unidentified fossil fragment	Shallow subtidal
Calcisiltite	Thickness from a few meters to six meters. Light to dark, with cherty layers and nodules, few pellets.	Massive to mechanical laminations and stylolites	Fossils are rare in this facies.	Deeper subtidal, more abundant in the northern sections.
Carbonate mudstone, black shale	Light to dark gray. The mudstone ranges in thickness from half to one meter. The black shale is very thin organic-rich sediment.	Massive beds	Few unknown fossils.	Basinal environments only in northern sections
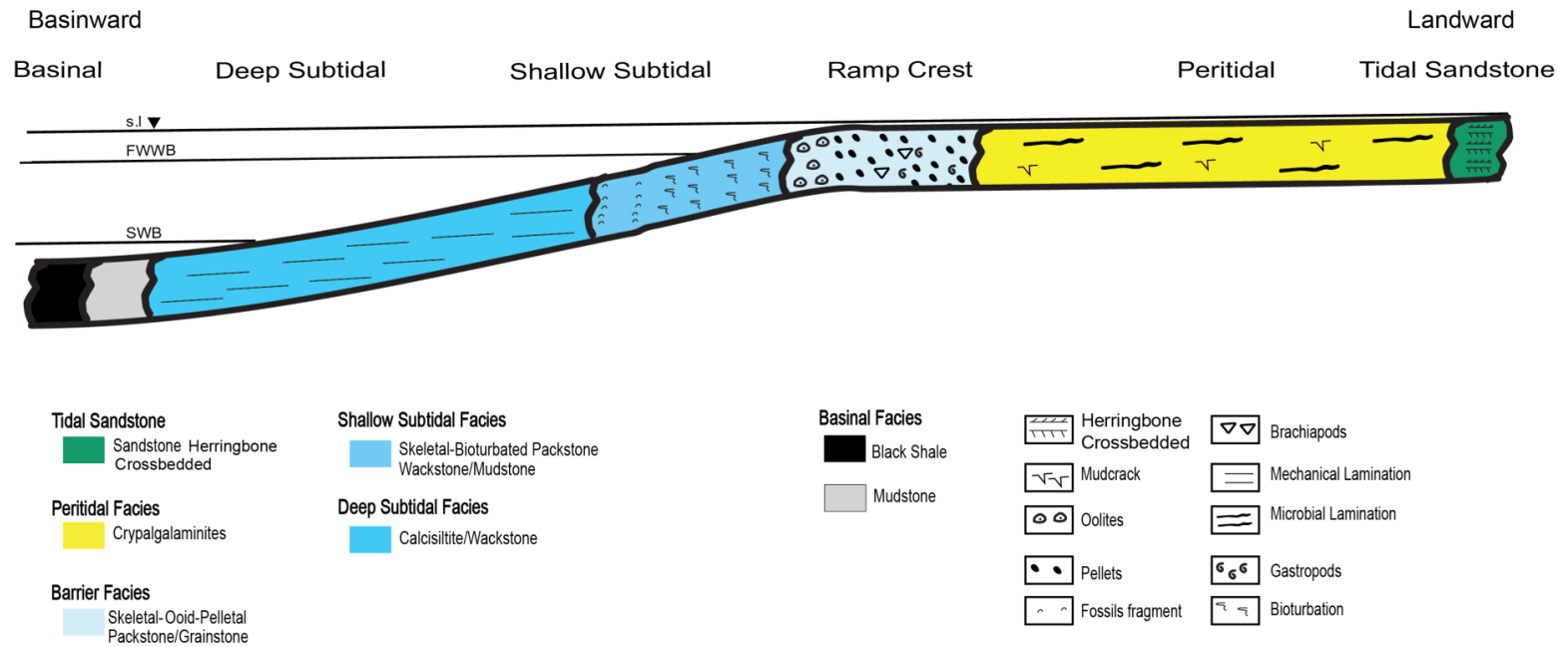
Fig. 4.4. Conceptual depositional model of Middle-Late Triassic Al Aziziyah Formation showing spatial relationship of facies across the low relief homclinal ramp. S.l = sea level; FWWB = Fairweather Wave Base; SWB = Storm Wave Base.

IV.1.3.1 Tidal sandstone

This facies (Fig. 4.5A) contains bidirectionally crossbedded red sandstone beds, which are 2 meters thick and composed primarily of well-rounded, well-sorted medium sand grains recording high-energy siliciclastic deposition by tidal currents (Hammuda et al., 1985). This facies occurs only at the Ghryan Dome section.

IV.1.3.2. Peritidal carbonate

This carbonate facies (Fig. 4.5B) is composed of dolomitized light tan to yellowish cryptalgalaminites, microbial laminites and stromatolites and commonly contains well–developed mudcracks, and chert nodules. Planar cryptalgalaminites and small microbial domes are the most abundant sedimentary structures in this unit and primarily occur in the Ghryan Dome section. Pellets occasionally are trapped in the microbial laminations. The abundance of evaporites, mudcracks and a lack of burrowing suggests that this facies was deposited in a semi-arid to arid climate. This facies represents the shallowest water carbonate deposition in the Al Aziziyah Formation.

IV.1.3.3. Ramp crest barrier carbonate

The ramp crest facies is characterized by ooid-skeletal-pelletal packstone-grainstone (Fig. 4.5C), containing irregular gray chert layers. The pellets are up to 2 mm, without clear orientation, rod-like in the longitudinal section, circular in the transverse section and are relatively uniform. Beds of this facies range in thickness from less than one meter to almost two meters. The skeletal fragments in this facies are brachiopods,

gastropods and small unidentified bioclastic fragments. In some sections, these shell fragments are locally mixed with ooids to form grapestone. Most of the oolites have a radial internal structure or are composite ooids, containing more than one ooid grain. Oolites show radial and concentric layers (Ferguson & Ibe, 1981; Ferguson, 1987). The oolitic nuclei commonly are skeletal fragments and non-skeletal grain nuclei most commonly are pellets. The pelletal-ooid packstone/grainstone facies record high-energy depositional conditions along the ramp crest that separated restricted evaporitic facies to the south from the open-marine conditions to the north.

IV.1.3.4 Shallow subtidal carbonate

This facies consists of thin-medium beds (Fig. 4.5D) of bioturbated skeletal packstone-wackstone-mudstone in beds ranging up to one meter in thickness. Bioturbated, fine-grained, light to dark-gray mudstone and pelletal-skeletal wackestone are the most common lithologies in this unit. The bioturbation in this facies completely disturbed the bedding indicating a bioturbation index of 5-6 (Droser and Bottjer, 1986). This facies was deposited in shallow, well-oxygenated waters that promoted abundant bioturbation directly basinward of the ramp crest facies.

IV.1.3.5 Deep subtidal carbonate*:*

This facies consists of medium-thick beds (up to four meters thick) of laminated calcisiltite, with hummocky cross-stratification, mechanical laminations and local chert layers (Fig. 4.5E), interbedded with pellet wackstone or lime mudstone. These facies

were deposited within storm wave base and recorded alternating moderate to high–energy storm events interbedded with lower energy muddy background sedimentation.

IV.1.3.6 Basinal facies

These facies consists of thin-bedded mudstone layers interbedded with extremely thin black organic-rich shale. These facies only occur within the northernmost sections (e.g., Bu Arghop and Ras Lafa sections) and may substantially thicken toward the offshore portion of the Jifarah Basin (Abohajar et al., 2009).

IV.1.4 Methods

Two stratigraphic sections from the Al Aziziyah Formation in northwest Jifarah Basin (Figs. 4.1C and 4.3) were measured and sampled bed-by-bed. 320 thin sections from these two sections were etched with dilute HCl and stained with Alizarin Red and potassium ferricyanide solution (Dickson, 1966) for differentiation of calcite and dolomite (ferroan and non-ferroan) and studied by polarized and binocular microscopy. In addition, the cathodoluminescence of 50 polished thin sections was studied using a Technosyn Model 8200 MK II with an attached camera (Marshall, 1988; Tucker, 1988; Frank et al., 1995). Cathodoluminescent and petrographic analysis of thin sections identifies the diagenetic features, type of cements and their relative timing. A total of 287 whole rock matrix carbon and oxygen isotopic values were compared with the carbon and oxygen isotope values from 17 cement samples. Stable isotopic samples were analyzed in the Texas A&M Stable Isotope Geoscience Facility, College Station, Texas.
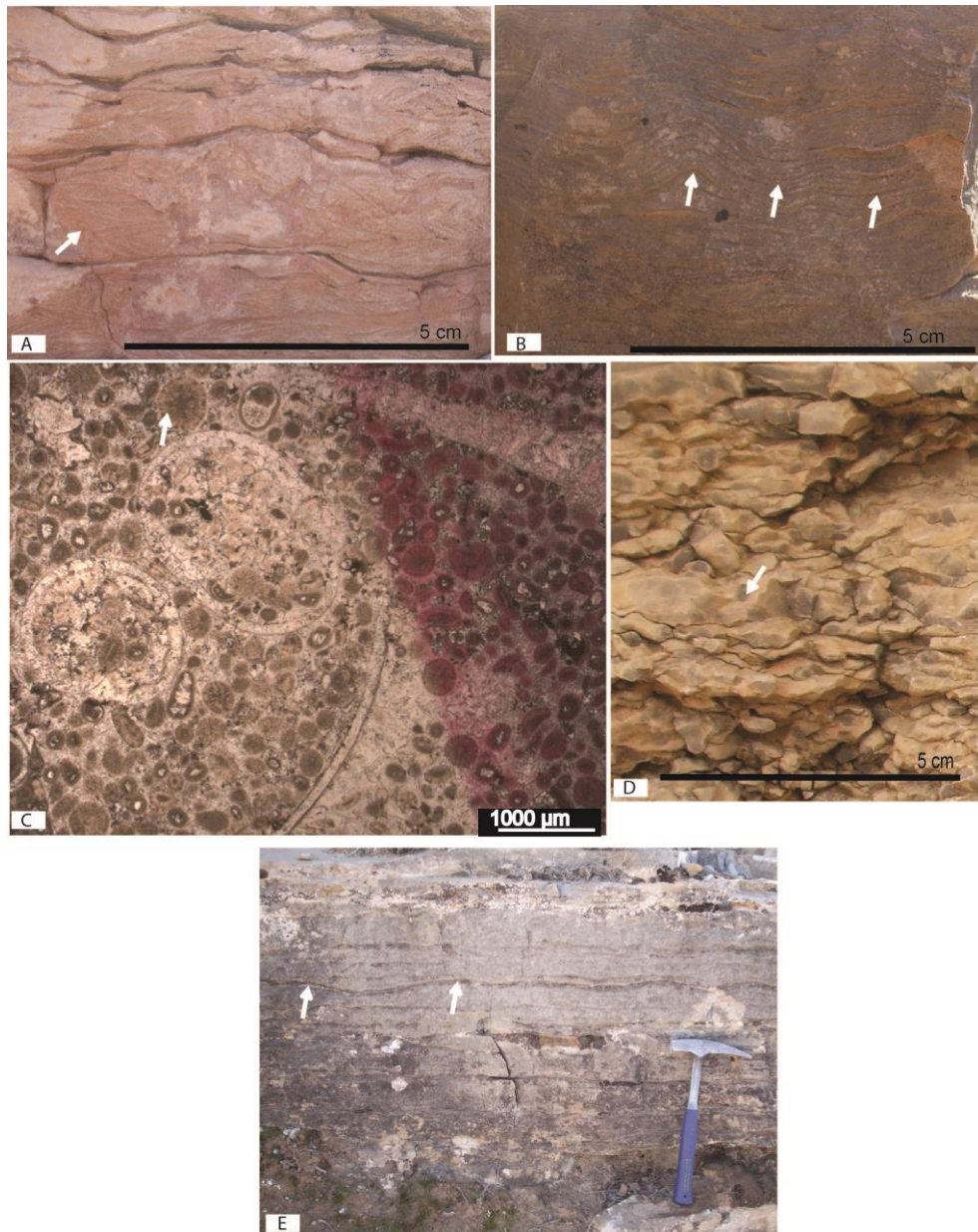
Fig. 4.5. Photographs (A, B, D and E) and photomicrograph (C) of Middle-Late Triassic Al Aziziyah Formation facies. A: Tidal Sandstone B: Peritidal, C: Barrier, D: Shallow Subtidal and E: Deep Subtidal. The picture and arrows show: A- Bidirectionally crossbedded red sandstone beds; B- Planar and domal cryptalgalaminites; C- ooid-skeletal-pelletal packstone-grainstone; D- bioturbation and E- Laminated calcisiltite, with hummocky cross-stratification and mechanical laminations.

In addition, trace elements for 70 calcite and pore-filling dolomite cement samples were analyzed at the Texas A&M Microprobe Laboratory.

Trace elements were determined on a four spectrometer Cameca SX50 electron microprobe at an accelerating voltage of 15 KV at a beam current of 50 nA, and at a beam diameter of 10 μm. The SX50 was equipped with Back Scattered Electron (BSE), Secondary Electron (SE) and cathodoluminescence detectors, as well as a Princeton Gamma Tech energy dispersive spectrometer (EDS). All quantitative analyses employed the wavelength-dispersive X-ray spectrometers (WDS). Analyses determined after standardization using very well characterized compounds or pure elements. Thin sections were coated with ~ 15 nm of high purity carbon prior to analysis to eliminate charging. BSE imaging determined out in atomic number mode at an accelerating voltage of 15 kV and a beam current of 10 nA using a 6-component BSE detector. The brightness of an object in this mode is directly proportional to the mean atomic number for a horizontal polished surface. Typical accuracy for major elements (> 10 wt. %) is about = +/- 1 to 2 % of the amount present; the uncertainty at low concentrations increases as the concentration decreases, with the uncertainty reaching 100% at the lower limit of detection (LLD). The lower limit of detection for most elements is typically100 to 1000 ppm and was calculated for all analyses.

IV.1.5 Diagenetic events, stable isotope geochemistry and elemental analysis

IV.1.5.1 Diagenetic events

The sequence of diagenetic events in a carbonate system depends on factors such as the sediment type, grain size and texture, mineralogy, nature of pore fluids and climate (Tucker and Wright 1990; Tucker 1993; Flugel 2004). Petrographic study of thin-sections and their cathodoluminescence indicate that the diagenetic processes in the Al Aziziyah Formation include micritization, cementation, dissolution, neomorphism, dolomitization, physical compaction, chemical compaction and fracturing (Fig. 4.6). Cements formed during early (syndepositional), intermediate and late diagenesis. Early cements are isopachous, fringing, and equant spar, intermediate cement is blocky calcite cement whereas, late cement is pore-filling dolomite and silica.

IV.1.5.1.1 Micritization

Micritization in the Al Aziziyah Formation affected many skeletal and non-skeletal particles including fossils, pellets and intraclasts. Micritization produced thin dark colored micrite envelopes around some grains and in others this process led to destruction of most of the grains with replacement of patches of micrite (Fig. 4.7A-B). The only traces of the original nature of this sediment result from the preservation of the stable micrite envelopes. Micritization formed by organisms boring carbonate grains, and results in hazy, ill-defined grain boundaries.

Diagenetic Processes	Diagenetic Events		
	Middle-Late Triassic Syndepositional	Intermediate	Late burial
Micritization	▬		
Type one dolomite (D1)	▬		
Isopachous fibrous cements	▬		
Dissolution		▬	
Blocky calcite cement		▬	
Neomorphism		▬	
Physical compaction		▬	
Type two dolomite (D2)		▬	
Pore filling blocky calcite cement			▬
Silica			▬
Stylolitization			▬
Type three dolomite (D3)			▬
Fracturing			▬

Fig. 4.6. Paragenetic sequence of the Al Aziziyah Formation in the study area; Cements formed during early, intermediate and late diagenesis. Early cements are isopachous, fringing, and equant spar, intermediate cements is blocky or equant calcite whereas, late cement is pore-filling calcite, dolomite and silica.

IV.1.5.1.2 Cementation

Cements in the Al Aziziyah Formation are: 1) an isopachous bladed or fibrous, 2) equant spar, 3) dolomite cement and 4) silica. Isopachous bladed or fibrous fringing cement formed as the first generation cement around most ooids and bioclasts (Fig. 4.7B).. Fibrous and bladed shapes formed on the grain rims or surrounding micrite envelopes (Fig. 4.8A). Equant irregular calcite cement occurs between the grains as the second generation cement (Fig. 4.8A). This cement also formed within grain-supported lithofacies comprising large crystals (Fig. 4.8B). This cement generally occupies the remaining pore space after isopachous fringing cementation. This cement varies from small on pore margins growing progressively larger crystals toward the center of pores. Equant irregular dolomite and pore-filing dolomite cements occur between and within the grains as the second and third generation cement (Fig. 4.8A).
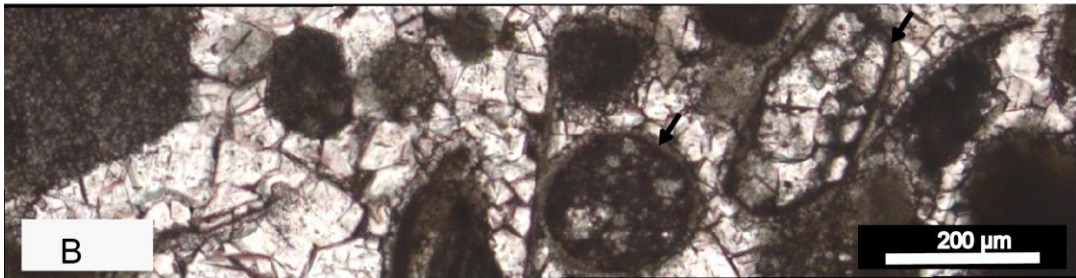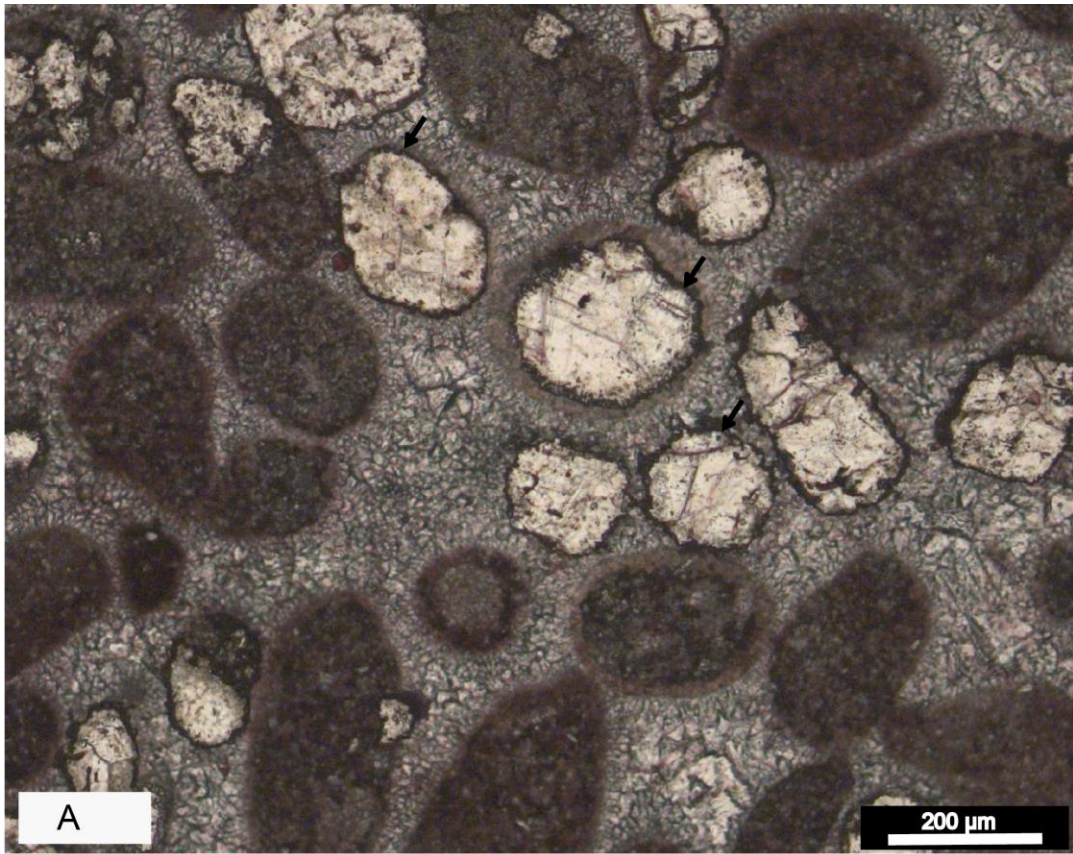
Fig. 4.7. Photomicrograph of micritization around the grains (A&B). The black arrows indicate micritization around the grains.

Silica cement is rare, partially replacing grains preserving original fabrics and grain types (Fig. 4.8C). Silica also occurs replacing pore-filling cement with smaller silica crystals along the pore margins and larger silica crystals in pore interiors (Fig. 4.8D).

IV.1.5.1.3 Physical compaction

Evidence of mechanical or physical compaction includes fractured bioclasts, deformation and truncation of bioclasts. A few samples of skeletal limestone have a compacted fabric and broken grains (Fig. 4.8E) and also show increasingly sutured and concave–convex contacts. Chemical compaction is indicated by stylolites and dissolution seams (Fig. 4.8F). In addition, a few samples also show fracturing of ooids and skeletal grains (Fig. 4.9A).

IV.1.5.1.4 Neomorphism

One type of neomorphism occurs in many of the Al Aziziyah Formation samples: the change of lime mud to coarser crystals in mud-supported facies (Fig. 4.9B). This type of neomorphism is common in the Al Aziziyah Formation.

IV.1.5.1.5 Dissolution

A few skeletal grains were leached leaving only a micrite envelope and other samples show extensive dissolution of most of the cement and grains (Figs. 4.9C-4.9F). Large volumes of vuggy and some moldic porosity were produced by this process. Dissolution ranges from slight to extensive (Figs. 4.9C-4.9F).
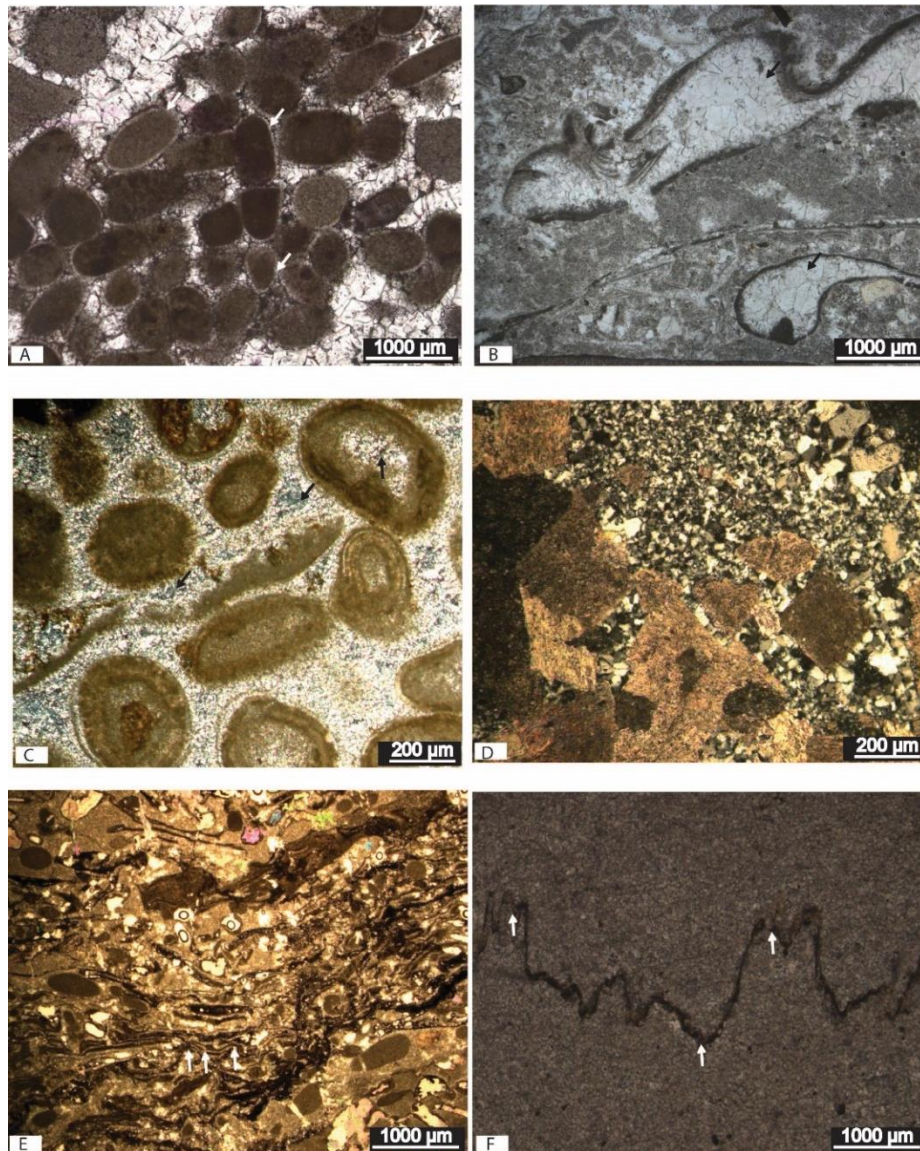
Fig. 4.8. Photomicrographs A) Isopachous rimming cement surrounding pellets. B) Plane polarized crystal blocky cements filling fossil fragment. C-D). Silica cements filling pore space between ooids and skeletal grains and dolomite. E) Stylolite; F) stylolite in carbonate mudstone. The arrows are pointed toward: A-Isopachous cement; B- blocky or Equant; C- silica cement; E and F are pointing toward stylolites.

117
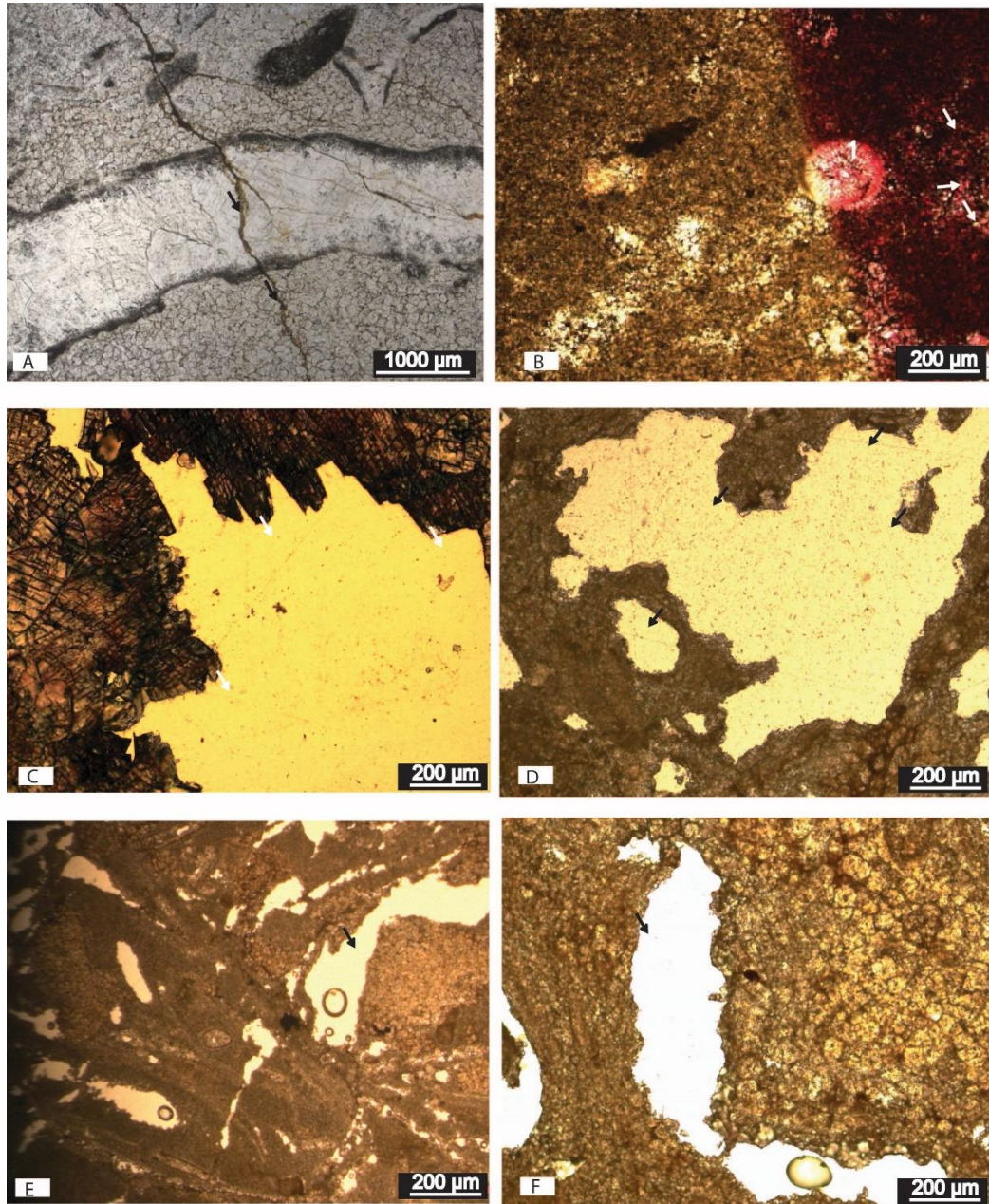
Fig. 4.9. Photomicrographs showing the effect of diagenetic processes in the Al Aziziyah samples. A-B fracture and neomorphism in mudstone. C-F dissolution in limestone. The arrows are ponting toward A- fracture, B-neomorphism, C-F-dissolution pores.

118

IV.1.5.2 Dolomite types

Dolomite in the Al-Azizyah Formation is sub-divided into three types. Type one (D1) is light grey and brown, and fine to medium-crystalline unimodal and polymodal non-planar to planar-s mosaic dolomite crystals with euhedral to subhedral shapes generally ≤50 μm in size (Fig. 4.10A). Type two dolomite (D_2) has medium to coarse (100–300 μm) unimodal and polymodal crystal size and it is subhedral to euhedral (Fig. 4.10B). These dolomite crystals are light brown to brown and have cloudy cores and clear rims in most of their crystals (Figs. 4.10B and C), though some of these dolomite crystals are very dark and have zonation in some crystals (Fig. 4.10D). Type three dolomites (D_3) occur as late pore-filling dolomite cement. Pore-filling dolomites are of two types: a) clear planar fine to medium (100-200 μm) crystals (Fig. 4.10E), b) coarse crystalline (>300 μm) saddle dolomite (Fig. 10F).
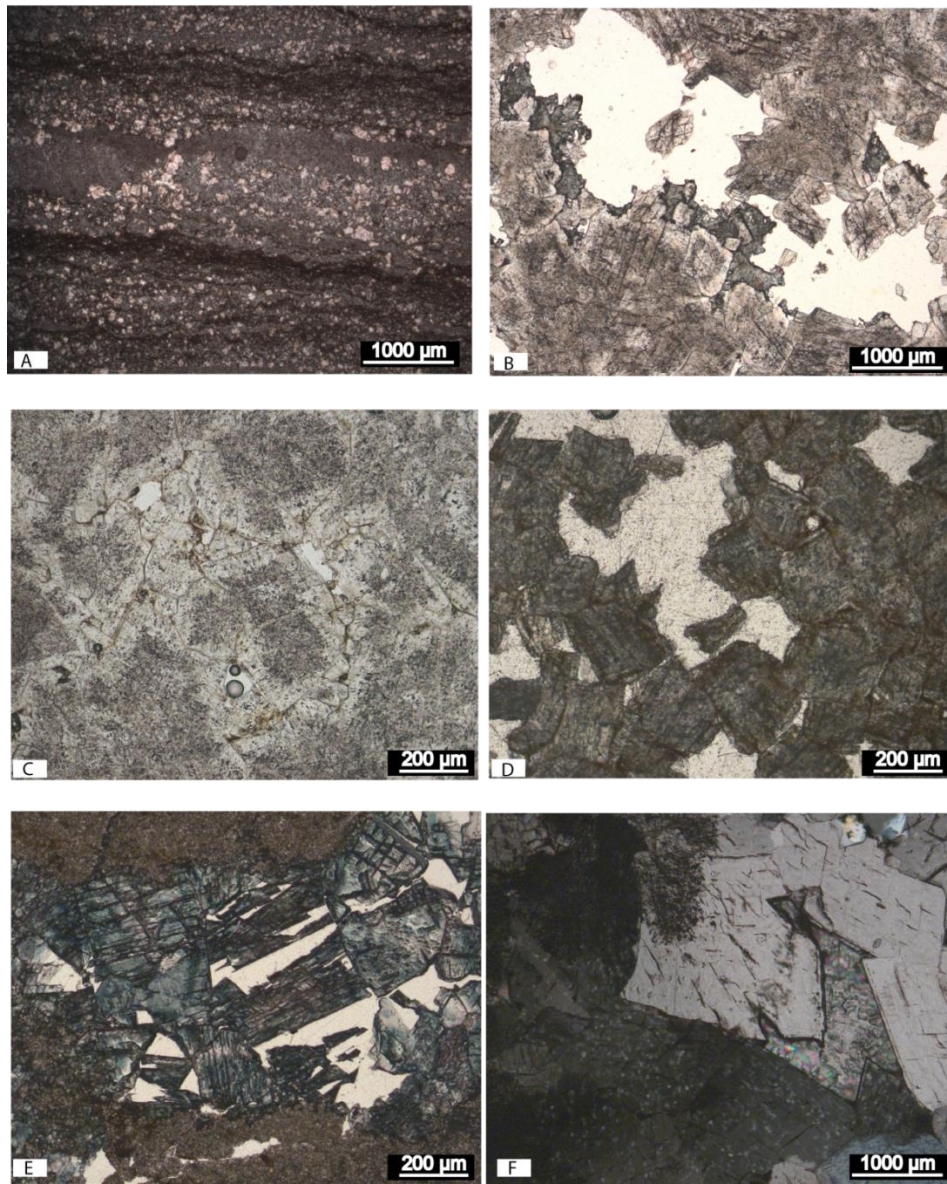
Fig. 4.10. Photomicrographs of dolomite types in Al Aziziyah Formation. A) Fine crystalline dolomite (D_1). B-D) medium to coarse crystalline dolomite (D_2) replacing original texture with cloudy cores and clear rims. E) Medium to coarse crystalline greenish stained dolomite (D_3). F) Pore filling coarse crystalline saddle dolomite (D_3).

IV.1.5.3 Stable isotope geochemistry

The carbon isotope values of mudstone matrix in the Al Aziziyah Formation ranges from -7.8 to +3.9‰ (Moustafa et al., 2014) and are correlated with isotopic values from calcite and dolomite cements to determine the differences between the whole rock and cement values. Carbon isotope values of the calcite and pore-filling dolomite cement (Table 4.2; 7 samples from calcite cement and 11 from dolomite cement) range from -1.5 to -0.9‰ and -1.3 to +1.8 (VPDB) respectively and oxygen isotope values of the calcite and dolomite cements range from -6.2 to -4.3‰ and -7.6 to -4.1 respectively (Fig. 4.11).

IV.1.5.4 Elemental analysis

Elemental analysis (Ca, Mg, Fe, Mn, and Sr) of selected thin sections from the Al Aziziyah Formation are shown in figures 4.12 and 4.13. Sr values in calcite cement and pore-filling dolomite cements range from 0 to 944 ppm and 0 to 214 ppm respectively. Mn values in calcite cement and pore-filling dolomite cement range from 0 to 2156 ppm and 250 to 12001 ppm respectively. Fe values in calcite cement and pore-filling dolomite cement range from 77 to 4160 ppm and 146 to 18750 ppm respectively. Na values in calcite cement and pore-filling dolomite cement range from 96 to 816 ppm, and 20 to 790 ppm respectively. Average values of trace elements in calcite and pore-filling dolomite cements are 248 ppm and 250 ppm for Na, 168 ppm and 72 ppm for Sr, 1031 ppm and 9750 ppm for Fe, and 349 ppm and 940 ppm for Mn. The lower detection limit of the cement values are Na (70 ppm), Sr (200 ppm), Fe (150 ppm) and Mn (100 ppm).

Table 4.2

Stable isotope values from different cement types. GD=Ghryan Dome; KB=Kaf Bates.

Sample	List (m)	$\delta^{13}C$	$\delta^{18}O$	Comments
C_1-GD-3	0.2	-0.7	-4.6	Coarse pore filling calcite of possible large skeletal grains (Blocky cement)
C_2-GD-3	0.2	-0.5	-4.3	Corse pore filling calcite cement (Blocky cement)
C_3-GD-3	0.2	-0.7	-4.7	Corse pore filling calcite cement (Blocky cement)
C_1-GD-12	4.6	1.2	-7.6	Coarse pore filling dolomite of possible large skeletal grains (Blocky cement)
C_2-GD-12	4.6	-0.2	-6.6	pore filling dolomite cement
C_3-GD-12	4.6	0.4	-4.1	pore filling dolomite cement
C_1-GD-15	6	-1.5	-6.2	Blocky calcite cement
C_2-GD-15	6	-1.2	-5.7	Blocky calcite cement
C_3-GD-15	6	-1.3	-5.4	Blocky calcite cement
C4-KB-25	15.3	-1.0	-4.9	Fine pore filling dolomite
C_1-KB-30	18	-1.3	-7.1	pore filling dolomite cement (blocky cement)
C_1-GD-76	53.5	-0.9	-7.3	pore filling dolomite
C_1-GD-100	78.8	1.8	-5.1	pore filling dolomite
C_2-GD-100	78.8	1.7	-5.1	pore filling dolomite
C-KB-118	96.3	0.9	-6.1	pore filling calcite cement
C_1-KB-133	104	1.3	-6.1	pore filling dolomite
C_2-KB-133	104	1.4	-6.2	pore filling dolomite
C3-KB-133	104	1.3	-5.9	pore filling dolomite
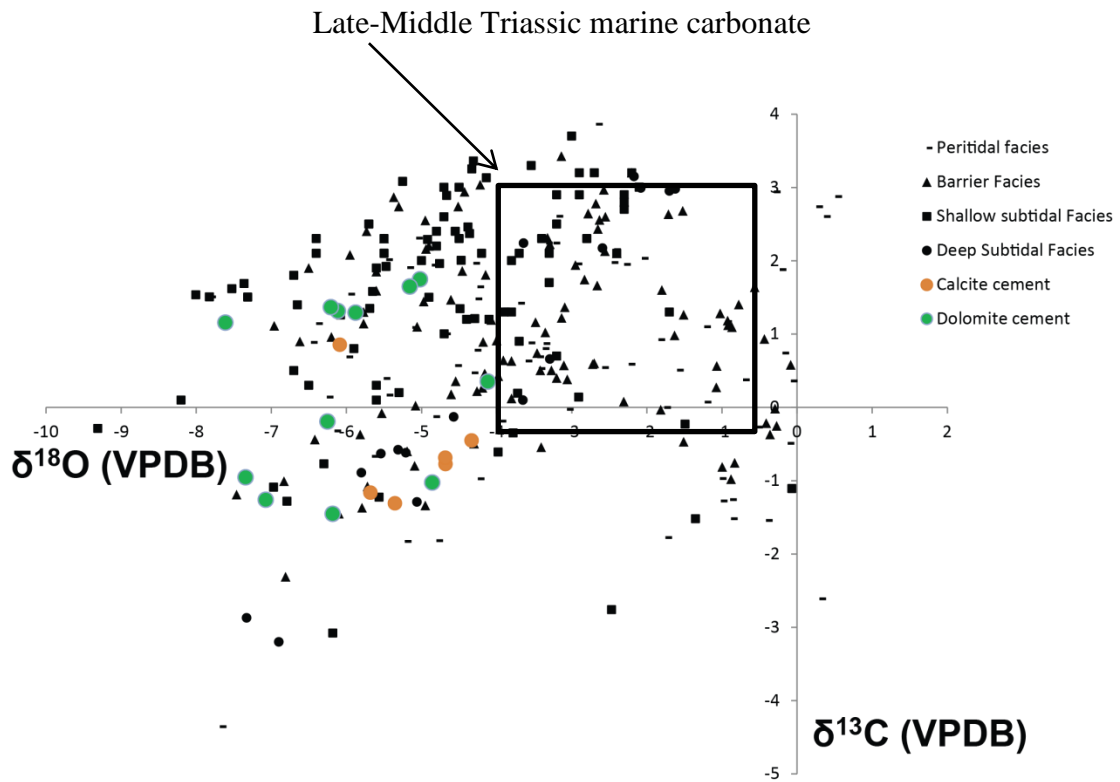
Fig. 4.11. Comparison between $\delta^{18}O$ and $\delta^{13}C$ value of study samples from matrix and cement. This trend is similar to inverted J-trend (Lohmann, 1988) indicating the influence of meteoric to shallow burial diagenesis on much of the Al Aziziyah Formation. The box for Triassic marine values is adapted from Korte et al., 2005.
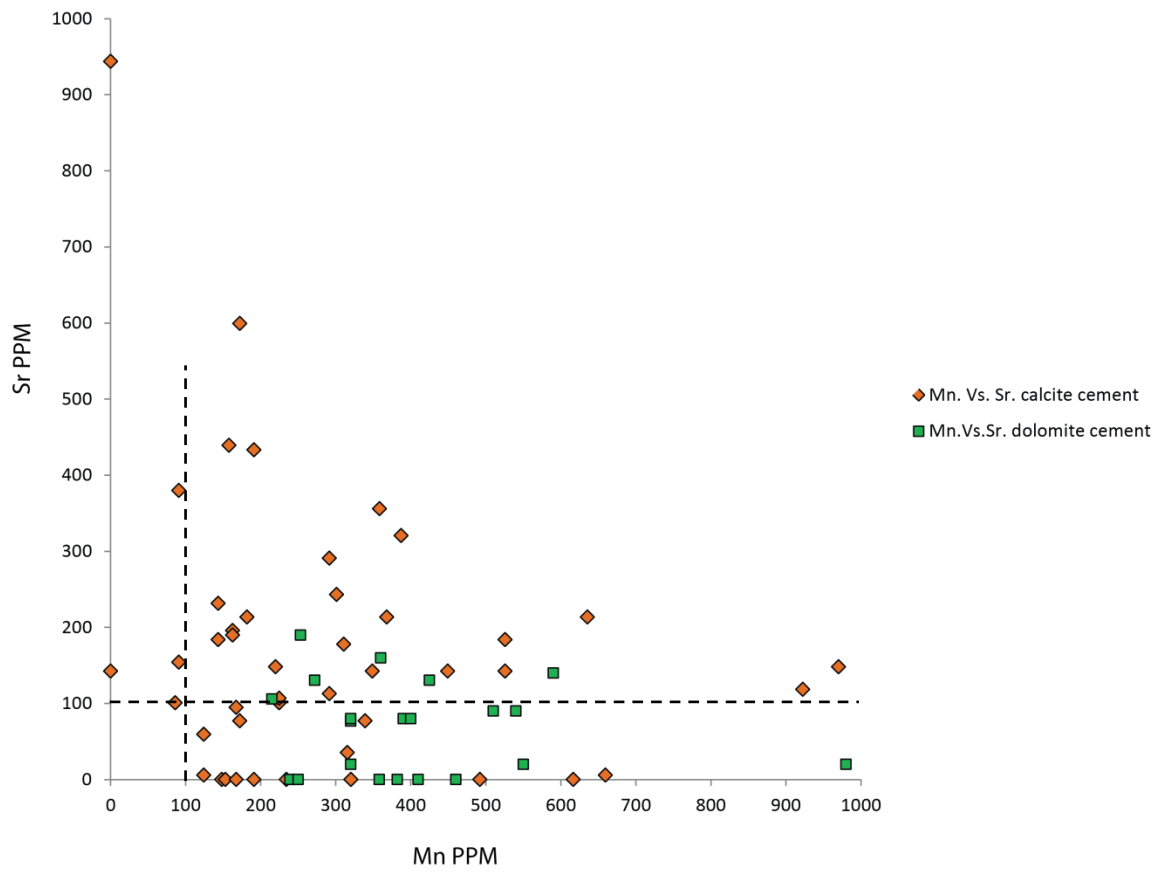
Limit of detection (LLD)

Sr. 200 ppm LLD. Calcite
Mn. 100 ppm LLD. Dolomite

Fig. 4.12. Cross plot of Mn versus Sr in carbonate cement samples of the Al Aziziyah Formation.

124
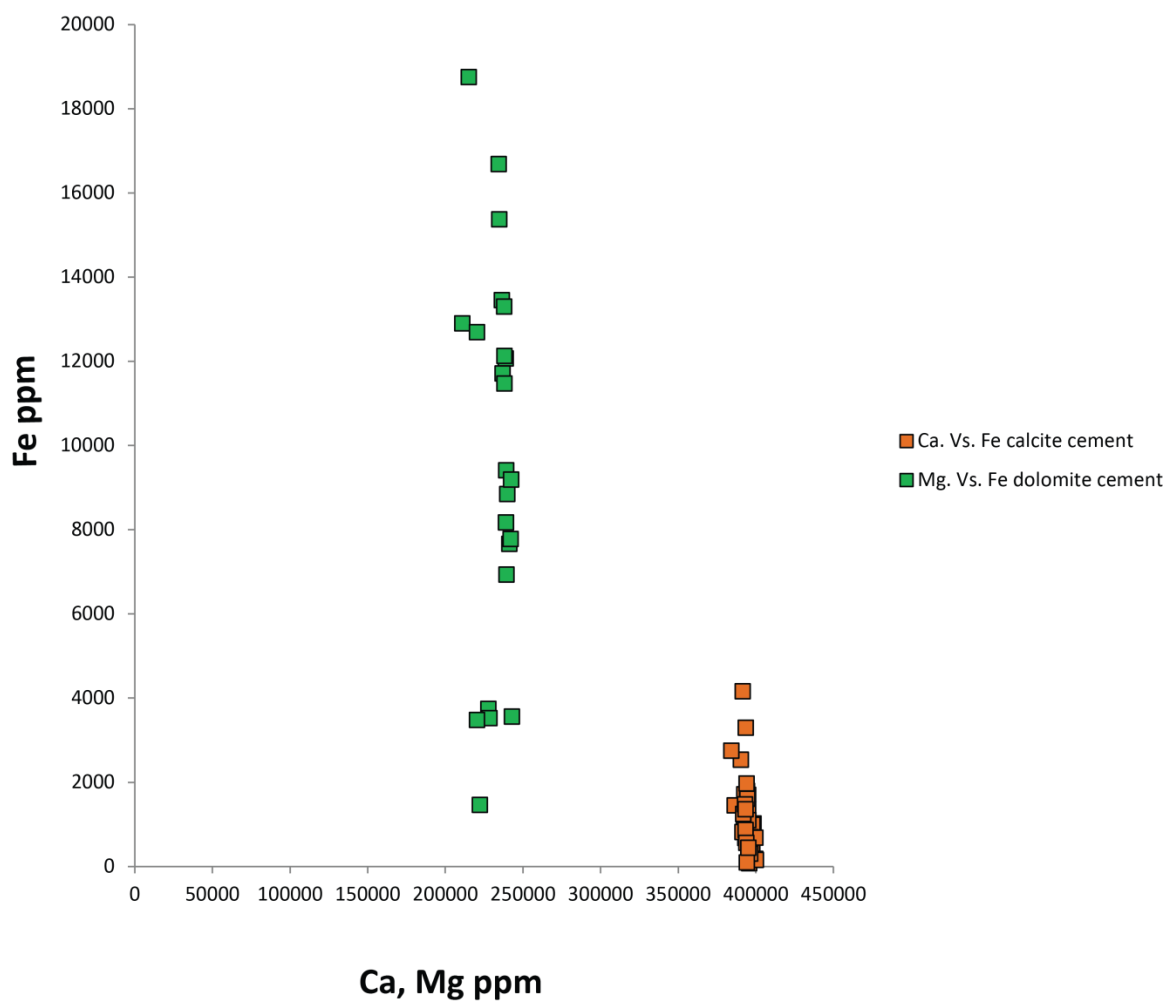
Limit of detection (LLD)

Fe.150 ppm LLD
Ca. 560 ppm LLD . Calcite
Mg. 30 ppm LLD. Calcite
Ca. 320 ppm LLD. Dolomite
Mg. 230 ppm LLD. Dolomite

Fig 4.13. Cross plot of Ca, Mg versus Fe in carbonate samples of the Al Aziziyah Formation indicating high Fe within the dolomite cements (green color).

IV.1.6 Discussion and interpretations

IV.1.6 1 Elemental analysis

The most common naturally occurring minor and trace elements in carbonate minerals are Mg, Mn, Fe, and Sr (Bathurst, 1975; Popp et al., 1986). A carbonate phase may dissolve partially or fully upon exposure to undersaturated waters and its elements are transferred to the ambient solution. So its diagenetic calcite will be different than the original carbonate (Popp et al., 1986; Grossman, 2012). Some trace elements like Mn and Fe are not abundant in the natural carbonate mineral, because they are insoluble in oxic waters (Arthur et al., 1988). However, Mn and Fe are abundant in anoxic diagenetic fluids (Marshall, 1992; Grossman, 2012). Other trace elements like Sr, S, and Na are rich in natural carbonate minerals and may disappear in diagenetic minerals. The presence of the trace elements (Sr, S, and Na) indicates preserved marine signatures (Veizer, 1983; Mii et al., 1999; Grossman, 2012).

In addition, increasing concentrations of Mn and Fe elements in cements are related to diagenetic fluids having higher Mn and Fe values (e.g. Pingitore et al., 1988; Brand and Veizer, 1980). Redox potential also controls Fe and Mn values (Frank et al., 1982). If the amount of Mn and the Mn/Fe ratio are high enough then luminescence will occur in calcite cements (Frank et al., 1982). The shallowest water facies of Al Aziziyah Formation facies were influenced by increased siliciclastic influx at the Ghryan Dome section. Therefore, siliciclastic influx can increase diagenetic fluids and Mn values in shallow marine carbonate environments.

Elemental cross plots from calcite and pore-filling dolomite cements are shown in Figs. 4.12-4.13. Sr and Mn values from well-preserved Triassic brachiopods are more than 400 ppm and less than 250 ppm respectively (Korte et al., 2005). Al Aziziyah Formation cement samples have low Sr (Average values of Sr in calcite and pore-filling dolomite cements are 168 ppm and 72 ppm respectively) and high Mn values (Average values of Mn in calcite and pore-filling dolomite cements are 349 ppm and 940 ppm respectively) suggesting their original compositions were altered. Strontium concentration of the Al Aziziyah Formation samples is much less than Triassic sea water values (Milliman, 1974; Korte et al., 2005). The low Sr concentration of the Al Aziziyah Formation cements implies either the fluids in this unit had a lower Sr/Ca ratio than Triassic seawater (Korte et al., 2005), or they were altered during meteoric diagenesis (McCorkle et al., 1995), or the original mineralogy was primarily low Mg calcite (Spotl and Burns 1991). Meteoric diagenetic effects can be interpreted from high Mn values and bright CL. However, the original mineralogy is best understood from preservation of internal fabric of the ooids, which indicates a radial crystal structure (aragonite) for most of the Al Aziziyah ooids (Fig. 4.5C).

The high Fe^{2+} values particularly suggest that Al Aziziyah Formation was affected by pore fluids in reducing environments within a shallow burial setting. The high Fe also indicates that additional Fe was added during the diagenetic history as Fe^{2+} of reducing environments in burial diagenesis should be in order of ~1,000 ppm or higher (Drever 1982). High Fe values (>12,000 ppm) are very clear in the last stage dolomite cement (Fig. 4.13). Pore-filling dolomite cement has lower Sr (Fig. 4.12) content than the calcite

cement suggesting it recrystallized and became excessively depleted during Sr purification of the dolomite (Land, 1980).

IV.1.6.2 Stable isotope geochemistry

The oxygen and carbon isotopic composition of seawater varies through geologic time (Veizer et al., 1999). Therefore, it is necessary to understand the initial composition of the Triassic marine carbonate to make correlations with the isotopic values from the cement (marine or not). Accordingly, the isotopic values of well-preserved brachiopod shells from Triassic seawater range from -0.5 to +3.0‰ δ^{13}C and -3.9 to -0.6‰ δ^{18}O (Korte et al., 2005). Stable isotopic values from whole rock, calcite and dolomite cements from the cross plots of the Middle-Late Triassic Al Aziziyah Formation (Fig. 4.11) show two different trends from carbonate cements on cross plots: first, a trend with depleted δ^{13}C values and depleted δ^{18}O; and second has a trend with enriched δ^{13}C values and depleted δ^{18}O values. In general, open systems and high water–rock ratio lead to loss of primary isotopic values, where closed systems and low water–rock ratios favor retention of original isotopic composition (Lohmann, 1988). The first trend of increasing negative δ^{18}O values in Al Aziziyah samples probably reflects increasing temperature during shallow burial diagenesis (Allan and Matthews, 1982). Little variation in δ^{13}C values of these samples could have resulted from original inorganic carbon derived as well as less differentiation between ^{13}C/^{12}C ratios than ^{18}O/^{16}O ratios with increasing temperature or rock-buffering of the δ^{13}C system (Allan and Matthews, 1982). The second trend with more depletion of carbon isotope values is similar to the inverted J

trend (Lohmann, 1988) and is usually formed by flushing of organic-rich, warm waters through the rocks during meteoric diagenesis or shallow burial conditions (Allan and Matthews, 1982).

In addition, comparison of isotopic data from cement with whole rock shows greater depletion and enrichment of oxygen and carbon isotope values from the matrix due to diagenetic effects from shallowest water facies (Moustafa et al. 2014; Fig. 4.11). Evaporation most likely caused the more positive $\delta^{18}O$ values within the peritidal and barrier facies. Still, early fresh water diagenetic effects during the Middle-Late Triassic are the main reasons for more negative $\delta^{18}O$ values (Moustafa et al., 2014). High productivity during the deposition of the Al Aziziyah Formation and/or the abundance of aragonite mixing (Swart, 2008) with calcite are the most likely causes of the local $\delta^{13}C$ enrichment relative to the general $\delta^{13}C$ curve for brachiopod shells (Allan and Matthews, 1982).

IV.1.6.3 Diagenetic events

Petrographic study of thin-sections and their cathodoluminescence indicate that the diagenetic events in the Al Aziziyah Formation are 1- Early (syndepositional), which include micritization, type one dolomite and isopachous fibrous cements); 2- Intermediate (dissolution, blocky calcite cement, neomorphism, physical compaction and type two dolomite; and 3- Late stage (pore filling blocky calcite cement, silica, stylolitization, type three dolomite and fracturing (Fig. 4.6).

IV.1.6.3.1 Early (syndepositional)

IV.1.6.3.1.1 Micritization

Micritization is the first diagenetic process that occurs near the sediment–water interface of the Al Aziziyah Formation and also represents the first event in most settings under low-energy conditions (Tucker and Wright, 1990; Flugel, 2004). This process is produced by boring of microorganisms (bacteria, algae and fungi) on carbonate grain surfaces (Flugel, 2004). Some thin sections samples show dissolved grains with preserved grain edges (Fig. 4.7A-B), which also indicates microorganism activities (Flugel, 2004). A few grains were dissolved and replaced by cement and their edges were preserved as micrite envelope (Fig. 4.7A).

IV.1.6.3.1.2 Type one dolomite (Microbial dolomite)

The microbial dolomite model proposes that sulfate-reducing bacteria activities in an arid, evaporite setting can overcome kinetic barriers to form proto-dolomite in the anoxic zone immediately beneath the sediment-water interface (Vasconcelos et al., 1995; Vasconcelos and McKenzie, 1997). Continuation of this microbial activity with early diagenesis after deposition leads to an ageing process, which eventually leads to formation of stoichiometric dolomite (Vasconcelos and McKenzie, 1997; Mastandrea et al., 2006; Bontognali et al., 2010; Sadooni et al., 2010). Dolomite type one (D_1) is associated with evaporite pseudomorphs, seawater, which were modified either by evaporation or mixing with meteoric or hypersaline waters (Dunham and Olson, 1980; Tucker, 1982; Frisia, 1994, Mutti and Simo, 1994), was the most likely source for Mg^{2+}

130

for this dolomite type. The peritidal facies of the Al Azizyah Formation has very small, fabric preservative dolomite crystals (D1) within crypalgalaminites (Fig 4.10A). Staining shows the dolomite is non-ferroan. The fine dolomite within the peritidal facies of the Al Aziziyah Formation is interpreted to have formed very soon after depositional due to microbial activities.

IV.1.6.3.1.3 Fibrous cements

Marine cements in the Al Aziziyah Formation are: an isopachous bladed or fibrous grain rimming. Isopachous fringing cement formed as the first generation cement around ooids and bioclasts and records high saturation state of $CaCO_3$ and low sedimentation rate during their formation (Flugel, 2004). This cement formed as aragonite as indicated by the abundance of ooid grains that have both concentric lamina and radial structures that later dissolved and neomorphism to calcite cement (Budd, 1988). Most fibrous and bladed cements stain pink with Alizarin Red and potassium ferricyanide solution indicating its low Fe calcite composition and these cements have very bright luminescence zones under CL indicating Mn abundance >> Fe abundance during precipitation (Figs. 14B1 and D1). However, some isopachous fringing cements are unstained with potassium ferricyanide indicating later replacement by dolomite (Fig. 4.7A). There are two types of changes recorded in the aragonite to calcite or dolomite: First the aragonite neomorphoses to calcite but traces of the micro-architecture of the original grain are preserved indicated by radial crystals (Fig. 4.5C). Secondly, the entire

original crystal (possibly aragonite) was dissolved, leaving a mold that was later filled by pore-filling calcite or dolomite cement (Scoffin, 1987).

IV.1.6.3.2 Intermediate

IV.1.6.3.2.1 Dissolution

Undersaturated of pore fluids with respect to carbonate lead to dissolution of metastable carbonate grains and cements in the Al Azizyah Formation. Fluids, charged with organic acids, carbon dioxide, and/or hydrogen sulfide derived from organic matter diagenesis and sulfate reduction were the likely fluids that caused significant dissolution (Mazzullo & Harris, 1992; Berner, 2002; Flugel, 2004). Exposure of the Al Aziziyah Formation to subaerial conditions during the early Late Triassic probably resulted from regional relative sea level fall. Meteoric fluids penetrated underlying sediment causing dissolution of grains, cements and matrix and creating selective dissolution patterns (Fig. 4.9C and D) with some large pores (Fig. 4.9E and F).

IV.1.6.3.2.2 Blocky equant calcite cement

Equant spar cement formed between the grains in most of the samples (Fig. 4.7A) and large spar crystals formed within the grains in few samples (Fig. 4.8B). Most equant spar cements stain pink but some are unstained with Alizarin red indicating their dolomite composition (Fig. 4.8A). Equant spar (blocky) cement has alternating dark, bright and dull luminescence zones under CL indicating varying amounts of Mn and Fe during its precipitation (Fig. $4.14B_2$, D_2, F_1 and F_2). Cements precipitated in the shallow burial

environment commonly are composed of clear, coarse calcite spar (Tucker and Wright, 1990; Flugel, 2004). Compared with marine cements, burial spar typically is depleted in Mg, Sr and Na, but may have significant amounts of Fe and Mn (Choquette and James, 1987). CL microscopy and trace element abundances indicate that much of the calcite cement in the Al Aziziyah Formation are depleted in the Sr and Na and enriched in Fe and Mn and most likely formed during meteoric or shallow burial diagenesis. Equant irregular dolomite occurs between the grains as second generation cement. This equant irregular dolomite cement is similar in morphology to equant dolomite cement (Fig. 4.8A).

IV.1.6.3.2.3 Neomorphism

Neomorphism occurs in the presence of water during dissolution and precipitation or re-precipitation (Bathurst, 1975; Longman, 1977) and is interpreted to be an intermediate stage event. Filling of some shells with sparry calcite that formed from neomorphism of metastable aragonite occurs in some samples of the Al Aziziyah Formation (Fig. 4.9B1).
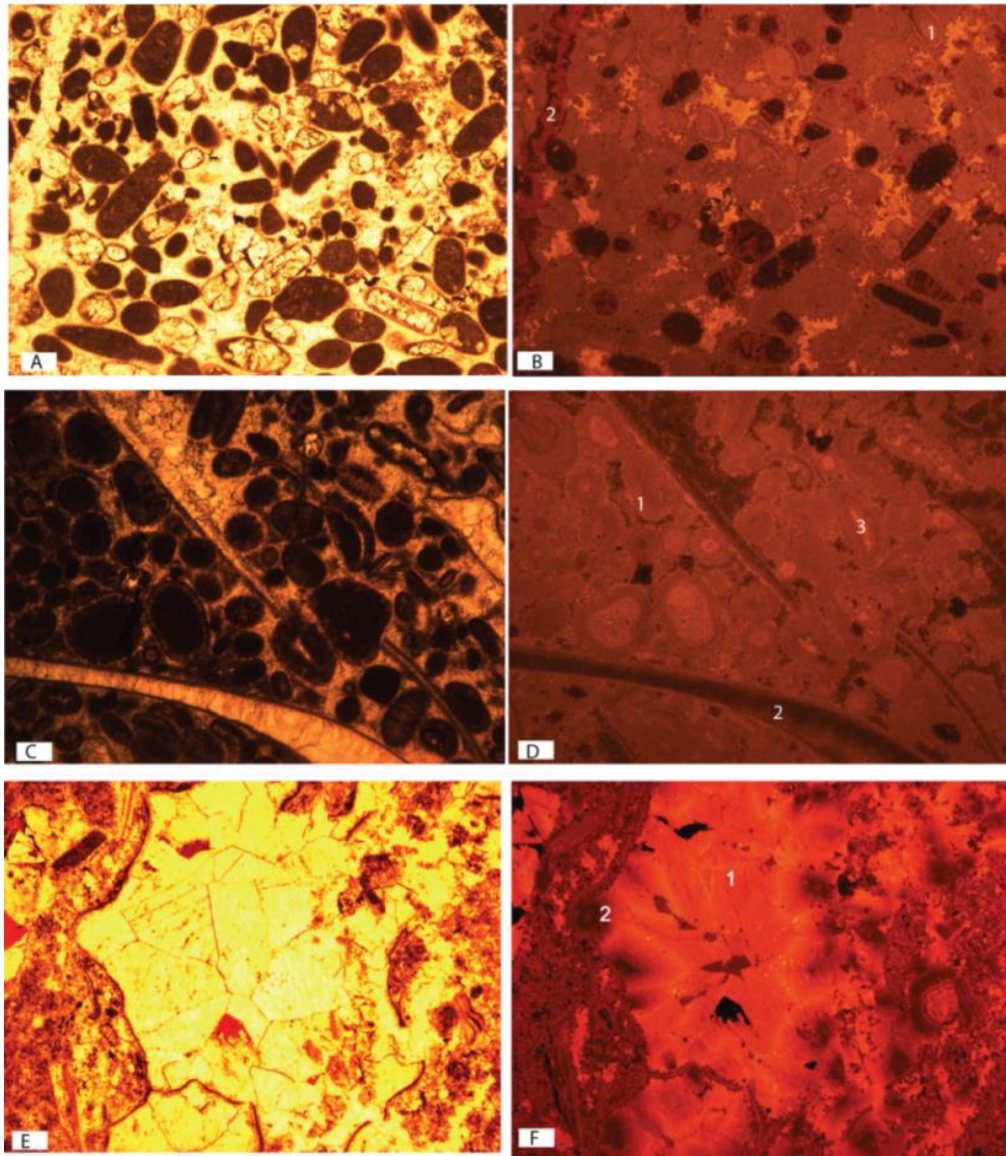
Fig. 4.14. Photomicrograph of unpolorized light and cathodoluminescence of cements (5 mm each view). A-B isopachous (1). B-D pore-filling (2 and 3) with isopachous (1), and E-F large blocky calcite cement (1 and 2).

IV.1.6.3.2.4 Compaction

Compaction affected Al Aziziyah Formation after deposition and led to physical changes in the sediments as a result of increasing overburden of sediment (Flugel, 2004). Compaction occurs in some thin sections and is best recorded in skeletal packstone (Fig. 4.8E).

IV.1.6.3.2.5 Type 2 dolomite (Reflux dolomite)

The seepage reflux model forms dolomite beneath restricted environments, where evaporation is intense and highly concentrated, sinking brines precipitate dolomite by moving many volumes of water with high Mg/Ca ratios through the sediment (Land, 1986; Morse and Makenzie, 1990; and Allan and Wiggins, 1993; Machel, 2004). In this model the underlying sediment need not to be supratidal, but dolomite can form in any shallow water depositional environment. The dolomite formed in the barrier facies of the Al Aziziyah Formation was likely produced as seepage reflux brines passed through these rocks during intermediate stage diagenesis. Type 2 dolomite (D2) mostly occurs as a replacement in Al Aziziyah Formation beds with moldic porosity and silica filling void spaces. Staining indicates that D2 dolomite is non-ferron in most of the samples, and has dull to bright CL suggesting the involvement of meteoric water in its formation. The most likely source for Mg^{2+} for this dolomite type is seawater. In addition, the clear rims around the cloudy dolomite rhombs (Fig. 4.10B and C) may have formed from more diluted solutions due to high Mn^{+2} and low Fe^{+2} (Land et al., 1975; Amthor et al., 1993; Mahboubi et al., 2010).

IV.1.6.3.3 Late Stage Diagenesis

IV.1.6.3.3.1 Pore filling blocky calcite cement

This pore filling blocky calcite cement formed late and it associated with dolomite type three (Fig. 4.15A &B; Fig. 4.16 A and B). In addition, staining indicates that the blocky calcite cement is non-ferroan. Petrographic, geochemical and cathodoluminescent data (depleted Sr and Fe; and enriched in Mn, bright to dark luminescence (Fig. 4.15A and B) indicates that these dolomites formed under shallow burial depths. The abundance of Fe, Mn and bright to dark CL in pore-filling dolomite D_3 indicate it formed by burial processes.

IV.1.6.3.3.2 Silica cement

Silica cement represents the last stage of pore filling in two ways. 1- Silica replaced the cement between the grains and preserved the original depositional fabric. For example, oolitic limestone was cemented by silica and its original fabric is well preserved (Fig. 4.8C). 2- Silica also replaced pore-filling cement after dolomitization. Silica filled the pores that were created earlier by dolomitization and also filled some fractures (Fig. 4.8D). Therefore, silica cement is interpreted to have formed during a burial stage of diagenesis.

IV.1.6.3.3.3 Stylolitization

Stylolites were product by chemical compaction under increasing temperature and pressure conditions (Flugel, 2004); these types of features are abundant in the mudstone facies of the Al Aziziyah Formation (Fig. 4.8F).

IV.1.6.3.3.4 Dolomite type 3 (Burial dolomite)

Burial dolomite (Land, 1986; Morse and Makenzie, 1990; and Allan and Wiggins, 1993) forms in the subsurface after lithification of carbonate sediments (Land, 1986; Morse and Mackenzie 1990; and Allan and Wiggins 1993). As temperature increases, the Mg/Ca ratio required to produce dolomite decreases and many subsurface waters evolve into dolomitizing solutions. The most common fluid sources for burial dolomitization are: (1) Mg-rich residual evaporite brines, (2) modified seawater, and (3) shale compaction waters (Land et al., 1975; Amthor et al., 1993; Mahboubi et al., 2010). The D_3 pore-filling dolomite (Fig. 4.10E and F) occurs as cement filling molds and vugs with sweeping extinction and is interpreted as saddle dolomite (Fig. 4.10F).

D_3 has black, dull and bright CL with significant amounts of Fe and Mn, which indicate a shallow burial setting. Burial cements (calcite or dolomite) typically are depleted in Mg, Sr and Na, but it may have significant amounts of Fe and Mn (Fig. 4.16A and B; Choquette and James, 1987). In addition, staining indicates that D_3 is non-ferroan in most samples and ferroan in a few samples (Fig. 4.10E). Petrographic, geochemical and cathodoluminescent data (depleted Na and Sr and enrichment in Fe; Mn, bright to dark luminescence (Fig. 4.15A &B) and depleted oxygen isotope ($\delta^{18}O$ from -7.6 to -4.1) indicates that these dolomites formed under shallow burial depths. The abundance of Fe,

137

Mn and bright to dark CL in pore-filling dolomite D_3 indicate it formed by burial processes.

IV.1.6.3.3.5 Fracturing

Fractures in the Al Azizyah Formation were produced as temperature and pressure increased (Flugel, 2004). A few samples show fracturing of ooids and skeletal grains (Fig. 4.9A). These types of features are abundant in the mudstone and packstone facies of the Al Aziziyah Formation. Most of the fractures are clear indicating these fractures formed during a late stage of diagenesis.

IV.1.7 Paragenetic sequence

Petrographic characteristics and geochemical results indicate diagenetic processes in the Al Aziziyah Formation occurred in early, intermediate and late diagenetic environments (Figs. 4.6). Early diagenetic processes occurred in marine settings as indicated by micritization, microbial dolomite and non-ferroan isopachous cements. Intermediate diagenetic environments formed in shallow meteoric settings and are indicated by dissolution, blocky equant calcite cements, neomorphism, physical compaction and non-ferroan, euhedral to subhedral, medium-size dolomite (D_2).
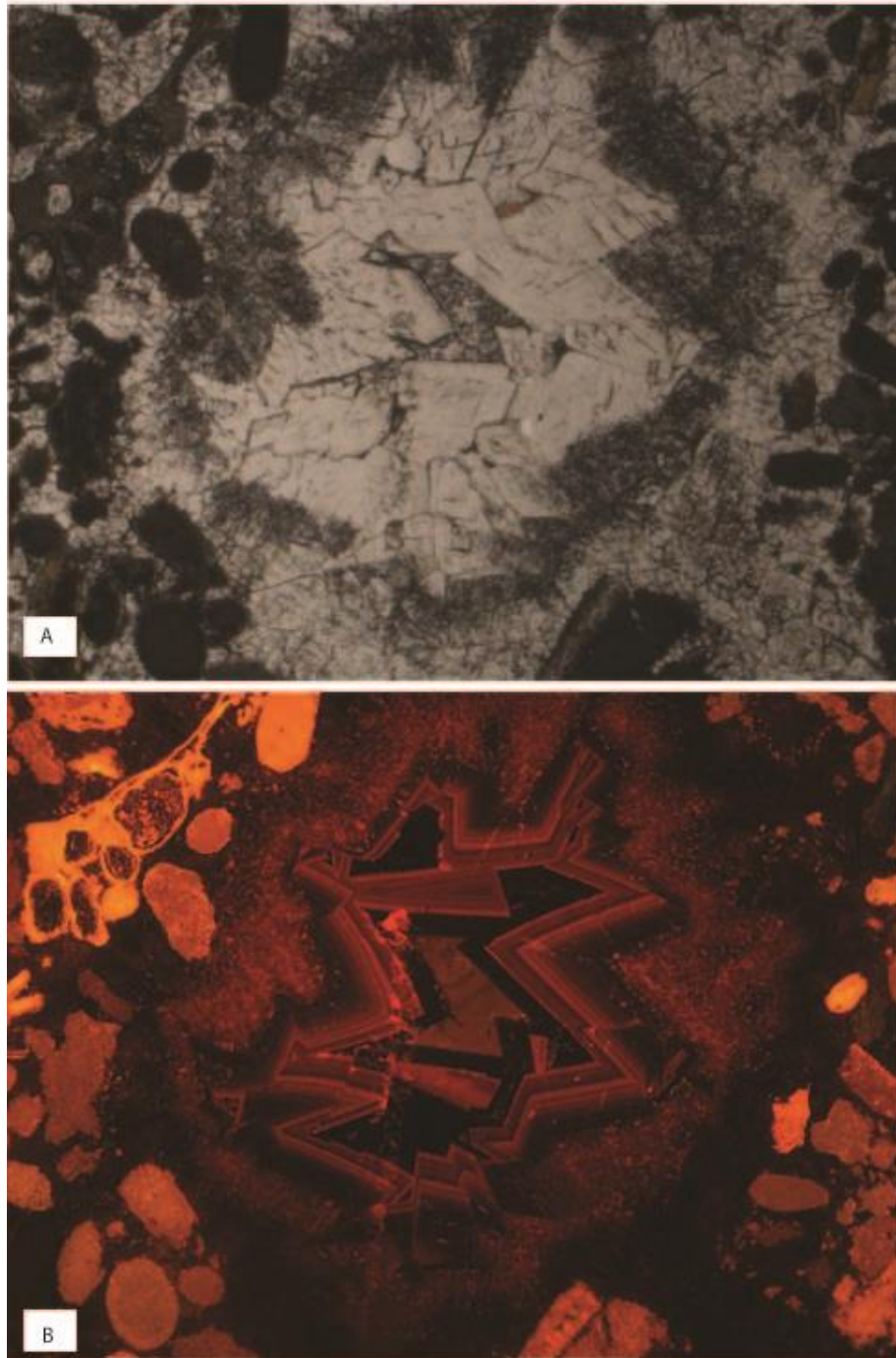
Fig. 4.15. Plane polarized photomicrograph (A) and cathodoluminescence photomicrograph (B) of pore filling coarse crystalline dolomite (D$_3$ type) and its CL zonation (5 mm each view).
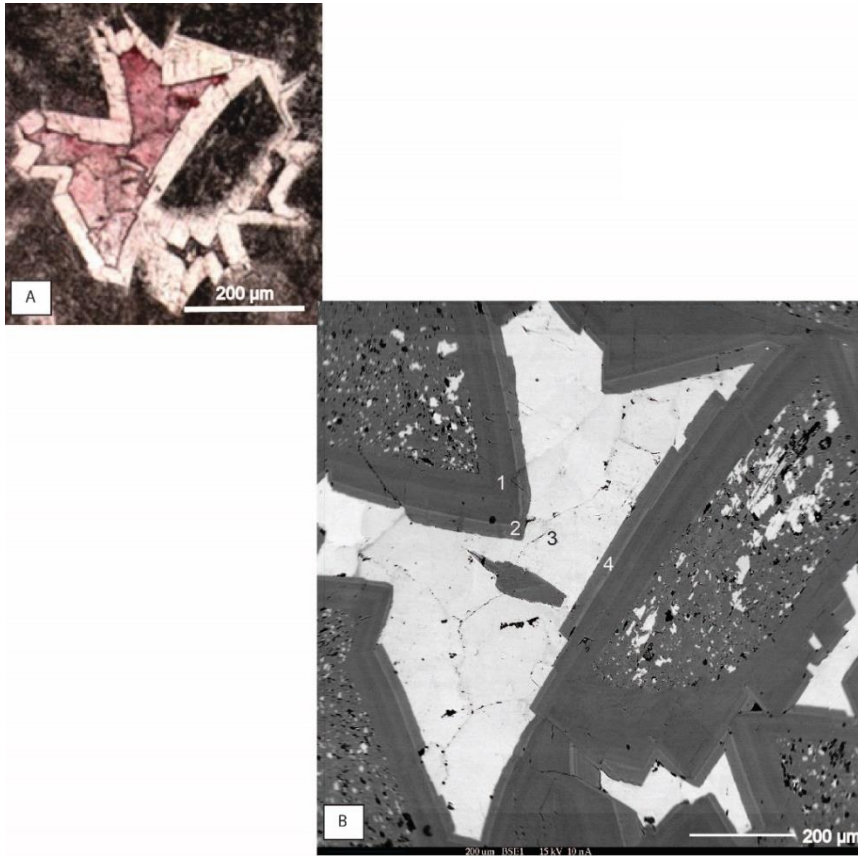
Sample N	Mn (PPM)	Lower limit of detection (LLD)	Fe (PPM)	Lower limit of detection (LLD)
1	390	100	3740	150
2	360	100	12900	150
3	2156	100	4160	150
4	460	100	12690	150

Fig. 4.16. Photomicrograph (A) and Back Scattered Electron (BSE) image (B) of complex dolomite filling cement , of A- stained thin section of dolomite (unstained) and calcite (pink) and B-Trace elements distribution within dolomite (gray; 1, 2, and 4) and calcite (white; 3). Table shows the trace elements distribution within dolomite and calcite. Note that dolomite cement 2 and 4 have the same trace elements values. Therefore, 2 and 4 represent the same events.

Burial processes affected the Al Aziziyah Formation in shallow burial settings. At this burial stage, diagenetic processes formed pore filling calcite cement, silica cement, stylolitization, D_3, and fracturing. D_3 formed with increasing Fe content in cements during reducing conditions. Stylolites, and fractures cross-cut the other phases, in particular the pore-filling cement (Fig. 4.7A). Based on the rarity of saddle dolomite, burial depth was likely not great (e.g., Budd, 1997; Warren, 2006). Marine and meteoric processes mostly occur in the early and intermediate stages, but chemical and physical compaction, fracturing and silica cementation occur in later stages of burial (e.g. Flugel 2004; Vincent et al., 2007). Based on geochemical studies in general, cements precipitated during late burial diagenesis have high amounts of Fe and Mn and less Sr and Na.

IV.1.8 Monsoonal climate Influence

The Al Aziziyah Formation contains an abundance of mudcracks, evaporite pseudomorphs and silicified evaporite nodules in its peritidal facies without karst features, suggesting an arid or semi-arid climate (e.g., Golonka and Ford, 2000; Preto et al., 2010). In addition, the upper boundary of the Al Aziziyah Formation is a sharp unconformable surface with overlying rusty colored continental sandstone of the Abu Shaybah Formation (Fatmi 1977; Asserto and Benelli, 1971; Magnier, 1963; Desio et al., 1963; Desio et al., 1960; Burollet 1963; Muttoni et al., 2001) indicates seasonal variations in net precipitation due to monsoonal effect. Libya was very close to the equator during the Triassic and the rainfall spring and fall and not very much during either season (Parrish, 1993). So increased aridity in Libya is consistent with a weak

monsoonal climate. These changes from carbonate facies to carbonate facies with evaporite and sand indicate strong seasonal variations in net precipitation due to monsoonal effect. The Al Aziziyah Formation carbonate facies also has rare dissolution and meteoric cements filling vuggy porosity suggesting meteoric fluids, recharged from the subaerial exposure surfaces flowed through the strata dissolving it and precipitating cements. In addition, most fibrous, bladed and blocky cements, stain pink with Alizarin red and have very bright luminescence zones under CL indicating Mn abundance >> Fe abundance during their precipitation from meteoric fluids. Diagenetic events outlined here from the Al Aziziyah Formation are similar to Landinian and Carnian events record in Triassic sections around the Mediterranean (Garzanti, 1985a; Frisia-Bruni et al., 1989; Mutti, 1994). The eastern equatorial region of Pangea and its peritidal facies show evidence of arid climate and less meteoric effect indicated from very few samples with extensive dissolution Therefore, the Al Aziziyah Formation carbonate facies, and their diagenetic events are linked to a monsoonal climate.

IV.1.9 Conclusions

The Middle-Late Triassic Al Aziziyah Formation in the Jifarah Basin of northwest Libya is composed mainly of carbonate facies that were affected by several diagenetic processes as characterized by their petrography, trace element, and stable isotope signatures. Petrographic study of thin-sections and their cathodoluminescence indicate that the diagenetic events in the Al Aziziyah Formation are 1- Early (syndepositional), which include micritization, type one dolomite and isopachous fibrous cements); 2-

142

Intermediate (dissolution, blocky calcite cement, neomorphism, physical compaction and type two dolomite; and 3- Late stage (pore filling blocky calcite cement, silica, stylolitization, type three dolomite and fracturing. The petrographical features, geochemical data and the distribution of dolomite suggest that microbial processes initiated dolomite formation in peritidal settings (D_1) and reflux-zone dolomitization was the most likely process for the formation of the dolomites D_2. The pore-filling saddle dolomite D_3 formed as a late cement. Libya was very close to the equator during the Middle to Late Triassic and the Al Aziziyah Formation sediments were deposited under arid climatic conditions and may be linked to its monsoonal climate setting.

CHAPTER V

CONCLUSIONS

This study presents the stratigraphic framework integrated with high resolution carbon isotope of the Middle-Late Triassic Al Aziziyah Formation. The Middle-Late Triassic (Ladinian-Carnian) Al Aziziyah Formation was deposited on a gently sloping carbonate ramp within the Jifarah Basin of Northwest Libya. The Al Aziziyah Formation consists of gray limestone, dolomite, and dolomitic limestone interbedded with shale. The main lithofacies are interpreted as 1) tidal crossbedding sandstone; 2) carbonate mudstone or cryptalgalaminites, deposited in peritidal environments; 3) skeletal-oolitic pelletal packstone/grainstone that formed an extensive shoal at the ramp crest; 4) skeletal bioturbated wackestone/mudstone, formed in a shallow subtidal environments; 5-hummocky bedded calcisiltite deposited within a deep subtidal environment within storm wave base; and 6- rare carbonate mud or organic-rich black shale deposited in a basinal setting. Eight measured sections (Ghryan Dome, Ras Mazal East, Ras Mazal West, Kurrush Dome, Kaf Bates, Al Aziziyah Town, Ras Lafal and Bu Arghop) record a depositional dip cross section of the Al Aziziyah Formation within the Jifarah Basin were sampled and analyzed for facies analyzed and sequence stratigraphy to build the stratigraphic framework of Al Aziziyah Formation. The Al Aziziyah Formation is predominantly a 2nd-order (5-20 m.y. duration) subtidal carbonate ramp with peritidal facies restricted to the southernmost sections. Peritidal facies was arid with mudcracks, evaporite nodules and stromatolites. Ramp crest shoals were predominantly pellet

144

packstone-grainstone, whereas subtidal carbonates are thin-medium beds with hummocky cross-stratification, mechanical lamination and low to high density bioturbation. The transition from the underlying Kurrush Formation to the Al Aziziyah Formation is marked by a change from fine sand and red clay to carbonate. In the most updip location the transition from the Al Aziziyah Formation to the overlying Abu Shaybah Formation is an iron and phosphatic surface (composite exposure and flooding surface) overlain by a bone bed and fine sand. Seven sequences within the Ghryan Dome have been identified based on facies staking patterns, filed observations and carbon stable isotopes (S_1-S_7). However, north of the Ghryan Dome section, three more sequences were mapped (S_8-S_{10}).The Ghryan Dome and Kaf Bates sections were also sampled and analyzed for carbon and oxygen isotope chemostratigraphy to integrate high-resolution carbon isotope data with an outcrop-based sequence stratigraphic framework, to build the stratigraphic correlation, and to provide better age control of the Al Aziziyah Formation. This study also discusses the relation between the facies architecture of the Al Aziziyah Formation and the carbon isotope values and the possible influence of depositional environments on the isotopic values. Moreover, the Al Aziziyah Formation within the Jifarah Basin were sampled and analyzed for diagenesis to describe the diagenetic processes and sequence of paragenetic events that affected the Middle–Late Triassic Al Aziziyah carbonate facies. The correlation between the Ghryan Dome and Kaf Bates sections indicates five sequences (sequences 3-7) of increasing and decreasing in δ^{13}C values. The Carnian ocean circulation was restricted in the some parts of the basin. Therefore, the Al Aziziyah Formation δ^{13}C chemostratigraphic curve can be

145

partially correlated with the proposed Triassic global δ^{13}C curve. This correlation indicates that the Al Aziziyah Formation was deposited during the Ladinian and during part of the Carnian stage. The δ^{13}C values of the Al Aziziyah Formation range from -7.8 to +3.9‰, while the δ^{18}O values range from -9.3 to +0.5‰. These wide ranges contrast with the narrow published ranges for marine calcite from well-preserved Triassic brachiopod shells (-0.5 to +3.0‰ for δ^{13}C and -3.9 to -0.6‰ for δ^{18}O). The positive δ^{13}C values in certain intervals relative to brachiopod values likely reflects local withdrawal of ^{12}C from the ocean due to increased productivity, as indicated by the deposition of organic-rich sediment, and/or whole rock sediment composed of calcite admixed with aragonite. The depletion of δ^{13}C in the Ghryan Dome and Kaf Bates sections is clearly associated with exposure surfaces and with shallow carbonate facies. However, heavier δ^{18}O values relative to Triassic brachiopods are related to evaporatic increase in ^{18}O, as indicated by the abundance of evaporites within the peritidal facies. On the other hand, the depletion of δ^{18}O is related to diagenesis due to freshwater input. Carbon isotope values of the calcite cement and pore-filling dolomite cement range from -1.5 to -0.9‰ and -1.3 to +1.8 and oxygen isotope values of the calcite and pore-filling dolomite cements ranges from -6.2 to -4.3‰ and -7.6 to -4.1 respectively, indicating different cement generations. Three types of dolomite occur within the Al Azizyah Formation. Dolomite 1 is very fine- to fine-crystalline (≤50 µm crystal diameter) and preserves depositional fabric well. Dolomite type 2 is coarse crystalline dolomite (100 to 300 µm crystal diameter) that destroyed the depositional fabric and some crystals have a clear outer rim to surrounding a precursor cloudy coarse dolomite core. Dolomite type 3 is a

146

coarse to very coarse dolomite that formed last in a shallow burial environment. The Middle-Late Triassic Al Aziziyah Formation in the Jifarah Basin of northwest Libya is composed mainly of carbonate facies that were affected by several diagenetic processes as characterized by their petrography, trace element, and stable isotope signatures. Processes include cementation, micritization, dissolution, neomorphism, compaction, dolomitization, and fracturing that occurred in early, intermediate and burial environments. The petrographical features, geochemical data and the distribution of dolomite suggest that microbial processes initiated dolomite formation in peritidal settings (D1) and reflux-zone dolomitization was the most likely process for the formation of the dolomites D2. The pore-filling saddle dolomite D3 formed as a late cement. Libya was very close to the equator during the Middle to Late Triassic and The Al Aziziyah Formation sediments were deposited under arid climatic conditions. Therefore, the Al Aziziyah Formation carbonate facies, diagenesis cements are linked to monsoonal climate setting.

REFRENCES

Abohajar, A., Krooss, B., Harouda, M., Littke, R., 2009. Maturity and source-rock potential of Mesozoic and Palaeozoic sediments, Jifarah Basin, NW Libya. J. Petrol. Geol., 32, 327-341.

Ahr, W.M., 1973. The carbonate ramp: an alternative to the shelf model. Gulf Coast Assoc. Geol. Socs.Trans., 23, 221-225.

Allan, J. and Matthews, R., 1982. Isotope signatures associated with early meteoric diagenesis. Sedimentology, 29, 797-817.

Allan, j. r. and Wiggins, w. d., 1993. Dolomite reservoirs: Geochemical techniques for evaluating origin and distribution. Continuing education course note series No. 36, Am. Assoc. Petrol. Geologists, 129 p.

Amthor, J.E., Mountjoy, E.W., Machel, H.G., 1993. Subsurface dolomites in Upper Devonian Leduc Formation buildups, central part of Rimbey-Meadowbrook reef trend, Alberta, Canada. Bull. Can. Pet. Geol. 41, 164-185.

Anketell, J. M. and Ghellali, S. M., 1991A. A Palaeogeographic map of the Pre-Tertiary surface in the region of the Jafarrah Plain and its implication to the structural history of northern Libya. In The Geology of Libya (Eds M.J. Salem, A.M. Sbeta and M.R. Bakbak), Academic Press, London, 6, 381-2406.

Anketell, J.M. and Ghellali, S.M., 1991B. The Jifarah Formation – Aeolian and fluvial deposits of Quaternary age, Jifarah plain. In (Salem, M. J. and Belaid, M. N. editors): The Geol. Of Libya, V:1967 2013.

Arkell, W., Kummel, B. and CW, W., 1957. Mesozoic Ammonoidea. In: Treatise on

Invertebrate Paleontology (Ed. R.C. Moore RC). Ceol. Soc. America, Mollusca 4, L80-L490.

Arnott, R. W. C., 1995. The Parasequence Definition--Are Transgressive Deposits Inadequately Addressed? Journal of Sedimentary Research, 65(1).

Asserto, R., and Benelli, F., 1971. Sedimentology of the Pre-Cenomanian Formations of the Jebel Gharyan, Libya: in the First Symposium on the Geology of Libya, Gray. C., ed., Faculty of Science, University of Libya, p. 37-85.

Atudorei, N., 1999. Constraints on the Upper Permian to Upper Triassic marine carbon isotope curve. Case studies from the Tethys. Unpubl, PhD Thesis, Lausanne, 160pp.+ Appendix.

Balog, A., Haas, J., Read, J. F., and Coruh, C., 1997. Shallow marine record of orbitally forced cyclicity in a Late Triassic carbonate platform, Hungary. Journal of Sedimentary Research, 67(4).

Bathurst, R. G. C. 1975. Carbonate sediments and their diagenesis (2nd ed.) Elsevier, Amsterdam.

Becker, L., Poreda, R., Basu, A., Pope, K., Harrison, T., Nicholson, C. and Iasky, R. 2004. Bedout: a possible end-Permian impact crater offshore of northwestern Australia. Science, 304, 1469-1476.

Berner, R.A., 2002. Examination of hypotheses for the Permo–Triassic boundary extinction by carbon cycle modeling. Proc. Natl Acad. Sci. USA, 99, 4172-4177.

Bishop, W.F., 1975. Geology of Tunisia and adjacent parts of Algeria and Libya. AAPG bulletin, 59, 413-450.

Bontognali, T. R., Vasconcelos, C., Warthmann, R. J., Bernasconi, S. M., Dupraz, C.,Strohmenger, C. J., & McKenzie, J. A., 2010. Dolomite formation within microbial mats in the coastal sabkha of Abu Dhabi (United Arab Emirates). Sedimentology, 57(3), 824-844.

Boucot, A. J., Gray, J., 2001. A critique of Phanerozoic climatic models involving changes in the CO< sub> 2</sub> content of the atmosphere. Earth-Science Reviews, 56(1), 1-159.

Brand, U., 2004. Carbon, oxygen and strontium isotopes in Paleozoic carbonate components: an evaluation of original seawater-chemistry proxies. Chem. Geol., 204, 23-44.

Brand, U., Veizer, J., 1980. Chemical diagenesis of a multicomponent carbonate system--1: Trace elements. Journal of Sedimentary Research, 50(4).

Broecker, W.S., 1982. Glacial to interglacial changes in ocean chemistry. Prog. Oceanogr., 11,151-197.

Brown Jr, L. and Fisher, W., 1977. Seismic-stratigraphic interpretation of depositional systems: examples from Brazilian rift and pull-apart basins. Seismic Stratigraphy—Applications to Hydrocarbon Exploration: AAPG Mem., 26, 213-248.

Budd, D. A., 1988. Aragonite-to-calcite transformation during fresh-water diagenesis of carbonates: insights from pore-water chemistry. Geological Society of America Bulletin, 100(8), 1260-1270.

Burollet, P. F.,1963. Field trip guidebook of the excursion to Jebel Nefus

(Mesozoic/Tertiary section in Tripolitania). First Saharan symp., petrol. Explor.Soc. Libya, Tripoli, 17 pp.

Chen, Z., Tong, J., Kaiho, K., Kawahata, H. (2007) Onset of biotic and environmental recovery from the end-Permian mass extinction within 1–2 million years: a case study of the Lower Triassic of the Meishan section, South China. Palaeogeography, Palaeoclimatology, Palaeoecology, 252, 176-187.

Choquette, P. W., James, N. P., 1987. Diagenesis# 12. Diagenesis in Limestones-3. The deep burial environment. Geoscience Canada, 14(1).

Coe, A. L. (Ed.)., 2003. The sedimentary record of sea-level change. Cambridge University Press.

Cornell, W. C., Tekbali, A., 1993. Age and Environmental Significance of Palynomorphs Fromthealaziziyah Formation, Northwestern Libya. In: the Nonmarine Triassic (Eds S.G. Lucas and M. Mrales). New Mexico Museum of Natural History and Science Bulletin No.3.

Dal Corso, J., Preto, N., Kustatscher, E., Mietto, P., Roghi, G. and Jenkyns, H.C. 2011. Carbon-isotope variability of Triassic amber, as compared with wood and leaves (Southern Alps, Italy). Palaeogeography, Palaeoclimatology, Paleoecology, 302, 187-193.

Davies, P.J., Bubela, B. and Ferguson, J. 1978. The formation of ooids. Sedimentology, 25, 703-730.

Demaison, G., 1965. The Triassic salt in the Algerian Sahara. Salt basins around Africa. London, Inst. Petroleum, 91-100.

Dercourt, J., Ricou, L.E., Vrielynck, B. (Eds.), 1993. Atlas Tethys Palaeoenvironmental Maps.

Desio, A., Ranchetti, C. R., Invernizi, G., 1960. Sulla Strtigrafia del Trias in Tripolitaniae nel sud-Tunisino, Rev. Ltal-Paleontal. Stratigr, V .66, 273-322.

Desio, A., Ronchetti, R.C., Pozzi, R., Clerici, F., 1963. Stratigraphic studies in the Tripolitania Jabel, Libya. Rev.Ital. Paleontol. Stratigr. Mem., 9, 1-26.

Dewey, J.F., Burke, K.C., 1973. Tibetan, Variscan, and Precambrian basement reactivation: products of continental collision. J. Geol., 683-692.

Dickins, J. M., 1993. Climate of the Late Devonian to Triassic. Palaeogeography, Paleoclimatology, Paleoecology, 100(1), 89-94.

Drever, J.I., 1982. The geochemistry of natural waters: Englewood Cliffs, New Jersey, FrenticeHall, 388 p.

Droser, M. L., and Bottjer, D. J., 1986. A semiquantitative field classification of ichnofabric: Research method paper. Journal of Sedimentary Research, 56(4).

Dubiel, R. F., Parrish, J. T., Parrish, J. M., Good, S. C., 1991. The Pangaean megamonsoon: evidence from the Upper Triassic Chinle Formation, Colorado Plateau. Palaios, 347-370.

Dubois P, Umbach P., 1974. A propos du Trias de deux bassins se´ dimentaires franiais: le Bassin de Paris et le bassin du Sud-Est. Bull Soc Geol France 6: 796—707

Dunham, J. B. 1980. Shallow Subsurface Dolomitization of Subtidally Deposited Carbonate Sediments in the Hanson Creek Formanon (Ordovician—Silurian) of Central Nevada.

Dunham, R.J., 1962. Classification of carbonate rocks according to depositional texture, in Ham, W. E., Ed., Classification of Carbonate Rocks: American Association of Petroleum Geologists Memoir, v. 1, p. 108-121.

EL-Hinnawy, M., Cheshitev, G., 1975. Sheet Tarabulus (NI 33-13), Geological Map of Libya, scale 1:250,000, Explanatory Booklet, Industrial Research Centre, and Tripoli, pp. 118.

Embry, A. F., 2005. Parasequences in Third Generation Sequence Stratigraphy. In American Association of Petroleum Geologists Annual Convention, June 19-22.

Emiliani, C. 1955. Pleistocene temperatures. J. Geol., 538-578.

Fanton, K., Holmden, C., 2007. Sea-level forcing of carbon isotope excursions in epeiric seas: implications for chemostratigraphy. Can. J. Earth Sci., 44, 807-818.

Fatmi, A.N. 1977. The Upper Triassic (Carnian) Ammonite Genus Mojsisoviscites from Jabal Ghryan (Jabal Nefuse) Libya. The Libyan Journal of Science,Libya, 7A 35-48.

Fatmi, A.N., Eliagoubi, B.A., Hammuda, OS., 1980. Stratigraphic nomenclature of the pre-Upper Cretaceous Mesozoic rocks of Jabal Nafusah, NW. Libya, Second Symposium on the Geology of Libya, v. 1., M.J. Salem and M.T. Busrewil., eds., Academic Press, London, p. 57-66.

Ferguson, J., 1987. The significance of carbonate ooids in petroleum source-rock studies. Geological Society, London, Special Publications, 26(1), 207-215.

Ferguson, J., Ibe, A. C. 1981. Origin of light hydrocarbons in carbonate oolites. Journal of Petroleum Geology, 4(1), 103-107.

Flügel, E., 2004. Microfacies of carbonate rocks: analysis, interpretation and application. Springer. pp 400

Frakes, L.A., Francis, J.E., Syktus, J.I., 1992. Climatic modes of the Phanerozoic: Cambridge, Cambridge University Press, pp. 274.

Frank, J.R., Carpenter, A.B., Oglesby, T.W., 1982. Cathodoluminescence and composition of calcite cement in the Taum Sauk Limestone (Upper Cambrian), Southeast Missouri. J. sedim. Petrol. 52, 631-638

Frisia, S., 1994. Mechanisms of complete dolomitization in a carbonate shelf: comparison between the Norian Dolomia Principale (Italy) and the Holocene of Abu Dhabi Sabkha (pp. 55-74). Blackwell Publishing Ltd

Frisia Bruni, S. I. L. V. I. A., Jadoul, F., Weissert, H., 1989. Evinosponges in the Triassic Esino Limestone (Southern Alps): documentation of early lithification and late diagenetic overprint. Sedimentology, 36(4), 685-699.

Galfetti, T., Bucher, H., Brayard, A., Hochuli, P.A., Weissert, H., Guodun, K., Atudorei, V. Guex, J., 2007. Late Early Triassic climate change: insights from carbonate carbon isotopes, sedimentary evolution and ammonoid paleobiogeography. Palaeogeography, Palaeoclimatology, Palaeoecology, 243, 394-411.

Garzanti, E., 1985a. Petrography and diagenesis of Upper Triassic volcanic arenites (S. Giovanni Bianco, Gorno and Val Sabbia Formations, Bergamasc Alps): Boll. Soc. Geol. It., v. 104, p. 3-20.

Gischler, E., Swart, P.K. and Lomando, A.J., 2007. Stable isotopes of carbon and oxygen in modern sediments of carbonate platforms, barrier reefs, atolls, and

ramps: patterns and implications. In: Perspectives in Carbonate Geology: A Tribute to the Career of Robert Nathan Ginsburg (Eds S.K. Peter, E.J. Gregor and M.A. Judith), Int. Assoc. Sedimentol. Spec. Publ., 41, 61-74.

Golonka, J. and Ford, D., 2000. Pangean (late Carboniferous–Middle Jurassic) paleoenvironment and lithofacies. Palaeogeography, Palaeoclimatology, Palaeoecology, 161, 1-34.

Gradstein, F. M., Ogg, G., & Schmitz, M. (Eds.), 2012. The Geologic Time Scale. Elsevier, pp. 1176.

Gray, C., 1971. Structure and origin of the Garian Domes. In Symposium on the Geology of Libya, University of Libya, 307-319, Tripoli.

Grossman, E. L., 2012B. Ch. 10. Oxygen isotope stratigraphy. In F. M. Gradstein, J. G. Ogg, M. Schmitz, and G. Ogg (eds.), The Geologic Time Scale 2012, Elsevier, 195–220.

Grossman, E. L., 2012A. Applying Oxygen Isotope Paleothermometry in Deep Time. In L. C. Ivany and B. T. Huber (eds.), Paleontological Society Papers, v. 18. Paleontological Society, p. 39-67.

Grossman, E. L., Yancey, T. E., Jones, T. E., Bruckschen, P., Chuvashov, B., Mazzullo, S. J., and Mii, H. S., 2008. Glaciation, aridification, and carbon sequestration in the Permo-Carboniferous: the isotopic record from low latitudes. Palaeogeography, Palaeoclimatology, Palaeoecology, 268, 222-233.

Grossman, E.L., 1994. The carbon and oxygen isotope record during the evolution of Pangea: Carboniferous to Triassic. Geol. Soc. Am. Spec. Pap., 288, 207-228.

Grotzinger, J.P., Fike, D.A. and Fischer, W.W.2011. Enigmatic origin of the largest-known carbon isotope excursion in Earth's history. Nature Geoscience, 4, 285-292.

Hajikazemi, E., Al-Aasm, I., Coniglio, M. 2012. Chemostratigraphy of Cenomanian–Turonian carbonates of the Sarvak Formation, Southern Iran. J. Petrol. Geol., 35, 187-205.

Hallett, D., 2002. Petroleum Geology of Libya. Elsevier Science B.V., Amsterdam,503 pp.

Hallock, P., & Schlager, W., 1986. Nutrient excess and the demise of coral reefs and carbonate platforms. Palaios, 389-398.

Halverson, G.P., Hoffman, P.F., Schrag, D.P., Maloof, A.C., Rice, A.H.N., 2005 Toward a Neoproterozoic composite carbon-isotope record. Geol. Soc. Am. Bull., 117, 1181-1207.

Hammuda, O. S., Sebeta, A.M., Mouzughi, A.J., Eliagoubi, B.A., 1985. Stratigraphic nomenclature of the northwestern offshore of Libya. Earth Sciences.

Handford, C. R., Loucks, R. G., 1993. Carbonate depositional sequences and systems tracts-responses of carbonate platforms to relative sea-level changes. Memoirs-American Association Of Petroleum Geologists, 3-3.

Haq, B. U., Hardenbol, J., and Vail, P. R., 1987. Chronology of fluctuating sea levels since the Triassic. Science, 235(4793), 1156-1167.

Hecht, F., Fürst, M., Klitzsch, E., 1964. Zur geologie von Libyen. Geologische Rundschau, 53(2), 413-470. In: Mégnien, C. (Ed.), Synthèse géologique du Bassin de Paris, Mém., 101. BRGM, pp. 37–74.

Holmden, C., Creaser, R., Muehlenbachs, K., Leslie, S. Bergström, S., 1998 Isotopic evidence for geochemical decoupling between ancient epeiric seas and bordering oceans: Implications for secular curves. Geology, 26, 567-570.

Holser, W.T., Schönlaub, H.-P., Attrep, M., Boeckelmann, K., Klein, P., Magaritz, M., Orth, C.J., Fenninger, A., Jenny, C. Kralik, M., 1989. A unique geochemical record at the Permian/Triassic boundary. Nature, 337, 39-44.

Hudson, J. D., 1977. Stable isotopes and limestone lithification. Journal of the Geological Society, 133(6), 637-660.

Immenhauser, A., Della Porta, G., Kenter, J.A., Bahamonde, J.R. 2003 An alternative model for positive shifts in shallow-marine carbonate $\delta^{13}C$ and $\delta^{18}O$. Sedimentology, 50, 953-959.

Immenhauser, A., Kenter, J.A., Ganssen, G., Bahamonde, J.R., Van Vliet, A., Saher, M.H., 2002. Origin and significance of isotope shifts in Pennsylvanian carbonates (Asturias, NW Spain). J. Sed. Res., 72, 82-94.

Irwin, M. L., 1965. General theory of epeiric clear water sedimentation. AAPG Bulletin, 49(4), 445-459.

Isozaki, Y., 1997. Permo-Triassic boundary superanoxia and stratified superocean: records from lost deep sea. Science, 276, 235-238.

Kaufman, A. J., Knoll, A. H., 1995. Neoproterozoic variations in the C-isotopic composition of seawater: stratigraphic and biogeochemical implications. Precambrian Research, 73(1), 27-49.

Kerans, C., Tinker, S., 1997. Carbonate Sequence Stratigraphy, SEPM Spec. Publ.

Knoll, A.H., Bambach, R., Canfield, D., Grotzinger, J., 1996. Comparative Earth history and Late Permian mass extinction. Science-New York Then Washington, 452-457.

Korte, C. and Kozur, H.W., 2010. Carbon-isotope stratigraphy across the Permian–Triassic boundary: a review. Journal of Asian Earth Sciences, 39, 215-235.

Korte, C., Kozur, H. W., Veizer, J., 2005. δ^{13}C and δ^{18}O values of Triassic brachiopods and carbonate rocks as proxies for coeval seawater and palaeotemperature: Paleogeography, Paleoclimatology, Paleoecology, v. 226, p. 287–306.

Krull, E., Retallack, G., Campbell, H., Lyon, G. 2000. δ^{13}Corg chemostratigraphy of the Permian-Triassic boundary in the Maitai Group, New Zealand: Evidence for high-latitudinal methane release. NZ J. Geol. Geophys., 43, 21-32.

Krull, E.S., Lehrmann, D.J., Druke, D., Kessel, B., Yu, Y., Li, R. 2004. Stable carbon isotope stratigraphy across the Permian–Triassic boundary in shallow marine carbonate platforms, Nanpanjiang Basin, south China. Palaeogeography, Palaeoclimatology, Palaeoecology, 204, 297-315.

Kump, L.R., Arthur, M.A. 1999. Interpreting carbon-isotope excursions: carbonates and organic matter. Chem. Geol., 161, 181-198.

Land, L. S., 1986. Environments of limestone and dolomite diagenesis: some geochemical considerations. In: Warme, j. e. and Shanley, k. w. (Editors), carbonate depositional environments, modern and ancient, part 5: Diagenesis 1. Colorado School of Mines Quart., 81, 26-41.

Land, L.S., 1980. The isotopic and trace element geochemistry of dolomite: The state of the art. In Zenger, D.H., Dunham, J.B. & Ethington, R.L., eds., Concepts and

Models of Dolomitization. SEPM Special Publications, Tulsa, 28, 87-110.

Land, L.S., Salem, M.R.I., Morrow, P.W., 1975. Paleohydrology of ancient dolomites: Geochemical evidence: American Association of Petroleum Geologists Bulletin, v. 59, p. 1602-1625.

Laubscher, H., Bernoulli, D., 1977. Mediterranean and Tethys. In The ocean basins and margins (pp. 1-28). Springer US.

Lehrmann, D.J., Minzoni, M., Li, X., Yu, M., Payne, J.L., Kelley, B.M., Schaal, E.K., Enos, P., 2012. Lower Triassic oolites of the Nanpanjiang Basin, south China: Facies architecture, giant ooids, and diagenesis—implications for hydrocarbon reservoirs. AAPG Bull. 96, 1389–1414.

Lohmann, K.C., 1988. Geochemical patterns of meteoric diagenetic systems and their application to studies of paleokarst. In: Paleokarst, pp. 58-80. Springer.

Longman, M. W. 1977. Factors controlling the formation of microspar in the Bromide Formation. Journal of Sedimentary Research, 47(1).

Lucas, S. G., 1998. Global Triassic tetrapod biostratigraph andbiochronology. Palaeogeography, Palaeoclimatology, Palaeoecology, 143(4), 347-384.

Machel, H. G., 2004. Concepts and models of dolomitization: a critical reappraisal. Geological Society, London, Special Publications, 235(1), 7-63.

Magnier, P. 1963. Etude stratigraphique dans le Gebel Nefousa et le Gebel Garian (Tripolitaine, Libya). Bulletine-Societe Geologique de, 5, 89-94.

Mahboubi, A., Moussavi-Harami, R., Carpenter, S. J., Aghaei, A., Collins, L. B., 2010. Petrographical and geochemical evidences for paragenetic sequence interpretation

of diagenesis in mixed siliciclastic–carbonate sediments: Mozduran Formation (Upper Jurassic), south of Agh-Darband, NE Iran. Carbonates and evaporites, 25(3), 231-246.

Marshall, .J. D., 1988. Cathodoluminescence of Geological Materials. Unwin-Hyman, Boston, Mass., 146 pp.

Marshall, J. D., 1992. Climatic and oceanographic isotopic signals from the carbonate rock record and their preservation. Geological Magazine, 129(02), 143-160.

Mastandrea, A., Perri, E., Russo, F., Spadafora, A., & Tucker, M. (2006). Microbial primary dolomite from a Norian carbonate platform: northern Calabria, southern Italy. Sedimentology, 53(3), 465-480.

Mazzullo, S. J., & Harris, P. M. 1992. Mesogenetic dissolution: its role in porosity development in carbonate reservoirs (1). AAPG bulletin, 76(5), 607-620.

McCorkle, D. C., Martin, P. A., Lea, D. W., Klinkhammer, G. P. (1995). Evidence of a dissolution effect on benthic foraminiferal shell chemistry: δ^{13}C, Cd/Ca, Ba/Ca, and Sr/Ca results from the Ontong Java Plateau. Paleoceanography, 10(4), 699-714.

Mitchum Jr, R., Vail, P., Thompson, S. III., 1977. Seismic stratigraphy and global changes of sea level: Part 2. The depositional sequence as a basic unit for stratigraphic analysis: Section 2. Application of seismic reflection configuration to stratigraphic interpretation. AAPG. Mem. 26, 205–212.

Morante, R., 1996. Permian and early Triassic isotopic records of carbon and strontium in Australia and a scenario of events about the Permian-Triassic boundary. Hist.

Biol., 11, 289-310.

Morse, J. and Mackenzie, F. T., 1990. Geochemistry of sedimentary carbonates. Elsevier, New York, 707p.

Moustafa, M. S.; Mriheel, I. Y.; Pope, M., 2012. Sequence Stratigraphy of the Middle-Late Triassic Al Aziziyah Formation, Jifarah Basin, NW Libya. Abstract, AAPG Annual Convention, Long Beach, California.

Moustafa, M. S.; Pope, M., Grossman, E., & Mriheel, I. Y., 2014. Integrated Facies-Based Stratigraphic Architecture, Chemostratigraphy and Diagenesis of the Middle-Late (Ladinian–Carnian) Triassic Al Aziziyah Formation, Jifarah Basin, NW Libya. Abstract, AAPG Annual Convention, Houston, Texas.

Mundil, R., Ludwig, K.R., Metcalfe, I., Renne, P.R., 2004. Age and timing of the Permian mass extinctions: U/Pb dating of closed-system zircons. Science, 305, 1760-1763.

Mutti, M., Simo, I. A., 1994. Distribution, petrography and geochemistry of early dolomite in cyclic shelf facies, Yates Formation (Guadalupian), Capitan Reef Complex, USA. Dolomites: A volume in honour of Dolomieu. International Association of Sedimentologists, Special Publication, (21), 91-109.

Mutti, M., 1994. Association of tepees and palaeokarst in the Ladinian Calcare Rosso (Southern Alps, Italy): Sedimentology, v. 41, p. 621–641.

Mutti, M., Weissert, H., 1995. Triassic monsoonal climate and its signature in Ladinian-Carnian carbonate platforms (Southern Alps, Italy). Journal of Sedimentary Research, 65(3).

Muttoni, G., Garzanti, E., Alfonsi, L., Cirilli, S., Germani, D., & Lowrie, W., 2001. Motion of Africa and Adria since the Permian: Paleomagnetic and paleoclimatic constraints from Northern Libya. Earth and Planetary Science Letters, 159-174.

Palaeoclimatology, Palaeoecology, 143(4), 347-384.

Panchuk, K.M., Holmden, C.E. and Leslie, S.A. 2006. Local controls on carbon cycling in the Ordovician midcontinent region of North America, with implications for carbon isotope secular curves. J. Sed. Res., 76, 200-211.

Parona, C. F., 1914. Per la geologia della Tripolitania. Atti della Reale Accademia delle Scienze di Torino, 50, 16-38.

Parrish, J. T., 1993. Climate of the supercontinent Pangea. The Journal of Geology, 215-233.

Patterson, W.P. and Walter, L.M., 1994. Depletion of ^{13}C in seawater ΣCO_2 on modern carbonate platforms: Significance for the carbon isotopic record of carbonates. Geology, 22, 885-888.

Payne, J.L. and Kump, L.R., 2007. Evidence for recurrent Early Triassic massive volcanism from quantitative interpretation of carbon isotope fluctuations. Earth Planet. Sci. Lett., 256, 264-277.

Payne, J.L., Lehrmann, D.J., Wei, J., Orchard, M.J., Schrag, D.P., Knoll, A.H. (2004) Large perturbations of the carbon cycle during recovery from the end-Permian extinction. Science, 305, 506-509.

Pingitore Jr, N. E., Eastman, M. P., Sandidge, M., Oden, K., Freiha, B., 1988. The coprecipitation of manganese (II) with calcite: an experimental study. Marine

Chemistry, 25(2), 107-120.

Popp, B. N., Podosek, F. A., Brannon, J. C., Anderson, T. F., Pier, J., 1986. < sup> 87</sup> Sr/< sup> 86</sup> Sr ratios in Permo-Carboniferous sea water from the analyses of well-preserved brachiopod shells. Geochimica et Cosmochimica Acta, 50(7), 1321-1328.

Preto, N., Kustatscher, E., Wignall, P. B., 2010. Triassic climates—State of the art and perspectives. Palaeogeography, Palaeoclimatology, Palaeoecology, 290(1), 1-10.

Preto, N., Spötl, C., Guaiumi, C., 2009. Evaluation of bulk carbonate δ13C data from Triassic hemipelagites and the initial composition of carbonate mud. Sedimentology, 56, 1329-1345.

Raulin, C., Frizon de Lamotte, D., Bouaziz, S., Khomsi, S., Mouchot, N., Ruiz, G., Guillocheau, F., 2011. Late Triassic-Early Jurassic block tilting along E-W faults, in southern Tunisia: new interpretation of the Tebaga of Medenine. Journal of African Earth Sciences 61, 94–104.

Read, J. F., 1998. Phanerozoic carbonate ramps from greenhouse, transitional and ice-house worlds: clues from field and modelling studies. Geological Society, London, Special Publications, 149(1), 107-135.

Read, J.F., 1985. Carbonate platform facies models. AAPG bulletin, 69, 1-21.

Reinhardt, L., Ricken, W., 2000. The stratigraphic and geochemical record of Playa Cycles: monitoring a Pangaean monsoon-like system (Triassic, Middle Keuper, S. Germany). Palaeogeography, Palaeoclimatology, Palaeoecology,161(1), 205-227.

Renne, P.R., Basu, A.R., 1991. Rapid eruption of the Siberian Traps flood basalts at the

Permo-Triassic boundary. Science, 253, 176-179.

Rubino J. L., Galeazzi, S. Sbeta,A. M., 2000. Guide book supplement day 1, the Triassic succession of Jabal Nefusah, NW Libya, pp. 23.

Sadooni, F. N., Howari, F., El-Saiy, A., 2010. Microbial dolomites from carbonate-evaporite sediments of the coastal sabkha of Abu Dhabi and their exploration implications. Journal of Petroleum Geology, 33(4), 289-298.

Saltzman, M. and Thomas, E., 2012. Carbon isotope stratigraphy. In: The geologic time scale (Eds J.G.O. F. M. Gradstein, M. Schmitz, and G. Ogg), pp. 207-232.

Saltzman, M.R., Sedlacek, A.R., 2013. Chemostratigraphy indicates a relatively complete Late Permian to Early Triassic sequence in the western United States. Geology, 41, 399-402.

Sarg, J.F., 1988. Carbonate sequence stratigraphy. In: Wilgus, C.K., Hastings, B.S., Kendall, C.G.St.C., Posamentier, H.W., Ross, C.A., Van Wagoner, J.C. (Eds.), Sea-Level Changes: An Integrated Approach. Soc. Econ. Paleontol. Mineral., Spec. Publ. 42, 155–181.

Sarg, J.F., Markello, J.R., Weber, L.J., 1999. The second-order cycle, carbonate-platform growth, and reservoir, source and trap prediction: in P.M. Harris, A.H. Saller, and J.A. Simo, eds., Advances in Carbonate Sequence Stratigraphy: Application to Reservoirs, Outcrops and Models, Society for Sedimentary Geology Special Publication 63, SEPM, Tulsa, OK, 11-34.

Sbeta, A. M., 2008, Field guide to the Triassic and Early Cretaceous successions of Jabal Nafusah NW Libya, pp. 76.

Schlager, W., 2003. Benthic carbonate factories of the Phanerozoic. International Journal of Earth Sciences, 92(4), 445-464.

Scholle, P., 1995. Carbon and sulfur isotope stratigraphy of the Permian and adjacent intervals. In: The Permian of Northern Pangea, pp. 133-149. Springer.

Shackleton, N.J. and Opdyke, N.D., 1973. Oxygen isotope and palaeomagnetic stratigraphy of Equatorial Pacific core V28-238: Oxygen isotope temperatures and ice volumes on a 10< sup> 5</sup> year and 10< sup> 6</sup> year scale. Quatern. Res., 3, 39-55.

Shaw, A.B., 1964. Time in Stratigraphy. McGraw-Hill, New York, N.Y., 365.

Sibley, D. F., 1982. The origin of common dolomite fabrics: clues from the Pliocene. Journal of Sedimentary Research, 52(4).

Sibley, D.F and Gregg, J.M., 1987. Classification of dolomite rock textures. Journal of sedimentary Research, 52(4).

Simms, M. J., Ruffell, A. H., 1990. Climatic and biotic change in the Late Triassic. Journal of the Geological Society, 147(2), 321-327.

Sloss, L. L., 1953. The significance of evaporites. Journal of Sedimentary Research, 23(3).

Spotl, C., Burns, S. J.,1991. Formation of ^{18}O-depleted dolomite within a marine evaporitic sequence, Triassic Reichenhall Formation, Austria. Sedimentology, 38(6), 1041-1057.

Stampfli, G. M., Borel, G. D., 2002. A plate tectonic model for the Paleozoic and Mesozoic constrained by dynamic plate boundaries and restored synthetic oceanic

isochrons. Earth and Planetary Science Letters, 196(1), 17-33.

Stanley Jr, G.D., Swart, P.K., 1995. Evolution of the coral-zooxanthenllae symbiosis during the Triassic: A geochemical approach. Paleobiology, 179-199.

Stoll, H.M., Schrag, D.P., 2000. High-resolution stable isotope records from the Upper Cretaceous rocks of Italy and Spain: Glacial episodes in a greenhouse planet? Geol. Soc. Am. Bull., 112, 308-319.

Swart, P. K., Oehlert, A. M., Mackenzie, G. J., Eberli, G. P., and Reijmer, J. J. G., 2014. The fertilization of the Bahamas by Saharan dust: A trigger for carbonate precipitation?. Geology, 42(8), 671-674.

Swart, P.K., 2008. Global synchronous changes in the carbon isotopic composition of carbonate sediments unrelated to changes in the global carbon cycle. Proc. Natl Acad. Sci. USA, 105, 13741-13745.

Swart, P.K., Eberli, G., 2005. The nature of the δ^{13}C of periplatform sediments: Implications for stratigraphy and the global carbon cycle. Sed. Geol., 175, 115-129.

Swart, P.K., Reijmer, J., Otto, R., 2009. A reevaluation of facies on Great Bahama Bank II: Variations in the δ^{13}C, δ^{18}O and mineralogy of surface sediments. In: Perspectives in Carbonate Geology: A Tribute to the Career of Robert Nathan Ginsburg (Eds S.K. Peter, E.J. Gregor and M.A. Judith),Int. Assoc. Sedimentol. Spec. Publ., 41, 47-59.

Swire, P.H., Gashgesh, T. M., 2000. The bio- chrono- and lithostratigraphy and hydrocarbon prospectivity of the NW Ghadamis Basin and Jifarah Trough, Libya,

in Salem, M. J., and Oun, K.M., eds., The second symposium on the sedimentary Basins of Libya, Earth Science Society of Libya (ESSL), 174-215

Tanner, L.H., 2010. The Triassic isotope record. Geol. Soc. London Spec. Publ., 334, 103-118.

Traverse, A., Ginsburg, R. N., 1966. Palynology of the surface sediments of Great Bahama Bank, as related to water movement and sedimentation. Marine Geology, 4(6), 417-459.

Tucker, M. E., 1982. Precambrian dolomites: Petrographic and isotopic evidence that they differ from Phanerozoic dolomites. Geology, 10, 7-12.

Tucker, M.E. Wright, V.P., 1990. Carbonate Sedimentology. Blackwell Science. P 482

Tucker, M.E., 1988. Techniques in Sedimentology. Blackwell Science Ltd, Oxford.

Vahrenkamp, V.C., 1996. Carbon isotope stratigraphy of the Upper Kharaib and Shuaiba Formations: implications for the Early Cretaceous evolution of the Arabian Gulf region. AAPG bulletin, 80, 647-661.

Vail, P. R., Mitchum Jr, R. M., Thompson III, S., 1977. Seismic Stratigraphy and Global Changes of Sea Level: Part 4. Global Cycles of Relative Changes of Sea Level. Section 2. Application of Seismic Reflection Configuration to Stratigraphic Interpretation, 83-97.

Vail, P.R., Todd, R.G., Sangree, J.B., 1977. Seismic stratigraphy and global changes of sea level, Part five: chronostratigraphic significance of seismic reflections, in Payton, C.E., ed., Seismic Stratigraphy—Applications to Hydrocarbon Exploration: Tulsa, OK, AAPG. Mem., 26, 99-116.

Van Wagoner, J.C., H.W. Posamentier, R.M. Mitchum, P.R. Vail, J.F. Sarg, T.S. Loutit, J. Hardenbol., 1988. An overview of sequence stratigraphy and key definitions, in C.W. Wilgus et al., eds., Sea level changes: an integrated approach: SEPM Special Publication 42, 39–45.

Vasconcelos, C., McKenzie, J. A., 1997. Microbial mediation of modern dolomite precipitation and diagenesis under anoxic conditions (Lagoa Vermelha, Rio de Janeiro, Brazil). Journal of Sedimentary Research, 67(3).

Vasconcelos, C., McKenzie, J. A., Bernasconi, S., Grujic, D., and Tiens, A. J., 1995. Microbial mediation as a possible mechanism for natural dolomite formation at low temperatures. Nature, 377(6546), 220-222.

Veizer, J. 1983. Chemical diagenesis of carbonates: theory and application of trace element technique.

Veizer, J., Ala, D., Azmy, K., Bruckschen, P., Buhl, D., Bruhn, F., Carden, G.A., Diener, A., Ebneth, S. Godderis, Y., 1999. ^{87}Sr/86Sr, δ^{13}C and δ^{18}O evolution of Phanerozoic seawater. Chem. Geol., 161, 59-88.

Vincent, B., Emmanuel, L., Houel, P., Loreau, J. P., 2007. Geodynamic control on carbonate diagenesis: petrographic and isotopic investigation of the Upper Jurassic formations of the Paris Basin (France). Sedimentary Geology, 197 (3), 267-289.

Wefer, G. Berger, W.H., 1991. Isotope paleontology: growth and composition of extant calcareous species. Mar. Geol., 100, 207-248.

Weissert, H., Lini, A., Föllmi, K.B. Kuhn, O., 1998. Correlation of Early Cretaceous carbon isotope stratigraphy and platform drowning events: a possible link?

Palaeogeography, Palaeoclimatology, Palaeoecology, 137, 189-203.

Woodard, S.C., Thomas, D.J., Grossman, E.L., Olszewski, T.D., Yancey, T.E., Miller, B.V. Raymond, A., 2013 Radiogenic isotope composition of Carboniferous seawater from North American epicontinental seas. Palaeogeography, Palaeoclimatology, Palaeoecology, 370, 51-63.

Woodruff, F., Savin, S.M. Douglas, R.G., 1980. Biological fractionation of oxygen and carbon isotopes by recent benthic foraminifera. Mar. Micropaleontol., 5, 3-11.

Ziegler, P. A., 1990. Geological Atlas of Western and Central Europe, Shell Internationale Petroleum Maatschappij BV/Geological Society of London.

Zivanovic, M., 1975. Geological map of Libya, Sheet Bani Walid (33-2), explanatory booklet: Industrial research center, Tripoli, 54-60.

APPENDIX A

ISOTOPE DATA FOR GHRYAN DOME (GD) AND KAF BATES (KB)

SECTIONS

PF=PERITIDAL FACIES; BF=BARRIER FACIES; SF= SHALLOW SUBTIDAL

FACIES; DF=DEEP SUBTIDAL FACIES

Height (m) GD	Facies	δ¹³C (VPDB)	δ¹⁸O (VPDB)	δ¹³C (VPDB) 5 pt. avg.	δ¹⁸O (VPDB) 5 pt. avg.
0.2	BF	0.4	-4.5		
0.8	PF	-0.3	-6.2		
1.4	PF	-0.1	-4.8	-0.1	-4.6
1.8	PF	0.0	-3.1	0.1	-3.9
2.2	PF	-0.2	-3.9	0.1	-3.6
2.9	BF	0.5	-3.4	0.3	-3.2
4.1	BF	0.6	-2.7	0.2	-2.8
4.6	BF	0.1	-2.3	0.2	-2.6
5	PF	0.0	-1.8	0.3	-2.7
5.7	BF	0.3	-4.2	-0.1	-3.6
6	PF	-0.1	-4.3	-0.3	-4.2
7.9	BF	0.2	-4.6	0.0	-4.8
9.3	PF	0.4	-5.5	0.2	-5.0
9.7	PF	0.2	-5.5	0.2	-5.1
10.3	BF	0.4	-3.9	0.3	-4.8
10.7	BF	-0.4	-5.8	0.2	-4.6
11.2	PF	0.9	-3.6	0.5	-3.9
13.2	PF	0.5	-2.6	0.5	-3.5
13.8	BF	0.5	-4.2	0.5	-3.6
14.7	SF	0.1	-2.9	0.6	-4.6
15.3	SF	1.2	-4.3	1.1	-4.1
15.7	SF	2.0	-4.5	1.4	-4.2
19.2	BF	1.1	-5.1	1.5	-4.2
19.7	BF	1.7	-2.7	1.7	-3.4
20.2	BF	1.9	-2.9	1.7	-3.1
20.7	BF	1.7	-2.8	1.6	-2.9
21.2	BF	1. 4	-3.1	1.3	-3.1
21.7	BF	0.6	-3.1	0.7	-3.1
22.2	BF	0.5	-3.3	0.4	-3.4
22.7	BF	-0.5	-3.4	0.3	-3.6
25.7	BF	0.4	-4.4	1.1	-4.0
32.7	SF	3.1	-4.1	2.2	-4.1
32.8	DF	3.2	-3.8	2.9	-4.2
33.2	DF	3.1	-4.3	3.1	-4.2
34.3	SF	2. 9	-4.7	3.1	-4.3
34.7	SF	3.3	-3.5	3.1	-4.1
35.2	BF	2.9	-4.4	2.6	-4.3
35.5	BF	2.7	-4.5	2.4	-4.2
35.8	BF	-0.5	-4.3	1.2	-4.1
36.3	BF	1.2	-3.1	1.5	-3.9
36.8	BF	3.0	-4.2	2.2	-4.4
37.8	BF	2.7	-5.3	2.6	-4.6
38.3	PF	2.0	-5.5	2.7	-4.5
39.3	PF	*3.9*	-2.7	3.1	-3.7
39.8	PF	2.6	-3.2	2.9	-3.5

Height (m) GD	Facies	$\delta^{13}C$ (VPDB)	$\delta^{18}O$ (VPDB)	$\delta^{13}C$ (VPDB) 5pt. avg.	$\delta^{18}O$ (VPDB) 5 pt. avg.
40.3	BF	3.4	-3.1	2.9	-3.9
41.3	BF	2.9	-5.4	2.6	-4.7
41.9	BF	0.9	-6.6	2.1	-4.8
42.2	BF	2.9	-2.6	2.4	-3.7
42.7	BF	2.6	-2. 8	2.4	-3.3
43.3	BF	2.6	-2.6	2.4	-3.3
43.8	BF	1. 5	-4.6	2.0	-4.0
44.5	BF	2.3	-5.1	2.1	-3.9
45	BF	2.2	-3.3	2.2	-3.1
45.5	PF	2.9	-0.3	2.5	-2.5
46	BF	2.8	-2. 7	2.3	-3.2
46.5	PF	1.1	-6.4	1.9	-4.2
47	BF	1.8	-4.1	2.0	-4.0
47.5	BF	2.6	-2.6	2.2	-3.3
48	BF	2.4	-2.7	2.3	-2.7
48.5	BF	2.1	-2.6	2.2	-2.5
49	PF	1.9	-2.5	2.1	-2.5
49.5	PF	2.0	-2.1	2.0	-2.4
50	PF	1.9	-2.9	1.9	-2.7
50.5	PF	2.1	-2.4	1.8	-2.8
51	PF	0.7	-3. 5	1.4	-3.1
51.5	PF	2.2	-3.2	1.5	-3.1
52.5	PF	0.9	-3.4	1.1	-2.9
53	PF	0.6	-2.2	0.9	-2.4
53.5	PF	0.9	-1.8	0.5	-2.0
54	PF	0.5	-1.6	-0.4	-2.4
55	PF	-1.8	-1.8	-1.5	-2.8
55.5	PF	*-4.4*	-7.7	-2.4	-3.9
56	PF	-1.3	-0. 9	-1.9	-2.4
57.5	PF	-0.9	-1.0	-1.5	-1.7
60.8	SF	-1.5	-1.4	-1.2	-2.0
62.3	PF	-1.3	-1.0	-1.1	-3.2
63.8	SF	-0.3	*-9.3*	-0.7	-5.8
64.3	SF	-1.2	-5. 6	-0.4	-6.0
66	PF	0.7	-5.9	0.4	-6.3
66.5	PF	1.3	-5.9	.9	-6.2
67	PF	0.9	-6.5	1.2	-6.6
70.8	SF	1.7	-7.4	1.4	-7.1
71.3	PF	1.5	-7.8	1.5	-7. 5
71.8	SF	1.6	-7.5	1.6	-7.6
72.3	SF	1.5	-7.3	1.6	-7.3
72.8	SF	1.5	-8.0	1.6	-7.0

Height (m) GD	Facies	δ^{13}C (VPDB)	δ^{18}O (VPDB)	δ^{13}C (VPDB) 5 pt. avg.	δ^{18}O (VPDB) 5 pt. avg.
77.8	PF	1.9	-5.2	1.7	-4.7
78.3	PF	1.9	-4.3	1.7	-4.6
78.8	BF	1.7	-4.5	1.7	-5.0
79.3	SF	1.3	-6.1	1.5	-5.5
79.8	SF	1.4	-6.7	1.4	-5.7
80.5	SF	1.3	-4.5	1.3	-5.1
81.8	PF	1.0	-4.7	1.2	-4.7
82.8	PF	1.6	-4.3	1.1	-4.1
83.8	PF	0.8	-4.3	0.6	-3.4
84.3	BF	-0.8	-0.9	0.1	-2.1
86.8	BF	0.0	-1.8	0.3	-1.6
87.5	BF	1.2	-0.9	0.8	-1.1
87.8	BF	1.4	-0.8	1.2	-1.0
88.3	BF	1.1	-0.9	1.2	-0.9
88.8	BF	1.3	-1.0	1.1	-1.0
89.3	BF	1.1	-0.9	0.8	-0.9
89.8	BF	0.3	-1.1	-0.3	-0.9
90.3	BF	-0.2	-0.4	-0.2	-0.7
90.8	BF	-0.8	-0.8	-0.5	-0.8
93.7	BF	-1.0	-0.9	-0.6	-0.9
94.3	BF	0.6	-1.1	0.0	-1.0
94.8	PF	0.1	-1.2	0.1	-1.0
95.3	PF	0.4	-0.7	0.3	-0.9
99.3	BF	0.0	-0. 3	0.4	-0.8
100.8	BF	1.3	-1.5	0.8	-1.4
101.3	PF	1.2	-0.9	0.8	-1.6
101.8	PF	0.5	-4.3	0.5	-2.2
104.7	PF	-0.3	-0.5	-0.1	-1.3
105.5	BF	-0. 3	-0.3	-0.3	-0.9
107	PF	-1.5	-0.9	-0.3	-0.7
108	BF	1.6	-0. 6	0.2	-1.2
109.5	PF	1.1	-1.2	-1.0	-1.9
110.3	BF	*-7. 8*	-5.6	-2.9	-2.6
112	BF	-0.4	-0.4	-2.5	-1.9
112.8	BF	-1.1	-0.1	-2.8	-1.7
113.3	BF	*-6.6*	-4.8	*-3.3*	-2.1
113.8	PF	-1.5	-0.4	-2.1	-1.1
114.3	PF	-0.5	-0.1	-1.0	-0.6
117.3	PF	0.4	-0.1	0.3	0.1
129	BF	0.6	-0.1	1.0	0.0
130	PF	2.9	*0.5*	1.9	-0.0
131.3	PF	1.9	-0.2	2.2	-0.3

Height (m) GD	Facies	$\delta^{13}C$ (VPDB)	$\delta^{18}O$ (VPDB)	$\delta^{13}C$ (VPDB) 5pt. avg.	$\delta^{18}O$ (VPDB) 5 pt. avg.
132.3	BF	2.6	-1.7	2.5	-0.6
133	PF	2.6	0.4	2.4	-0.2
134	PF	2.7	0.3	2.1	0.1
134.5	PF	0.7	-0.2	1.0	-0.1
136.3	BF	0.9	-0.4		

Height (m) KB	Facies	$\delta^{13}C$ (VPDB)	$\delta^{18}O$ (VPDB)	$\delta^{13}C$ (VPDB) 5 pt. avg.	$\delta^{18}O$ (VPDB) 5 pt. avg.
0.5	PF	0.6	-3.6		
1	PF	2.2	-3.3		
1.5	PF	1.4	-3.7	1.5	-3.4
2	PF	1.9	-2.3	1.3	-3.2
2.5	BF	0.1	-3.8	0.7	-3. 6
3	BF	0.2	-4.3	0. 6	-3.7
3.5	BF	1.2	-3.5	0.7	-3.7
4	BF	0.7	-3.5	0.7	-3.7
4.5	BF	0.6	-3.9	0.7	-3.7
6.5	DF	0.1	-3.7	0.8	-3.7
7	DF	2.2	-3.6	1.1	-3.7
7.5	DF	0.7	-3.3	1.0	-3.8
8	BF	0.1	-5.1	0.8	-4.4
8.5	BF	2.3	-3.3	0.8	-4.5
9.5	BF	-0.4	-6.4	-0.2	-5.5
11	DF	-0.6	-5.5	-0.3	-5.6
11.5	PF	0.1	-6.3	-0.6	-5.9
12	PF	-1.8	-4.8	-1.0	-5.5
12.5	SF	-1.1	-6.9	-0.8	-5.7
13	SF	0.2	-3.7	-0.4	-4.9
13.5	SF	-0.4	-5.8	-0.3	-4.7
14	SF	-0.4	-3.8	-0.4	-3.9
14.5	SF	-0.2	-1.5	-0.5	-2.9
15	BF	-1.1	-5.7	-0.7	-5.3
15.5	SF	-0.5	-3.6	-0.8	-4.7
16	SF	-1.3	-6.8	-0.9	-5.7
16.5	SF	-0.8	-6.3	-0.9	-5.6
17	SF	-0.6	-3.9	-1.4	-5.3
17.5	SF	-1.9	-5.7	-1.4	-5.4
18	BF	-1.4	-5.8	-1.4	-5.5
18.3	PF	-1.8	-5.2	-1.5	-5.4
18.5	PF	-0. 7	-5.7	-1.3	-5.1
19	BF	-1.3	-4.9	-1.6	-4.7
19.8	SF	-2.8	-2.5	-2.0	-4.4
20.8	BF	-1.5	-6.1	-1.9	-5.1
21.3	SF	-3.1	-6.2	-1.9	-5.4
21.8	DF	-0.1	-4.6	-0.9	-5.4
22.3	DF	-0.6	-5.3	-0.3	-5.3
23.3	SF	0.3	-6.5	0.4	-5.3
23.8	SF	2.3	-3.4	0.5	-5.0
24.3	DF	-0.6	-5.2	-0.5	-5.4
24.8	DF	-2.9	-7.3	-1.4	-5.9
25.3	DF	-1.3	-5.1	-1.2	-5.6
25.8	DF	-0. 9	-5.8	-0.5	-5.2
26.3	SF	1.3	-3.8	0.6	-4.5
26.8	SF	1.2	-4.1	1.0	-4.3
27.3	SF	1.2	-4.4	1.3	-4.2

Height (m) KB	Facies	δ^{13}C (VPDB)	δ^{18}O (VPDB)	δ13C (v-PDB) 5 pt. avg.	δ^{18}O (VPDB) 5 pt. avg.
84.3	SF	2.3	-4.9	2.4	-4.7
84.8	S.F	3.4	-4.3	3.0	-4.6
85.4	SF	3.3	-4.3	3.0	-4. 7
86	SF	3.1	-5.3	2.8	-5.1
86.5	SF	1.6	-5.7	2. 2	-5.4
87	SF	2.1	-5.5	2	-5.5
87.8	SF	1.9	-5.5	1.8	-5.5
88.4	SF	1.4	-5.7	1.7	-5.5
88.8	SF	1.4	-5.5	1.8	-5.2
89.3	BF	2.6	-4.9	2.3	-5.1
89.8	SF	3	-4.7	2.1	-5.0
90.3	SF	3.0	-4.5	1.3	-5.4
90.8	DF	-3.2	-6.9	-0.4	-6.3
91.3	DF	-1.2	-7.4	0.3	-6.6
91.8	DF	2.4	-5.9	0.6	-6.6
92.3	DF	0.5	-6.3	0.9	-6.6
92.8	SF	0.1	-8.2	1.2	-6.9
93.3	SF	2.6	-4.7	1. 8	-5.9
94.3	BF	2.1	-5.9	1.9	-6.0
94.8	BF	2.4	-5.7	2.0	-5.9
95.3	SF	0.5	-6.7	1.4	-6.1
95.8	BF	2.3	-5.5	1.7	-5.9
96.3	SF	0.8	-5.9	1.5	-5.9
96.8	SF	2.5	-5.7	2.0	-5.4
97.3	SF	2.1	-5.5	2.2	-4.6
97.7	BF	2.1	-2.4	2.4	-3.4
98.3	BF	3.2	-2.2	2.8	-2.6
98.8	BF	2.8	-2.3	2.8	-2.3
99.3	SF	2.9	-2.3	2.7	-2.5
99.8	SF	2.3	-2.8	2.3	-2.4
100.3	SF	1.3	-1.7	2.0	-2.3
100.8	SF	2.9	-2.9	2.3	-3.1
101.3	SF	2.1	-3.7	2.2	-4.1
101.8	SF	2.3	-6.4	2.2	-5.3
102.5	BF	1.9	-6.5	2.0	-5.8
103.3	BF	2.2	-4.9	1.9	-5.6
103.8	BF	1.6	-5.6	1.9	-5.3
104	BF	1.1	-5.8	2.1	-4.8
104.5	SF	3.7	-3	2.8	-3.7
104.8	SF	3.2	-2.7	3.6	-3.1
105.3	SF	3.2	-2.9	3.1	-2.9

Height (m) KB	Facies	$\delta^{13}C$ (VPDB)	$\delta^{18}O$ (VPDB)	$\delta^{13}C$ (VPDB) 5pt. avg.	$\delta^{18}O$ (VPDB) 5 pt. avg.
105.8	SF	2.9	-3.2	2.9	-3.1
106.3	SF	2.7	-2.3	2.6	-3.4
107	SF	2.2	-4.8	2.4	-4.0
108.3	BF	1.9	-5.6	2.4	-4.0
111.7	DF	2.9	-2.1	2.7	-2.9
112.3	DF	2.9	-1.6	2.8	-2.1
112.8	BF	2.7	-1.5	2.8	-1.8
113.3	SF	3.0	-2.1	2.8	-2.0
113.8	DF	2.2	-2.6	2.7	-2.2
114.3	DF	3.2	-2.2	2.8	-2.1
114.8	DF	2.9	-1.7	2.6	-2.4
115.5	BF	1.6	-1.8	2.6	-2.7
116	SF	2.1	-6.4		

APPENDIX B

RESULTS OF TRACE ELEMENT FROM CALCITE CEMENT FROM

GHRYAN DOME (GD) AND KAF BATES (KB) SECTIONS (PPM)).

MOLE % (NORMALIZED FOR MG, CA, FE, MN, SR (

NOTE THAT THE ITALIC VALUES INDICATE VALUES UNDER THE LIMIT

OF DETECTION (LLD)

Analysis	Height (m)	Ca (ppm)	Mg (ppm)	Fe (ppm)	Mn (ppm)	Sr (ppm)	S (ppm)	Na (ppm)	Al (ppm)	Si (ppm)
Reported LLD		560	30	150	100	200	80	70	130	140
3calcite_stdck#1		388014	35	*34*	803	*65*	*20*	*35*	0	175
5CaCO3_stdck#1		398361	*49*	*0*	354	*142*	24	182	21	*108*
3calcite_stdck#1		412701	*26*	*24*	817	309	*0*	139	21	*82*
GD76_a_pt06	53.5	398594	1220	178	*0*	944	*0*	291	0	*74*
GD76_a_pt07	53.5	397212	1909	824	*91*	380	115	200	102	*82*
GD76_c_pt01	53.5	398630	1119	1022	143	231	*56*	113	0	*63*
GD76_c_pt02	53.5	397877	1202	988	225	*101*	101	191	0	*28*
GD76_c_pt03	53.5	396748	1410	694	158	439	*0*	191	0	*25*
GD91_a_pt01	96.3	394381	2566	675	311	*178*	112	191	21	*4*
GD91_a_pt02	96.3	392995	2540	1369	301	243	*12*	139	0	*0*
GD91_b_pt01	96.3	397781	1534	482	292	*113*	125	126	9	*63*
GD91_b_pt02	96.3	397052	983	294	339	*77*	95	213	5	*61*
GD91_c_pt01	96.3	395050	2064	1383	*0*	*142*	124	122	7	*25*
GD91_c_pt02	96.3	397092	750	468	*86*	*101*	88	152	0	*57*
KB118_a_pt01	96.3	392591	2903	1711	163	*196*	95	104	0	*23*
KB118_a_pt02	96.3	395698	3004	280	*124*	*59*	166	191	0	*15*
KB118_a_pt03	96.3	394601	2131	1605	*124*	*6*	86	139	0	*72*

Analysis	Height (m)	Ca (ppm)	Mg (ppm)	Fe (ppm)	Mn (ppm)	Sr (ppm)	S (ppm)	Na (ppm)	Al (ppm)	Si (ppm)
KB118_a_ pt04	96.3	395346	4094	646	148	*0*	*66*	130	21	*68*
KB118_a_ pt05	96.3	393656	1958	3297	320	*0*	187	234	32	*30*
KB118_a_ pt06	96.3	396840	2722	193	*91*	*154*	171	161	0	*0*
KB118_a_ pt07	96.3	395398	3388	545	220	*148*	183	256	14	*0*
KB118_a_ pt08	96.3	393256	4157	675	153	*0*	119	204	0	*38*
KB118_b_ pt01	96.3	397368	2577	164	182	214	405	126	2	*112*
KB118_c_ pt01	96.3	390413	3979	2536	315	*36*	338	195	0	*21*
KB118_c_ pt02	96.3	397805	2027	468	225	*107*	291	213	0	*4*
KB118_c_ pt03	96.3	394465	2857	1793	163	*190*	32	182	7	*0*
KB118_c_ pt04	96.3	395762	2131	*77*	167	*0*	222	200	0	*30*
KB118_d_ pt01	96.3	395046	1548	1702	167	*95*	151	291	16	*53*
KB118_d_ pt02	96.3	395222	3442	598	143	*184*	125	295	0	*23*
KB118_d_ pt03	96.3	399783	2047	178	191	*0*	168	278	0	*89*
KB118_d_ pt04	96.3	394181	4143	1972	292	291	180	243	0	*4*
Average		395744	2371.5	957.7	183.3	165.3	136.1	191.7	8.4	37.9

Analysis	Height (m)	Ca (ppm)	Mg (ppm)	Fe (ppm)	Mn (ppm)	Sr (ppm)	S (ppm)	Na (ppm)	Al (ppm)	Si (ppm)
Reported LLD		560	30	150	100	200	80	70	130	140
5CaCO3_stdck#1		397953	*0*	*0*	373	451	143	117	*0*	188
3calcite_stdck#1		394157	*0*	*0*	1075	*0*	29	*74*	*0*	*139*
GD03_pt01	0.2	392391	3229	1118	526	*142*	293	816	*44*	*36*
GD03_pt02	0.2	395194	2811	1099	387	320	337	781	65	70
GD03_pt03	0.2	392054	3941	1234	970	*148*	202	291	141	*21*
GD03_pt04	0.2	399731	1271	680	191	433	312	360	*46*	87
GD03_pt05	0.2	394669	5207	1610	234	*0*	107	247	*78*	*0*
GD03_pt06	0.2	395674	3961	227	172	599	367	352	*53*	95
GD03_pt07	0.2	386428	3757	1451	1104	*0*	360	382	*30*	*0*
GD03_pt08	0.2	391422	2292	819	368	214	396	829	*58*	*21*
GD03_pt09	0.2	391974	5977	1249	172	*77*	234	187	*23*	*53*
GD12_pt03	4.6	391586	3771	4160	2156	*154*	72	464	*69*	203
GD12_pt09	4.6	384214	2828	2748	526	*184*	80	95	284	*95*
GD15_pt01	6	400147	1188	154	617	*0*	152	174	*30*	28
GD15_pt02	6	393428	3990	868	922	*119*	118	161	*0*	*0*
GD15_pt03	6	393928	2157	559	492	*0*	270	126	*46*	*0*
GD15_pt05	6	396467	3875	304	660	*6*	93	187	*108*	*21*
GD15_pt07	6	394249	3119	*96*	636	214	179	191	*67*	99
GD15_pt08	6	393080	4653	1475	349	*142*	299	200	*65*	*0*
GD15_pt09	6	393416	5213	1359	449	*142*	192	278	*76*	*0*
GD15_pt10	6	395234	2722	443	358	356	316	161	*25*	*0*
Average		393436.1	3471.7	1139.7	594.2	171.2	230.4	330.5	68.9	43.7

Analysis	Height (m)	Ca (PPM)	Mg (PPM)	Fe (PPM)	Mn(ppm)	Sr (PPM)	S(PPM)	Na (PPM)	Al(PPM)	Si (PPM)
LLD		320	230	150	100	200	40	70	20	40
3dolomite_stdck#1		220130	132740	610	160	*30*	*0*	*0*	50	200
GD12_pt01	4.6	227870	128480	3740	390	*80*	90	640	300	390
GD12_pt02	4.6	211050	122850	12900	360	*160*	20	790	120	160
GD12_pt04	4.6	220440	124040	12690	460	*0*	20	230	80	80
GD12_pt05	4.6	228500	126470	3520	320	*20*	80	200	60	40
GD12_pt06	4.6	222410	127860	1460	250	*0*	80	290	10	*20*
GD12_pt07	4.6	220420	129960	3480	320	*80*	70	130	50	*0*
GD12_pt08	4.6	215100	119560	18750	410	*0*	90	*20*	40	80
GD12_pt10	4.6	242950	115670	3560	400	*80*	250	270	190	*0*
GD12_pt11	4.6	239260	114500	9410	510	*90*	270	200	130	30
GD12_pt12	4.6	238100	112010	11470	540	*90*	130	160	130	*0*
GD12_pt13	4.6	239410	113840	6930	980	*20*	260	160	100	*0*
GD12_pt14	4.6	241280	111680	7660	1080	*20*	270	170	70	10
GD15_pt04	6	242150	111500	7780	590	*140*	150	180	110	70
GD15_pt06	6	242490	111200	9190	550	*20*	270	330	220	380

Analysis	Height (m)	Ca (ppm)	Mg (ppm)	Fe (ppm)	Mn (ppm)	Sr (ppm)	S (ppm)	Na (ppm)	Al (ppm)	Si (ppm)
Reported LLD		390	230	150	100	200	40	70	20	40
3dolomite_stdck#1		217663	131707	694	119	*24*	*26*	130	57	138
GD76_a_pt01	53.5	236484	108591	13449	320	*77*	160	243	175	*26*
GD76_a_pt02	53.5	237977	108715	13300	215	*107*	179	334	239	79
GD76_a_pt03	53.5	234433	108677	16684	382	*0.000*	160	278	281	75
GD76_a_pt04	53.5	238998	108092	12066	358	*0.000*	181	96	108	*36*
GD76_a_pt05	53.5	234874	108167	15368	425	*131*	139	282	334	351
GD76_b_pt01	53.5	238073	109568	12123	272	*131*	195	295	156	*2*
GD76_b_pt02	53.5	237044	107746	11709	12001	214	220	182	136	*28*
GD76_b_pt03	53.5	239175	109603	8170	239	*0*	210	156	141	*0*
GD76_c_pt04	53.5	240011	110098	8846	253	*190*	211	109	152	78

183

MOLE % (normalized for Mg, Ca, Fe, Mn, Sr only)						
Analysis	Height (M)	Ca (mole%)	Mg (mole%)	Fe (mole%)	Mn (mole%)	Sr (mole%)
3calcite_stdck#1		99.8	0.00	0.00	0.15	0.00
5CaCO3_stdck#1		99.9	0.00	0.00	0.05	0.00
3calcite_stdck#1a		99.8	0.00	0.00	0.15	0.05
GD76_a_pt06	53.5	99.3	0.50	0.05	0.00	0.10
GD76_a_pt07	53.5	99.0	0.80	0.15	0.00	0.05
GD76_c_pt01	53.5	99.2	0.45	0.20	0.05	0.05
GD76_c_pt02	53.5	99.2	0.50	0.20	0.05	0.00
GD76_c_pt03	53.5	99.2	0.60	0.10	0.05	0.05
GD91_a_pt01	71.3	98.8	1.05	0.10	0.05	0.00
GD91_a_pt02	71.3	98.6	1.05	0.25	0.05	0.05
GD91_b_pt01	71.3	99.2	0.65	0.10	0.05	0.00
GD91_b_pt02	71.3	99.5	0.40	0.05	0.05	0.00
GD91_c_pt01	71.3	98.9	0.85	0.25	0.00	0.00
GD91_c_pt02	71.3	99.6	0.30	0.10	0.00	0.00
KB118_a_pt01	96.3	98.4	1.20	0.30	0.05	0.00
KB118_a_pt02	96.3	98.7	1.25	0.05	0.00	0.00
KB118_a_pt03	96.3	98.8	0.90	0.30	0.00	0.00
KB118_a_pt04	96.3	98.2	1.65	0.10	0.05	0.00
KB118_a_pt05	96.3	98.5	0.80	0.60	0.05	0.00
KB118_a_pt06	96.3	98.8	1.10	0.05	0.00	0.00
KB118_a_pt07	96.3	98.4	1.40	0.10	0.05	0.00
KB118_a_pt08	96.3	98.1	1.70	0.10	0.05	0.00
KB118_b_pt01	96.3	98.8	1.05	0.05	0.05	0.00
KB118_c_pt01	96.3	97.8	1.65	0.45	0.05	0.00
KB118_c_pt02	96.3	99.0	0.85	0.10	0.05	0.00
KB118_c_pt03	96.3	98.5	1.15	0.30	0.05	0.00
KB118_c_pt04	96.3	99.0	0.90	0.00	0.05	0.00
KB118_d_pt01	96.3	99.0	0.65	0.30	0.05	0.00
KB118_d_pt02	96.3	98.4	1.40	0.10	0.05	0.00
KB118_d_pt03	96.3	99.0	0.85	0.05	0.05	0.00
KB118_d_pt04	96.3	97.8	1.70	0.35	0.05	0.05

MOLE % (normalized for Mg, Ca, Fe, Mn, Sr only)						
Analysis	Height (m)	Ca (mole%)	Mg (mole%)	Fe (mole%)	Mn (mole%)	Sr (mole%)
3dolomite_stdck#1		50.0	49.9	0.10	0.00	0.00
GD76_a_pt01	53.5	55.6	42.1	2.26	0.05	0.00
GD76_a_pt02	53.5	55.7	42.0	2.26	0.05	0.00
GD76_a_pt03	53.5	55.1	42.1	2.81	0.05	0.00
GD76_a_pt04	53.5	56.1	41.8	2.05	0.05	0.00
GD76_a_pt05	53.5	55.3	42.0	2.61	0.05	0.00
GD76_b_pt01	53.5	55.7	42.2	2.05	0.05	0.00
GD76_b_pt02	53.5	54.9	41.2	1.95	2.01	0.00
GD76_b_pt03	53.5	56.2	42.4	1.35	0.05	0.00
GD76_c_pt04	53.5	56.1	42.4	1.50	0.05	0.00

MOLE % (normalized for Mg, Ca, Fe, Mn, Sr only)						
Analysis	Height (M)	Ca (mole%)	Mg (mole%)	Fe (mole%)	Mn (mole%)	Sr (mole%)
3dolomite_stdck#1		50.1	49.8	0.10	0.05	0.00
GD12_pt01	4.6	51.5	47.9	0.60	0.05	0.00
GD12_pt02	4.6	49.9	47.9	2.21	0.05	0.00
GD12_pt04	4.6	50.7	47.1	2.10	0.10	0.00
GD12_pt05	4.6	52.0	47.4	0.55	0.05	0.00
GD12_pt06	4.6	51.2	48.5	0.25	0.05	0.00
GD12_pt07	4.6	50.4	49.0	0.55	0.05	0.00
GD12_pt08	4.6	50.5	46.3	3.15	0.05	0.00
GD12_pt10	4.6	55.6	43.7	0.60	0.05	0.00
GD12_pt11	4.6	55.0	43.4	1.55	0.10	0.00
GD12_pt12	4.6	55.2	42.8	1.90	0.10	0.00
GD12_pt13	4.6	55.3	43.4	1.15	0.15	0.00
GD12_pt14	4.6	55.9	42.7	1.25	0.20	0.00
GD15_pt04	6	56.1	42.5	1.30	0.10	0.00
GD15_pt06	6	56.0	42.4	1.51	0.10	0.00

MOLE % (normalized for Mg, Ca, Fe, Mn, Sr only)						
Analysis	Height (M)	Ca (mole%)	Mg (mole%)	Fe (mole%)	Mn (mole%)	Sr (mole%)
5CaCO3_stdck#1		99.9	0.00	0.00	0.05	0.05
3calcite_stdck#1		99.8	0.00	0.00	0.20	0.00
GD03_pt01	0.2	98.3	1.36	0.20	0.10	0.00
GD03_pt02	0.2	98.5	1.16	0.20	0.05	0.05
GD03_pt03	0.2	98.0	1.60	0.20	0.20	0.00
GD03_pt04	0.2	99.3	0.50	0.10	0.05	0.05
GD03_pt05	0.2	97.5	2.10	0.30	0.05	0.00
GD03_pt06	0.2	98.2	1.60	0.05	0.05	0.05
GD03_pt07	0.2	98.0	1.56	0.25	0.20	0.00
GD03_pt08	0.2	98.8	0.96	0.15	0.05	0.00
GD03_pt09	0.2	97.3	2.45	0.20	0.05	0.00
GD12_pt03	4.6	97.3	1.55	0.75	0.40	0.00
GD12_pt09	4.6	98.2	1.20	0.50	0.10	0.00
GD15_pt01	6	99.3	0.50	0.05	0.10	0.00
GD15_pt02	6	98.0	1.65	0.15	0.15	0.00
GD15_pt03	6	98.9	0.90	0.10	0.10	0.00
GD15_pt05	6	98.2	1.60	0.05	0.10	0.00
GD15_pt07	6	98.6	1.30	0.00	0.10	0.00
GD15_pt08	6	97.8	1.90	0.25	0.05	0.00
GD15_pt09	6	97.5	2.15	0.25	0.10	0.00
GD15_pt10	6	98.7	1.10	0.10	0.05	0.05